

INTERFEROMETRIC EXAMINATION OF
TEMPERATURE DISTRIBUTIONS
IN LIQUIDS:
REFRACTIVE INDEX AND
THERMAL CONDUCTIVITY

Thesis for the Degree of Ph. D.
MICHIGAN STATE UNIVERSITY
JAMES DAVID OLSON
1972

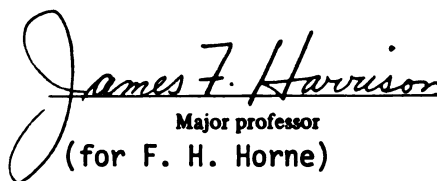
This is to certify that the
thesis entitled
INTERFEROMETRIC EXAMINATION OF TEMPERATURE DISTRIBUTIONS IN
LIQUIDS: REFRACTIVE INDEX AND THERMAL CONDUCTIVITY

presented by

JAMES DAVID OLSON

has been accepted towards fulfillment
of the requirements for

PH.D. _____ degree in CHEMISTRY

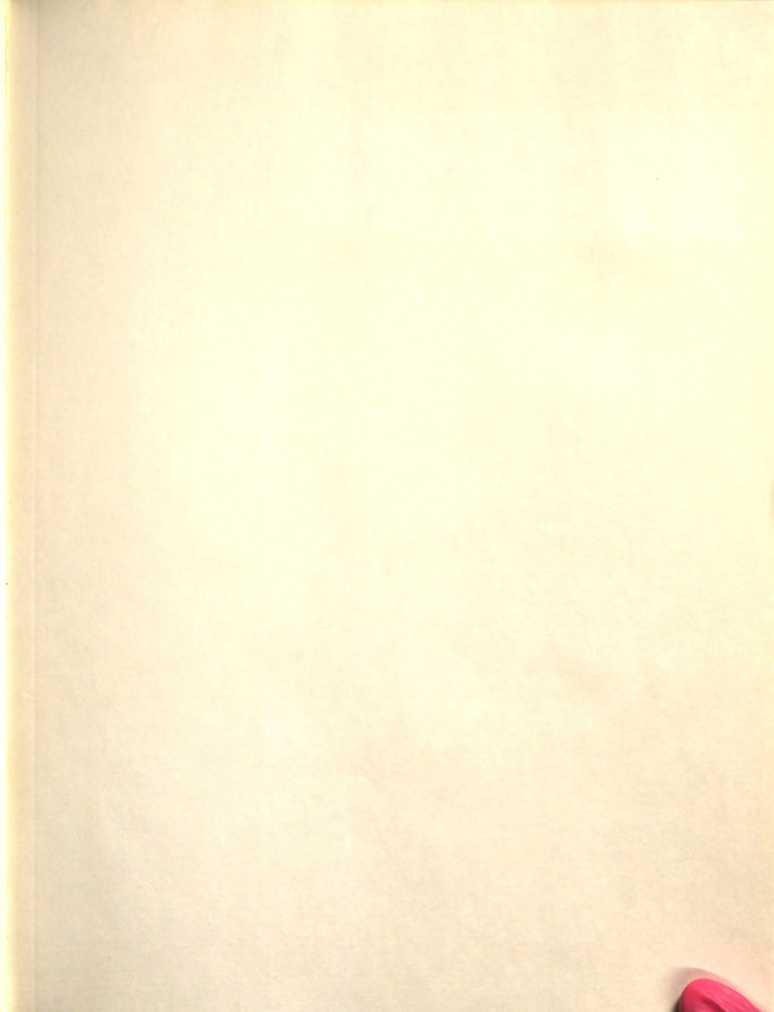

Major professor
(for F. H. Horne)

Date August 24, 1972

O-7639

LIBRARY
Michigan State
University





ABSTRACT

INTERFEROMETRIC EXAMINATION OF TEMPERATURE DISTRIBUTIONS IN LIQUIDS: REFRACTIVE INDEX AND THERMAL CONDUCTIVITY

By

James David Olson

A powerful interferometric method of studying refractive index gradients is developed and is applied to the study of vertical temperature variations in pure liquids. New methods for the direct determination of (i) temperature dependence of refractive index and (ii) thermal conductivity are developed and carried out.

An optical theory of the Bryngdahl wavefront shearing interferometer (J. Opt. Soc. Am., 53, 571 (1963)) is deduced in a general way without recourse to the mean value theorem or to phenomenological specification of the process producing the refractive index gradient. Full account is taken of displacement of the light beam by differential refraction. A final working equation is presented in terms of easily determined experimental quantities.

The availability of the new optical theory makes possible the development of a new method of determining the temperature dependence of the refractive index of liquids. The basis of the method is the interferometric examination of a liquid contained in a glass rectangular parallelepiped, bounded above and below by metal thermostating walls, in which a temperature gradient is established and maintained. Experimental results are presented for water, carbon tetrachloride, cyclohexane and benzene.

Steady state interference patterns produced by the nonelectrolytes do not have the appearance predicted by previous studies of the refractive index of these liquids: the interference fringes are parabolic rather than linear. Preliminary analysis of this anomalous behavior suggests that it is caused by slight nonlinearity in the steady state temperature distribution.

Thermal conductivity of the liquid is studied by analysis of the time dependent fringe shift observed during the establishment of the temperature gradient in the liquid. This technique is named pure thermal conduction because, in principle, it is the simplest experimental arrangement: it does not require calorimetry, and the experiment is performed in a convection free apparatus. Experimental results for water and carbon tetrachloride indicate that the new method, after technological refinement, will be of great usefulness.

577077

INTERFEROMETRIC EXAMINATION OF
TEMPERATURE DISTRIBUTIONS IN LIQUIDS:
REFRACTIVE INDEX AND THERMAL CONDUCTIVITY

By

James David Olson

A THESIS

Submitted to
Michigan State University
in partial fulfillment of the requirements
for the degree of

DOCTOR OF PHILOSOPHY

Department of Chemistry

1972

G79076

To my Parents

ACKNOWLEDGMENTS

I would like to thank the Department of Chemistry for financial support, especially its appointment as an Assistant Professor from 1964-69. I also gratefully acknowledge the support from the National Science Foundation.

I would like to thank the perceptive direction of Professor Robert A. Creswell during this research. His critical interest and advice during were extremely valuable.

To my Parents

I express my thanks to my parents for many helpful discussions concerning physical conductivity. Mr. William Taylor provided valuable assistance with the computational aspects of this work. I wish also to thank Mr. Ping Lee who assisted me with some of the experiments.

Finally, I am grateful to my wife Ellen for her encouragement and cheerfulness during the completion of this thesis.

ACKNOWLEDGMENTS

I would like to thank the Department of Chemistry for financial support, particularly for appointment as an Assistant Instructor for the academic year 1968-69. I also gratefully acknowledge financial support from the National Science Foundation.

I especially appreciate the perceptive direction of Professor Frederick Horne during this research. His critical interest and encouragement were constantly available.

I express my thanks to Dr. Sara Ingle for many helpful discussions concerning thermal conductivity. Mr. William Waller provided valuable assistance with the computational aspects of this work. I wish also to thank Mr. Ping Lee who assisted me with some of the experiments.

Finally, I am grateful to my wife Ellen for her encouragement and cheerfulness during the completion of this thesis.

TABLE OF CONTENTS

	Page
LIST OF TABLES	vi
LIST OF FIGURES.	viii
Chapter	
I. INTRODUCTION	1
II. WAVEFRONT SHEARING INTERFEROMETRY.	5
A. Introduction.	5
B. Optical Method.	7
C. Theory.	18
D. Relationship between Cell Coordinates and Final Image Coordinates	27
E. Analysis of Optical Data.	33
F. Applications.	35
III. EXPERIMENTAL APPARATUS AND PROCEDURE	38
A. Introduction.	38
B. Apparatus Improvements.	40
C. Chemicals	48
D. Data Reduction.	48
E. Experimental Procedure.	60
IV. TEMPERATURE DEPENDENCE OF REFRACTIVE INDEX	63
A. Introduction.	63
B. Working Equations	66
C. <u>A priori</u> Error Estimates.	71
D. Experimental Results for Water.	76
E. Results for CCl_4 , C_6H_{12} and C_6H_6	81
F. Discussion.	86
G. A Molecular Calculation Using (dn/dT)	87
H. Suggestions for Further Work.	94
V. ANOMALOUS PARABOLIC FRINGE SHAPES.	97
A. Introduction.	97
B. Analysis of the Parabolic Steady State Fringe Shapes	98
C. Discussion.	121

Chapter	Page
VI. PURE THERMAL CONDUCTION.	126
A. Introduction.	126
B. Experimental Methods.	127
C. A New Transient Method.	130
D. Theory of the Time Dependent Fringe Shift.	132
E. Experimental Results for Water and CCl_4	136
F. Discussion.	146
BIBLIOGRAPHY	149
APPENDIX A	155
APPENDIX B	158
APPENDIX C	163
4.1 Summary of experimental results for $(\text{dn}/\text{dT})_{\text{exp}}$ of carbon tetrachloride at $1.5 \times 10^3 \text{ Å}$	71
4.2 Summary of experimental results for $(\text{dn}/\text{dT})_{\text{exp}}$ for water.	73
4.3 Summary of experimental results for $(\text{dn}/\text{dT})_{\text{exp}}$ of carbon tetrachloride at $1.5 \times 10^3 \text{ Å}$	87
4.4 Summary of experimental results for $(\text{dn}/\text{dT})_{\text{exp}}$ of carbon tetrachloride at $1.5 \times 10^3 \text{ Å}$	88
4.5 Summary of experimental results for $(\text{dn}/\text{dT})_{\text{exp}}$ of carbon tetrachloride at $1.5 \times 10^3 \text{ Å}$	90
4.6 Data for $(\text{dn}/\text{dT})_{\text{exp}}$ of CCl_4 , refractive index and density as a function of temperature.	90
4.7 Effective refractive index and polarizability for CCl_4	91
5.1 Results of experiments for CCl_4 and nonlinear refractive index as a function of refractive index.	101
5.2 Results of experiments for CCl_4 and quadratic coefficient as a function of temperature.	105

LIST OF TABLES

Table		Page
4.1	Literature values for temperature dependence of refractive index at 25°C.	64
4.2	Literature values for $K_T \times 10^3$, temperature dependence parameter for thermal conductivity at 25°C	68
4.3	Typical values and experimental uncertainties of parameters in Eq. (4.11). . .	73
4.4	Summary of experimental results for $(dn/dT)_{25^\circ}$ of water at $\lambda = 6328 \text{ \AA}$	77
4.5	Summary of steady state fringe slope data for water.	79
4.6	Summary of experimental results for $(dn/dT)_{25^\circ}$ of carbon tetrachloride at $\lambda = 6328 \text{ \AA}$	83
4.7	Summary of experimental results for $(dn/dT)_{25^\circ}$ of cyclohexane at $\lambda = 6328 \text{ \AA}$	85
4.8	Summary of experimental results for $(dn/dT)_{25^\circ}$ of benzene at $\lambda = 6328 \text{ \AA}$	86
4.9	Data for Böttcher plot of CCl_4 refractive index and specific volume temperature dependence.	90
4.10	Effective molecular radii and polarizability for CCl_4 , C_6H_6 and C_6H_{12}	93
5.1	Results of curvefitting for alleged nonlinear temperature dependence of refractive index.	102
5.2	Results of curvefitting for gaussian nonlinear refractive index temperature dependence equation.	106

LIST OF FIGURES

Figure	Page
2.1 Schematic diagram of the interferometer. . . .	9
2.2 Schematic diagram of the cell.	11
2.3 Interferogram from an optically homogeneous test object.	15
2.4 Interferogram showing relocation of the cell center coordinate when a refractive index gradient is present in the cell.	17
2.5 Light path through the cell when a refractive index gradient is present	30
3.1 Schematic diagram of laser fringe counter. . .	46
3.2 Facsimile of computer output from program FRINGE.	56
3.3 Strip chart record of phototransistor voltage output during fringe displacement of μ -5. The arrow indicates position of $t = 0$	59
4.1 Interference fringe photographs: (a) isothermal slit photo, experiment v-13; (b) isothermal cell profile for water, experiment v-12; (c) steady state cell profile for water, $\Delta T = 5.59K$, experiment v-12	75
4.2 Böttcher plot for CCl_4 ; $n^2 / [(n^2 - 1)(2n^2 + 1)\bar{V}]$ vs. $(2n^2 - 2)/(2n^2 + 1)$	92
5.1 Interference fringe photographs: (a) steady state cell profile of CCl_4 in 8 mm cell, $\Delta T = 2.73K$, solid line (—) indicates midplane of cell, (b) steady state cell profile of C_6H_{12} in 8 mm cell, $\Delta T = 2.79K$, (c) steady state cell profile of C_6H_6 in 8 mm cell, $\Delta T = 2.79K$	100

Figure	Page
5.2 Temperature dependence of refractive index of C_6H_{12} . The solid line (—) is Eq. (5.1) and the broken (- - -) is the linear behavior predicted by the literature (Table 4.1).	105
5.3 Interference fringe photographs. This is the steady state cell profile of H_2O in 30 mm cell, $\Delta T = 10.83K$: (a) top (1/3) of cell, (b) middle (1/3) of cell, (c) bottom (1/3) of cell.	108
5.4 Interference fringe photographs. This is the steady state cell profile of CCl_4 in 30 mm cell, $\Delta T = 10.22K$: (a) top (1/3) of cell, (b) middle (1/3) of cell, (c) bottom (1/3) of cell.	110
5.5 Steady state cell profile of CCl_4 and H_2O in 30 mm cell. This composite drawing was made from Figures 5.3 and 5.4. The broken line (- - -) indicates the "break" in the CCl_4 fringes.	112
5.6 Interference fringe photographs: (a) isothermal slit photo for H_2O in 5 mm cell, (b) steady state cell profile of H_2O in 5 mm cell, $\Delta T = 10.09K$, (c) fringe pattern produced by free convection in CCl_4 heated from below.	116
6.1 "Goodness of fit" plot for thermal conductivity fitting of data from experiment v.	141
6.2 Plot of fringe shift at $z = 0$ as a function of time. The circles are the experimental points from v-4 and the solid line (—) is the least squares curve calculated from KINET.	144

CHAPTER I

INTRODUCTION

Nonuniform concentration and temperature distributions in liquids are two of the most difficult objects for the experimentalist to determine accurately. This type of measurement is required for determination of transport coefficients related to nonequilibrium processes; diffusion coefficients, thermal diffusion factors and thermal conductivities are three examples. Examination of the history of these experiments indicates that accepted values of the coefficients have been constantly revised with the advent of more and more sensitive methods for their determination.

In situ interferometry, which is the precision measurement of optical path length differences by observation of alternating light and dark patterns produced by interfering light waves, has long been recognized as the most sensitive method of detecting mass and energy transfer in liquids (Tyrell, 1961; Wolter, 1956; Ingelstamm, 1957). The extensive applications of Longsworth (1940, 1945, 1946, 1950) are examples of the determination of diffusion coefficients by an interferometric method. Gustafsson, et al. (1965) and Anderson (1968) have determined

thermal diffusion factors by an interferometric technique. An interferometric thermal conductivity method is described by Bryngdahl (1961).

Any interference phenomenon is related to spatial variations of the refractive index of the material under study. Because of this, the refractive properties of the liquid may, in principle, be examined simultaneously with the transport processes occurring in the liquid. This has not been done previously because (i) the determination of the transport coefficients was of utmost interest and (ii) an interferometric technique had not been developed to facilitate this type of experiment. However, in addition to the purely experimental reasons for studying the properties of the refractive index (Bauer, 1958; Coumou, 1964), this information can provide valuable fundamental knowledge about the molecular properties of the liquid (Waxler and Weir, 1963). Also, further refractive index studies are necessary to modify and improve the electromagnetic equation of state (Amey, 1968) which relates the refractive index to density, temperature and some function of the molecular polarizability.

The purpose of this thesis is to present an interferometric method of studying optical inhomogeneities in liquids which can be used to determine simultaneously (i) the spatial temperature distribution in a liquid perturbed from equilibrium by a temperature gradient, (ii) the

temperature dependence of the refractive index of the liquid and (iii) the thermal conductivity of the liquid. The basis of this method is the interferometric examination of a liquid in which a temperature gradient is established and maintained. We present experimental results for pure (one component) liquids although the technique could be extended to the study of mixtures.

We begin in Chapter II with a general optical theory of the particular instrument, the Bryngdahl wavefront shearing interferometer. The defects of previous theoretical treatments are corrected and a general discussion of the instrument's application to the study of transport processes is presented. It is shown that the instrument provides a sensitive yet easily executed method of measuring path length differences arising from mass and temperature distributions in liquids. Criteria for simultaneous study of transport processes and refractive index are discussed.

Chapter III is a description of the experimental apparatus used in conjunction with the wavefront shearing interferometer to study the development and effects of temperature gradients in liquids. The sample vessel is a classical pure thermal diffusion cell: a rectangular glass parallelepiped bounded above and below by thermostated metal plates. By changing the temperature of the metal plates, a temperature gradient is established and maintained in the liquid.

Experimental determination of the temperature dependence of the refractive index is discussed in Chapter IV. The optical theory of Chapter II is used to calculate (dn/dT) from the interference fringe behavior observed when a liquid has a temperature gradient established in it. Experimental results are presented for water, carbon tetrachloride, cyclohexane and benzene. The anomalous appearance of some of the steady state fringe shapes noted during the (dn/dT) experiments is discussed in Chapter V. This phenomenon appears to be related to the details of the steady state temperature distribution.

Finally, in Chapter VI we develop a new method for determining the thermal conductivity of the liquid. The basis of the method is the analysis of the time dependent behavior of the interference fringes. Experimental results are presented for water and carbon tetrachloride.

CHAPTER II

WAVEFRONT SHEARING INTERFEROMETRY

A. Introduction

Wavefront shearing interferometry, in which a distorted wavefront is compared with a sheared, or displaced, image of itself, is a highly sensitive method of determining optical path length differences and, in principle, refractive index distributions. The most convenient instrument, a Cartesian coordinate wavefront shearing interferometer, is the culmination of a study by Bryngdahl and co-workers (1957, 1960, 1961, 1963) of interferometers which employ Savart plate beam splitters. Advantages of Cartesian coordinate wavefront shearing interferometry include: (i) ease of operation, (ii) elimination of the necessity for a reference cell, (iii) a sharp interference image which is a Cartesian representation of the test object and (iv) increased sensitivity in studies of gradients of refractive index.

Unfortunately, the original optical theory (Bryngdahl, 1963) includes two simplifications which prevent the complete determination of some types of refractive index distribution encountered in the laboratory: (1) While

formally correct, the use of the mean value theorem for derivatives in order to relate the final interference image to the gradient of the refractive index normal to the optical axis in the test object introduces an unnecessary correction term in the final working equation. This correction vanishes only in the special case of a linear refractive index distribution, when the gradient is the same everywhere in the object. (2) The optical path length expression in the original article (Bryngdahl, 1963) is valid only when the path of the light ray through the test object is rectilinear. Such a path is obtained only if the refractive index gradient in the object is vanishingly small. The curvilinear path traveled by a light ray when a refractive index gradient is present in any object is treated in general by Svennson (1954, 1956). The physical manifestation of this aberration is bending of the light beam away from the original optical axis.

Other investigators (Gustafsson, et al., 1965; Wallin and Wallin, 1970; Mitchell and Tyrrell, 1972) have obtained optical theories for a similar interferometer in the course of investigations of thermal diffusion in dilute aqueous solutions. These treatments are consistent with ours, but they are not generally applicable since phenomenological equations which describe thermal diffusion are introduced early.

We present here a general optical theory for the Bryngdahl Cartesian coordinate wavefront shearing interferometer. The theory can be used to determine the refractive index distribution in an object, but it is independent of the phenomenological description of whatever produces the refractive index distribution. To obtain this improved theory we: (1) use an optical path length expression that includes corrections obtained by Svennson (1956) for a light ray traveling in a medium containing a refractive index gradient, (2) derive a method of relating the final interference image to the refractive index distribution in the cell without recourse to the mean value theorem and (3) include explicitly the additional effects of the ray-bending caused by the refractive index gradient.

B. Optical Method

Figure 2.1 is a schematic diagram of the interferometer arrangement called option II by Bryngdahl (1963). The only difference is the use of a laser as a light source because of its obvious advantages and ready availability. Detailed information about the modified Savart plates and other optical components is available in his article. We give here only an abbreviated description, with the help of the coordinate system* shown in Figure 2.2.

*y represents the vertical direction in this chapter but z represents the vertical direction in subsequent chapters. This chapter conforms to optics literature, while subsequent usage conforms to thermal transport literature.



Figure 1.1 - Schematic diagram of the instrument.

Figure 2.1.--Schematic diagram of the interferometer.

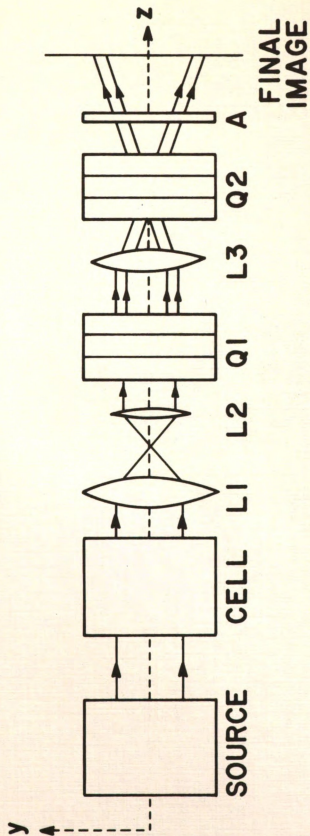




Figure 3.1--Schematic diagram of the cell.

Figure 2.2.--Schematic diagram of the cell.

Collimated, monochromatic, coherent light which is polarized in the ξ direction (this bisects the x and y axes and is inclined 45° from the plane containing the axes of the first Savart plate Q_1) passes through the test object. The test object may be any material in which an optical inhomogeneity exists or can be induced. In order to relate the general theory to the specific experiments discussed in later chapters, let the test object be a fluid-filled glass cell of length a and height h which is bounded above and below by opaque thermostating walls, as illustrated in Figure 2.2. Inside the cell, the wavefront is distorted by the refractive index distribution in the fluid. The wavefront is next reduced by the simple telescope system, lenses $L1$ and $L2$ (see Figure 2.1), to a size compatible with the optical characteristics of the modified Savart plates $Q1$ and $Q2$. The modified Savart plates are identical, each consisting of a half-wave plate sandwiched between two birefringent crystal plates. The axes of these plates lie in the same plane but are perpendicular to each other. The first modified Savart plate, $Q1$, splits the wavefront into two identical, vertically sheared wavefronts. The double image of the cell thus produced is focused by lens $L3$ into the second modified Savart plate $Q2$. This one introduces a small shear angle between the converging wavefronts and thus produces a constant path length difference. The image now passes through a polarization analyser A which

makes an interference pattern visible in the final image plane. The final image is a sharply focused double image of the x-y profile of the cell with interference fringes in the region of overlap. The fringe pattern can be related to the refractive index distribution in the cell by the optical theory of section C.

Several types of fringe patterns can be produced. Figure 2.3 shows the fringe pattern produced by an optically homogeneous test object. When the test object is optically inhomogeneous, the fringe pattern of Figure 2.4 and a variety of others can occur. Moreover, experiments can be conducted both during transient periods, when the refractive index gradient is changing, and in steady states. In a transient period the fringes move horizontally across the final image plane, and the fringe shape can change; for example, the fringe shape might change from the straight vertical bands of Figure 2.3 to the tilted or curved bands of Figure 2.4. In the steady state, no fringe movement is observed; however, the fringes may remain tilted and curved.

The shape of the fringes in the steady state is directly related to the details of the refractive index distribution in the cell. As we show in section C, a linear refractive index distribution produces straight vertical fringes identical to the ones observed in the homogeneous case. Hence, the only experimental information available in this case is the number of fringes which

Figure 2.3: Illustration of the orthogonal decomposition

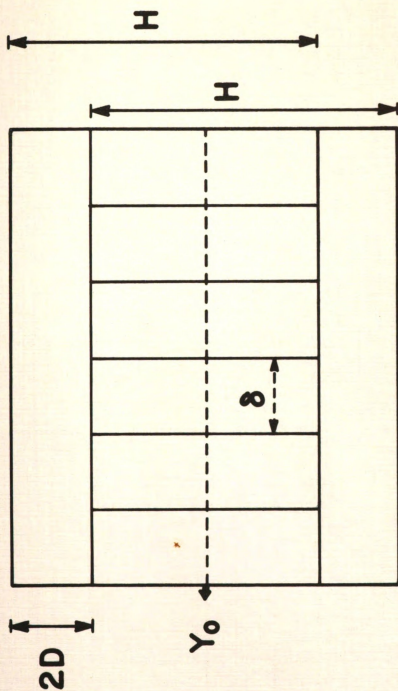


Figure 2.3: Illustration of the orthogonal decomposition

2D

y_0

Figure 2.3.--Interferogram from an optically homogeneous test object.



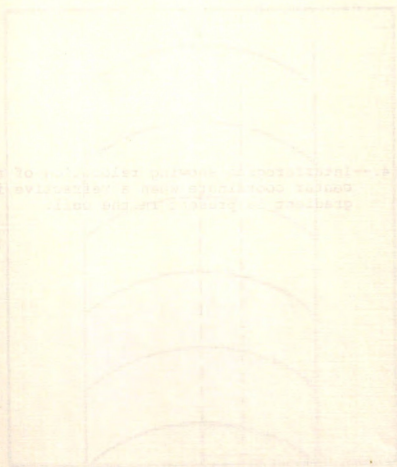
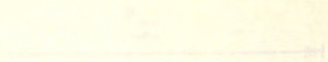
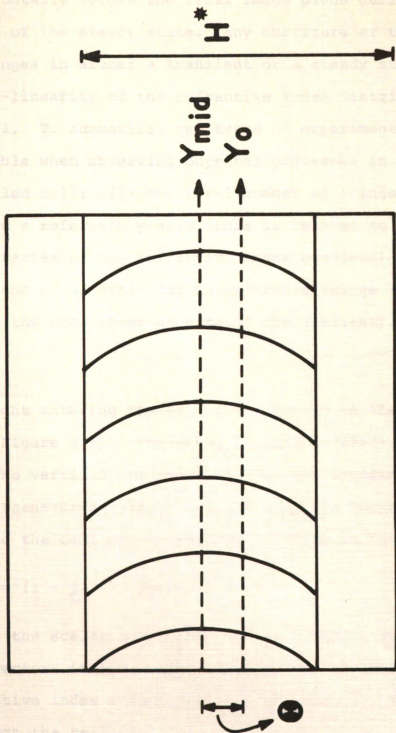


Figure 2. -- Indicated showing relative of the cell
 content coefficient when a relative index
 gradient is present in the cell.

Figure 2.4.--Interferogram showing relocation of the cell center coordinate when a refractive index gradient is present in the cell.



move horizontally across the final image plane during the attainment of the steady state. Any curvature or tilting of the fringes in either a transient or a steady state is due to non-linearity of the refractive index distribution in the cell. To summarize, two types of experimental data are available when observing physical processes in the liquid-filled cell: (1) the total number of fringes that have passed a reference y-axis (this is related to the linear character of the refractive index gradient) and (2) the x-y shape of a particular interference fringe (this is related to the non-linear aspects of the gradient).

C. Theory

Light entering the cell is polarized in the ξ direction (see Figure 2.1). Following Bryngdahl (1963), we describe the vertical component of the wave entering the cell by a transversal electric field strength vector, \underline{U} , referred to the cell coordinate system shown in Figure 2.2,

$$\underline{U} = (\underline{i} + \underline{j}) (A/\sqrt{2}) \exp(i k z) \quad (2.1)$$

where A is the scalar amplitude, $k = 2\pi/\lambda$, and \underline{i} and \underline{j} are the unit vectors in the x and y direction. If we denote the refractive index inside the cell by $n(x,y,z)$, the optical path through the cell is

$$W(x,y) = \int_0^a \{n(x,y,z)/\cos[\alpha(x,y,z)]\} dz \quad (2.2)$$

where $\alpha(x,y,z)$ is the tangential angle of the ray with the optical axis. The amplitude vector of the wave leaving the cell is

$$\vec{U} = (\hat{i} + \hat{j}) (A/\sqrt{2}) \exp\{i k[W(x,y) + z_0]\} \quad (2.3)$$

where z_0 is an arbitrary reference plane.

Next the light passes through the image reducing telescope formed by lenses L1 and L2. We introduce a new path length function

$$w(rx,ry) = W(x,y) \quad (2.4)$$

where r is the reduction factor of the lens system. The amplitude vector entering the first modified Savart plate Q1 is then

$$\vec{U} = (\hat{i} + \hat{j}) (A/r\sqrt{2}) \exp\{i k[w(rx,ry) + z_0]\} \quad (2.5)$$

In passing Q1, the component of \vec{U} in the x direction becomes polarized in the y direction and is displaced downward by an amount $(1/2)b_1$,

$$(1/2)b_1 = e(n_e^2 - n_o^2)/(n_e^2 + n_o^2), \quad (2.6)$$

where e is the thickness of each of the two birefringent plates and where n_e and n_o are the principal refractive indices. For 1 cm quartz plates in 6328 Å light, $(1/2)b_1 = 58.5\mu$. Likewise, the component in the y direction is displaced upwards by the same amount and becomes polarized in

the x direction. The amplitude vector after passing Q1 is

$$\begin{aligned} U = & \frac{i}{\lambda} (A/r\sqrt{2}) \exp\{i k[w(rx,ry + (1/2)b_1) + z_o + (1/2)\chi]\} \\ & + \frac{j}{\lambda} (A/r\sqrt{2}) \exp\{i k[w(rx,ry - (1/2)b_1) + z_o - (1/2)\chi]\} , \quad (2.7) \end{aligned}$$

where the quantity χ is introduced to take account of any path length difference due to the chance occurrence that the Savart plate may not be aligned so that the vector ξ is inclined 45° from the principal plane.

The light now enters L3 which focuses it into Q2 and magnifies it in order to produce the desired dimensions in the final image plane. The amplitude vector entering Q2 is

$$\begin{aligned} U = & \frac{i}{\lambda} (A/mr\sqrt{2}) \exp\{i k[V(mrx,mry + (1/2) mb_1) + z_o + (1/2)\chi]\} \\ & + \frac{j}{\lambda} (A/mr\sqrt{2}) \exp\{i k[V(mrx,mry - (1/2) mb_1) + z_o - (1/2)\chi]\} \quad (2.8) \end{aligned}$$

where m is the magnification factor from L3 and $V(mrx,mry)$ replaces $w(rx,ry)$ as the optical path length function.

On passing Q2, the image is sheared in the x direction, and a path length difference Δ is introduced which is related (Bryngdahl, 1961, 1963) to the incident and azimuthal angle of the light entering Q2,

$$\Delta = b_1 (mr_x/\ell) \cos i , \quad (2.9)$$

where ℓ is the distance from the focal plane of L3 to the final image plane and i is the incident angle. The amplitude vector becomes

$$\begin{aligned}
 U = & i \sqrt{A/mr\sqrt{2}} \exp\{i k[V(mrx - (1/2)b_1, mry - (1/2)mrb_1) + z_0 \\
 & + (1/2)\Delta - (1/2)\chi']\} + j \sqrt{A/mr\sqrt{2}} \exp\{i k[V(mrx \\
 & + (1/2)b_1, mry + (1/2)mrb_1) + z_0 - (1/2)\Delta + (1/2)\chi']\} , \quad (2.10)
 \end{aligned}$$

where χ' denotes any combined tilting of the Savart plates.

After passing the analyzer A, which is aligned in the η direction (see Figure 2.2), the resulting amplitude is

$$\begin{aligned}
 U = & U \cdot (i + j)/\sqrt{2} \\
 = & (A/2mr) \exp\{i k[V(mrx - (1/2)b_1, mry - (1/2)mrb_1) + z_0 \\
 & + (1/2)\Delta - (1/2)\chi']\} + (A/2mr) \exp\{i k[V(mrx + (1/2)b_1, mry \\
 & + (1/2)mrb_1) + z_0 + (1/2)\Delta - (1/2)\chi']\} \quad (2.11)
 \end{aligned}$$

Intensity at the final image is given by

$$\begin{aligned}
 I = |U|^2 = U \cdot U^* = & (1/2) (A/mr)^2 (1 + \cos\psi) , \\
 \psi = & k[V(mrx + (1/2)b_1, mry + (1/2)mb_1) \\
 & - V(mrx - (1/2)b_1, mry - (1/2)mb_1) - \Delta + \chi'] \quad (2.12)
 \end{aligned}$$

The periodicity of the interference fringes is thus given by $\psi = 2n\pi$ ($n = 0, 1, 2, \dots$).

We now seek an equation to describe families of curves of the same intensity in the final image plane.

$\cos i$ may be expanded,

$$\cos i = 1 - (1/2)O(i^2) ,$$

and Eq. (2.9) becomes

$$\Delta = b_1 \text{ mrx}/\ell - (b_1 \text{ mrx}/\ell) (1/2) O(i^2) . \quad (2.13)$$

Substituting Eq. (2.13) into the second of Eqs. (2.12) and solving for mrx, we find

$$\begin{aligned} \text{mrx} = & (\ell/b_1) [V(\text{mrx} + (1/2)b_1 \text{ mry} + (1/2)mb_1) \\ & - V(\text{mrx} - (1/2)b_1 \text{ mry} - (1/2)mb_1)] \\ & - (\ell/b_1) [(\psi/k) - \chi'] + (1/2)\text{mrx} O(i^2) . \end{aligned} \quad (2.14)$$

Hereafter, we consider only the usual case in which the refractive index is a function of y alone; then V , w , and W are independent of x and Eq. (2.14) becomes

$$\begin{aligned} \text{mrx} = & (\ell/b_1) \{ \Delta V(\text{mry}) - [(\psi/k) - \chi'] \} + (1/2)\text{mrx} O(i^2) , \\ \Delta V(\text{mry}) = & V(\text{mry} + (1/2)mb_1) - V(\text{mry} - (1/2)mb_1) . \end{aligned} \quad (2.15)$$

We now need an explicit expression for the path length of Eq. (2.2) in order to determine $\Delta V(\text{mry})$. The tangential angle α is zero for a ray that enters the cell parallel to the optical axis and travels a rectilinear path through the cell. In this case the path length expression is that used by Bryngdahl (1963),

$$W(y) = \int_0^a [n(y,z)/\cos\alpha] dz = an(y) . \quad (2.16)$$

However, when a refractive index gradient is present, the light ray does not travel the rectilinear path suggested

by Eq. (2.16). Following Svennson (1956), the expression for the optical path length which includes corrections for the effect of a gradient is,

$$W(y) = an(y) + (1/3)a^3[n'(y)]^2[n(y)]^{-1} + (1/15)a^5[n'(y)]^2n''(y)[n(y)]^{-2}, \quad (2.17)$$

where $n'(y) = dn/dy$ and $n''(y) = d^2n/dy^2$. In using Eq. (2.17), we assume that the light ray entering the cell is parallel to the z-axis but that it then travels a curvilinear path through the cell. Equation (2.17) gives the path length in terms of the entrance ($z=0$) y coordinate of the light ray since this will be different from the exit ($z=a$) y coordinate of the same ray. Since $W(y) = V(mry)$, Eqs. (2.15) and (2.17) yield

$$X = (a\ell/b_1)[\Delta n(y) + (1/3)a^2\Delta s'(y) + (1/15)a^4\Delta s''(y)] - (\ell/b_1)[(\psi/k) - \chi'] + (1/2)X O(i^2), \quad (2.18)$$

where $X = mrx$ is the horizontal fringe shift in the coordinates of the final image plane, and

$$\begin{aligned} \Delta n(y) &= n(y+\beta) - n(y-\beta) \\ \Delta s'(y) &= [n'(y+\beta)]^2[n(y+\beta)]^{-1} - [n'(y-\beta)]^2[n(y-\beta)]^{-1} \\ \Delta s''(y) &= [n''(y+\beta)][n'(y+\beta)]^2[n(y+\beta)]^{-2} \\ &\quad - [n''(y-\beta)][n'(y-\beta)]^2[n(y-\beta)]^{-2}, \end{aligned} \quad (2.19)$$

where $\beta = (1/2)b_1/r$, the shearing distance in cell coordinates.

Equation (2.18) must be transformed to a more useful experimental form since ℓ , the distance from the focal plane of L3 to the final image plane, is not easily measured accurately. Let δ be the distance between points of equal intensity on adjacent fringes in the final image; for example, as illustrated in Figure 2.3. Passing from one fringe to another represents a change in ψ of 2π so that

$$X + \delta = (a\ell/b_1) [\Delta n(y) + (1/3)a^2\Delta s'(y) + (1/15)a^4\Delta s''(y)] - (\ell/b_1) \{[(\psi - 2\pi)/k] - \chi'\} + (1/2)X O(i^2). \quad (2.20)$$

If we subtract Eq. (2.18) from Eq. (2.20) and recall that $k = 2\pi/\lambda$, we find $\delta = (\ell\lambda/b_1)$ or $(\ell/b_1) = (\delta/\lambda)$, and the final working equation which relates the fringe image to the refractive index distribution in the cell is

$$X = A[\Delta n(y) + (1/3)a^2\Delta s'(y) + (1/15)a^4\Delta s''(y)] + B$$

where $A = (a\delta/\lambda)$ and $B = -(\delta/\lambda)[(\psi/k) - \chi'] + X O(i^2)$. (2.21)

Equation (2.21) is comparable to Eq. (32) of Bryngdahl (1963, see Appendix A) with the following particular advantages: (i) Our equation contains only one correction term, $X O(i^2)$. If lens L3 is of suitable focal length, then $i < 10^{-2}$, and the deviation from the Cartesian form of Eq. (2.21) will be considerably less than 0.1%. (ii) There are no mean value theorem corrections of the type found in Eqs. (30) and (31) of Bryngdahl (1963).

(iii) Our equation retains explicitly the path length terms which arise from the curvilinear path followed by a light ray under the influence of a refractive index gradient. In some experimental instances, these additional terms might contribute negligibly to the total path length difference. In such cases a simple working equation of the type

$$X = A \Delta n(y) + B \quad (2.22)$$

may be used. Note also that if n is a linear function of y , then Δn is constant, n' is a constant and n'' is zero. Therefore, $\Delta s' = \Delta s'' = 0$, and the final image consists of straight vertical fringes. (iv) Although Bryngdahl's Eq. (32) looks like our Eq. (2.21), his equation contains a factor $(\Delta y')^{-1} = r/b_1$ in the first term. This factor renders his result incorrect dimensionally and numerically (Bartelt, 1968).

Experimental data for analysis by Eq. (2.21) are obtained from observation of both the fringe shift and the steady state fringe pattern in the final image plane. The fringe displacement X from an arbitrary vertical line selected before the refractive index gradient is developed in the cell is measured for each of a set of vertical coordinates in the final image plane. The fringe spacing δ is also measured. The set of X 's constitutes the data for the left-hand-side of Eq. (2.21), and the fringe spacing δ

permits calculation of the apparatus constant, $(a\delta/\lambda)$. The set of vertical coordinates in the final image and the shearing distance are reduced to cell coordinates by division by the magnification factor, m_r . (In the procedure described here, it is assumed that the vertical coordinate in the final image which corresponds to the center of the cell is chosen as $Y = 0$. This point is discussed further in section D.) The experimental data for Eq. (2.21) are thus a set of ordered pairs of (i) the distance (in cm) of the fringe shift in the final image plane and (ii) the particular vertical coordinate in the cell (between $-h/2$ and $h/2$) which corresponds to the image plane vertical coordinate at which (i) is measured.

Another experimental procedure is often more convenient. Equation (2.21) can be cast into the form,

$$(X/\delta) = (a/\lambda) [\Delta n(y) + (1/3)a^2\Delta s'(y) + (1/15)a^4\Delta s''(y)] + (B/\delta) . \quad (2.23)$$

Note that the left-hand-side of Eq. (2.23) is dimensionless. This indicates that a number of fringes rather than a fringe shift distance is measured to provide data for the left-hand-side of Eq. (2.23). This is accomplished experimentally by placing an arbitrary vertical reference line on one of the fringe minima before the establishment of the refractive index gradient in the cell. As the fringes are shifted horizontally during the establishment of the refractive

index gradient, the experimenter counts (manually or by use of a photoelectric device) the number of fringe minima that pass the reference line. However, it in general happens that the total fringe shift is not an integral number of fringes; i.e., the fringe motion stops when no fringe minimum is colinear with the reference line. In this case a fractional fringe displacement is calculated by (a) measuring the distance between the reference line and the last fringe minimum to pass the reference and (b) dividing this distance by the fringe spacing δ . This function is added to the integral number of fringes. As before the data are a set of ordered pairs; (i) the dimensionless fringe shift measured for (ii) each chosen vertical cell coordinate. The latter are obtained by reducing the vertical coordinates of the final image by the magnification factor m_r .

D. Relationship between Cell Coordinates and Final Image Coordinates

As mentioned above, the success of the use of Eq. (2.21) or (2.23) in experimental analysis of refractive index distributions depends on the ability to relate the coordinates of the final fringe image to the coordinates of the cell. This requires: (i) determination of the magnification factor and (ii) identification of the horizontal plane on the fringe pattern that corresponds to the center ($y = 0$) of the cell coordinate system. In the

case of an optically homogeneous cell, whose fringe pattern is shown schematically in Figure 2.3, these relationships are straightforward: the center of the final image (where $Y = Y_{\text{mid}}$) clearly corresponds to the center plane of the cell (where $y = 0$), and the height H of either of the superimposed final images is equal to the magnified height of the cell. The magnification factor, mr , is then simply the ratio of H to h , $mr = H/h$, and for any arbitrary set of Y coordinates,

$$y = (Y - Y_{\text{mid}})/mr. \quad (2.24)$$

In most experimental arrangements, Y_{mid} is chosen as $Y = 0$, and Eq. (2.24) becomes

$$y = Y/mr. \quad (2.25)$$

In general, however, the refractive index distribution in the cell is nonlinear, and the emergent ray is bent. The physical manifestation of the ray-bending effect of a refractive index gradient is shown in Figure 2.5. Ray-bending affects the relationship of the fringe coordinate system to the cell coordinate system in two ways: (a) The amount of bending changes with height in the cell, so that there is a net focusing of the light beam leaving the cell and a subsequent change in the magnification factor; (b) Part of the light beam may be cut off by the top or bottom of the cell, and consequently the center of the final fringe image

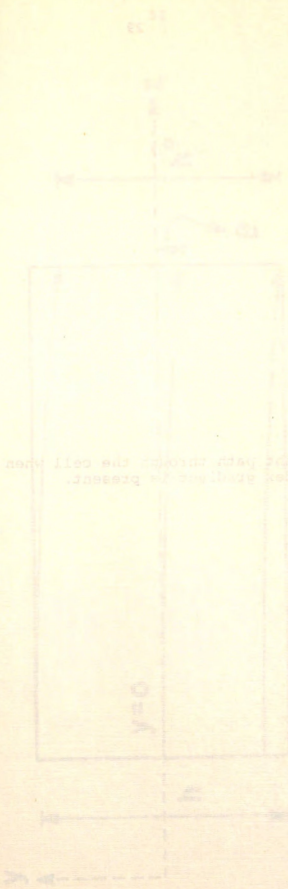
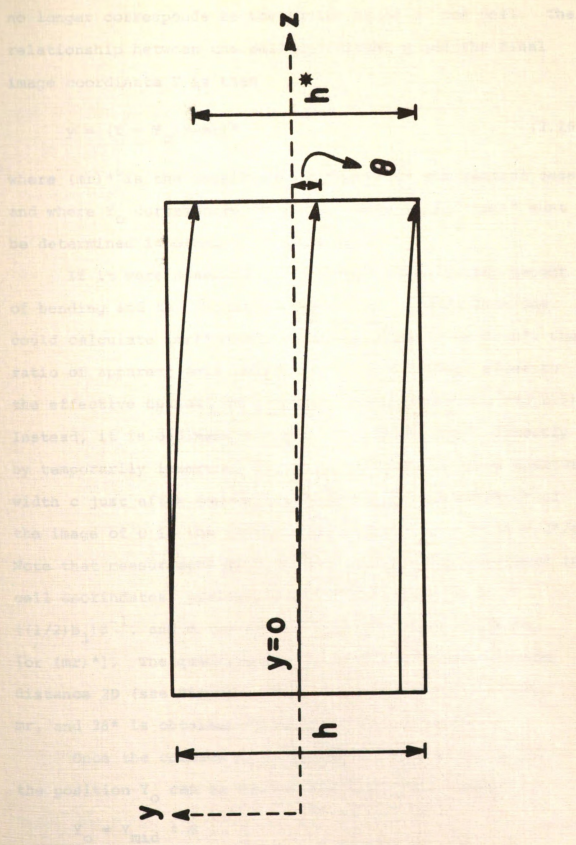


Figure 1.3. -- Light path through the cell when a refractive index gradient is present.

Figure 2.5.--Light path through the cell when a refractive index gradient is present.



no longer corresponds to the center plane of the cell. The relationship between the cell coordinate y and the final image coordinate Y is then

$$y = (Y - Y_0) / (mr)^* \quad (2.26)$$

where $(mr)^*$ is the magnification factor in the general case and where Y_0 corresponds to $y = 0$. Both Y_0 and $(mr)^*$ must be determined in order to analyze data.

If it were possible to determine directly the amount of bending and the amount of light beam cutoff, then one could calculate $(mr)^*$ directly by equating it to H^*/h^* , the ratio of apparent cell height in the final image plane to the effective optical cell height (see Figures 2.4 and 2.5). Instead, it is ordinarily easier to measure $(mr)^*$ directly by temporarily inserting a slit of accurately known aperture width c just after the cell and measuring the width C^* of the image of c in the final image plane. Then $(mr)^* = C^*/c$. Note that measurement of β (or β^*), the shearing distance in cell coordinates, yields r (or r^*) according to $r = ((1/2)b_1)\beta^{-1}$, and m (or m^*) is then obtainable from mr [or $(mr)^*$]. The quantity 2β is obtained by dividing the distance $2D$ (see Figure 2.3) by the magnification factor mr , and $2\beta^*$ is obtained by dividing $2D^*$ by $(mr)^*$.

Once the correct magnification factor is obtained, the position Y_0 can be determined from (see Figure 2.4)

$$Y_0 = Y_{mid} \pm \theta, \quad (2.27)$$

where (see Figures 2.4 and 2.5)

$$\Theta = (mr)^* \theta, \quad \theta = h - h^* . \quad (2.28)$$

Alternatively, since $(mr)^* = H^*/h^*$, Θ is obtained from more easily measured quantities,

$$\Theta = (mr)^* h - H^* . \quad (2.29)$$

The choice of signs in Eq. (2.27) is necessary because although θ and Θ are positive, the light beam may bend either up (+) or down (-), depending on the refractive index distribution in the cell.

Substitution of Eqs. (2.27) and (2.29) into Eq. (2.26) yields the final, general formula which relates Y to y for an arbitrary Y coordinate system,

$$y = [(Y - Y_{\text{mid}})/(mr)^*] \pm [h - H^*/(mr)^*] \quad (2.30)$$

Note that Eq. (2.30) reduces to Eq. (2.24) only when both $(mr)^* = mr$ and $h^* = h$.

The procedure can be simplified if a horizontal slit is placed before the cell and the aperture arranged so that the light beam entering the cell is symmetric about the $y = 0$ plane. In this case none of the light beam will be cut off, and the center of the fringe image will correspond to the center of the cell at the entrance coordinate. In practice, it is difficult to align the slit symmetrically about the $y = 0$ plane. Also, the amount of cell observable is decreased by this type of masking.

Wallin and Wallin (1970) suggest changing the angle of incidence of the light entering the cell to counteract the bending effect. This has the advantage of producing an exit beam that has the same exit coordinate as entrance coordinate but has the disadvantage of requiring a path length expression different from Eq. (2.17) in order to include terms which contain the entrance angle. A suitable expression could no doubt be derived, starting with the work of Svennson (1956), but its use would require accurate measurement of the angles of exit and accurate control of the angles of entrance. The techniques so far suggested for taking account of demagnification and coordinate relocation caused by ray-bending are probably not the only ones which might be useful; the particular physical arrangement of the interferometer and the properties of the system being studied may suggest other appropriate means to deal with these effects.

E. Analysis of Optical Data

After the correct final image coordinate relationship and the fringe displacement have been obtained, it is possible to calculate the refractive index distribution in the cell. Let the refractive index distribution in the cell be represented by the following equation:

$$n(y) = n_0 + f(y) . \quad (2.31)$$

The leading term in Eq. (2.31), n_0 , which is the absolute refractive index at the center of the cell, cannot be determined from analysis of the final image because it appears in the difference expressions,

$$n(y) = f(y + \beta) - f(y - \beta) , \quad (2.32)$$

which appear in Eq. (2.21). Rather, the specific values of the parameters in $f(y)$, which describes the functional variation of the refractive index about n_0 , are determined. The general form of $f(y)$ may be suggested by the shape of the fringes in the final image plane. The method of multiple linear regression (Anderson, 1968; Efroymsen, 1960; see Appendix C) for choosing a set of variables is valuable in this regard. To consider a specific example, the results might be expressed by a simple Taylor's series about $y = 0$,

$$\begin{aligned} n(y) = n_0 + (dn/dy)_{y=0} y + \dots + (i!)^{-1} (d^i n/dy^i)_{y=0} y^i \\ + \dots \end{aligned} \quad (2.33)$$

In this case, Eq. (2.33) is truncated after a sufficient number of terms and substituted into Eq. (2.23) which is written in cell coordinates for this purpose. This yields an expression containing (X/δ) as a function of y with the spatial derivatives as parameters,

$$(X/\delta) = X(y, dn/dy, d^2 n/dy^2, \dots, d^i n/dy^i) . \quad (2.34)$$

The optical experiment yields a set of $[(X, \delta), y]$ data from the number of fringes displaced and the fringe shape. As discussed following Eq. (2.22), the fringe data and the shear distance, D , can be reduced to cell coordinates by use of the magnification factor. The spatial derivatives [or similar parameters in other choices of $f(y)$] are obtained by least squares adjustment of Eq. (2.34) to the experimental data. This can be done by a number of parameter estimation techniques (see Appendix C) which are facilitated by the use of a digital computer. It should be noted that in this analysis, there are no assumptions made about the process producing the refractive index distribution.

F. Applications

The interferometer may be used to study physical processes such as mass and heat transport in the cell. Suppose we wish to relate the optical data to some property P which varies as a function of cell height, $P = P(y)$, and we also know that the refractive index is a function of P , $n = n(P)$. The refractive index can then be written as a function of cell height,

$$n = n[P(y)] \quad . \quad (2.35)$$

Equation (2.35) in effect specifies a particular $f(y)$ for use in Eq. (2.32). For example, in the case of initially

sharp boundary-layered isothermal diffusion experiments, a gaussian form of the refractive index gradient would be applicable. However, we must know explicitly either $P(y)$ or $n(P)$ to determine the other: that is, it is not possible to separate the property spatial distribution from the refractive index property dependence in one experiment. Hence, either of two mutually exclusive experimental objectives may be achieved: (i) Determination of the dependence of n on some property P whose y dependence is known: (ii) Determination of the y dependence of some property P whose relationship to n is known. Mass and heat transport experiments would fall into the latter category because the temperature and concentration dependence of the refractive index can be determined experimentally.

This method of analysis can be extended to account for more than one property which affects the refractive index and varies in the y direction, as, for example, in a pure thermal diffusion experiment. Equation (2.35) would then be written,

$$n = n[P_1(y), P_2(y), \dots, P_i(y)] . \quad (2.36)$$

In this case, all but one of the property spatial distributions and property refractive index dependences must be known completely to determine the process.

Application of the method to systems in which a very small Δn exists (for example, flow profiles in gases)

would require the shear distance D or the geometrical light path a to be increased in order to preserve high sensitivity. However, as D is increased, the region of overlap between the sheared wavefronts decreases, and the added sensitivity would eventually be countered by the decrease in the area of the test object studied. A compromise between these two effects must be found according to the needs of the particular experiment. Wallin and Wallin (1970) discuss a method of increasing sensitivity by rotation of the second Savart plate. The ultimate sensitivity is available in holographic analogs (Bryngdahl, 1969; Becsey, et al., 1970) of these methods; phase multiplication during reconstruction of the image increases sensitivity to any desired level.

The specific application of the interferometer to the study of the establishment and decay of a temperature gradient in a pure liquid will be discussed in Chapters IV, V and VI.

CHAPTER III

EXPERIMENTAL APPARATUS AND PROCEDURE

A. Introduction

The method of obtaining experimental fringe shift and fringe shape data is discussed in this chapter. These data can be analyzed by means of the optical theory developed in Chapter II to determine the temperature dependence of refractive index and thermal conductivity of the liquid.

The experimental apparatus used to study the effects of temperature nonuniformity in pure liquids is essentially the thermal diffusion apparatus built previously in this laboratory (Anderson, 1968). The liquid is contained in a rectangular glass sample cell bounded on the top and bottom by metal thermostating plates whose temperatures are controlled by circulating water reservoirs. The source of circulating water to each plate reservoir is controlled by a valve system so that the cell may be changed from an isothermal configuration (both plates thermostated by water from the same mean temperature bath, T_M) to a temperature difference configuration (water from a warmer bath, T_H , circulating in the upper reservoir and water from a cooler

bath, T_C , circulating in the lower reservoir). This arrangement allows a temperature difference to be applied vertically across the cell, a temperature gradient to be developed in the liquid as a function of time, and finally, a steady state temperature distribution to be maintained in the liquid. Observation of both the establishment and decay of a temperature gradient is possible.

Plate temperatures are measured with copper constantan thermocouples and a microvolt potentiometer. The continuous change of the plate thermocouple voltages is monitored by two strip chart recorders, each modified to record in 200 μv full scale steps. The circulating baths' temperatures are controlled by continuous heating and cooling regulated by a proportional temperature controller. The plates' temperatures are maintained constant within 0.003K fluctuations.

The cell is aligned in an optical train in which the vertical cell profile is illuminated by a laser and the image is optically analyzed by a Bryngdahl wavefront shearing interferometer. In some experiments, the interference fringes are recorded with a Polaroid MP-3 camera in the final image plane (see Figure 2.1). In other experiments, the Polaroid unit is removed from the final image plane and the horizontal movement of the fringes is monitored with a phototransistor.

A complete description of the apparatus design and objectives and details of the original apparatus construction are available elsewhere (Anderson, 1968, pps. 76-116). Anderson required maintenance of a carefully controlled temperature difference for ten to sixteen hours in order to obtain a thermal diffusion steady state. The present experiments, however, require only 15 to 45 minutes of controlled temperature difference. The effects of problems such as ambient temperature drift and temperature controller artifacts are therefore much less important for the present experiments. Short term temperature control is usually easy to obtain.

B. Apparatus Improvements

Several parts of the apparatus have been improved in the course of this research. However, the temperature monitoring equipment, the cell filling technique, the cell insulating technique, and the use of the MP-3 Polaroid camera are the same as described by Anderson (1968). Improvements are:

1. Temperature Control. The first step in improvement of temperature control was the installation of proportional temperature controllers to replace the mercury thermoregulators supplied by the bath manufacturer (Tamson). Model 2156 Versa-Therm controllers were purchased from Cole-Parmer, Chicago, Ill., and Model 408 "Banjo" probes were purchased

from YSI Co., Yellow Springs, Ohio. These eliminated the "temperature ripple" in the water baths by supplying a constant amount of power to the heating element in the bath to balance the constant cooling rate provided by a coil cooled with water from a refrigerated temperature bath. Any fluctuations in the bath temperature are balanced by proportionally greater or lesser amounts of power to the heating elements. Fluctuations were further reduced by heat exchangers (Anderson, 1968, p. 92). The plate temperatures are routinely maintained to within $\pm 0.003\text{K}$ of the desired temperature.

Optimum use of proportional temperature controllers requires a constant cooling rate. The Lab-line Tempmobile used by Anderson as a source of cooling water for the three baths was used with one modification. Flow meters and stopcocks were installed in order to monitor empirically and to reproduce cooling rates. Typically, cooling is maintained by a flow of about 250 ml/min of 13°C water. Slightly different rates are used to satisfy the individual requirements of the T_M , T_H , and T_C baths.

The two position valve (Anderson, 1968, p. 73) used to switch the bath water inlets to the plate reservoirs from the isothermal configuration to the temperature difference configuration was retained unchanged. However, the pinch clamps used to control access to the water bath by-passes were replaced by stopcocks for more convenient switchover.

2. Optical Components. The original optical train was replaced by equipment purchased from The Ealing Corporation, Cambridge, Massachusetts. The goals in this replacement were (a) reproducibility of the position of optical components and (b) capability of vertical and horizontal adjustment of lenses and modified Savart plates.

A two meter optical bench, equipped with a mm scale, replaced the two unconnected optical benches used previously. The optical carriers are equipped with a 0.1mm vernier which allows accurate reproduction of component position on the optical bench. Two carriers which can be adjusted vertically and horizontally are used to support the laser light source and align it along the optical axis. L1 is mounted in a lens holder also supported by a vertically and horizontally adjustable optical carrier. L2 is mounted in a focusing microscope objective holder which was modified by the Chemistry Department machine shop to serve as a lens holder. Q1 and Q2 are mounted in rotatable component holders which can be tilted 45° from the vertical axis as described in the optical theory (see Chapter II, section B). L3 is also mounted in a focusing microscope objective holder. A precision polarization analyzer completes the optical components of the interferometer. In order to provide the magnification of the final image necessary to take Polaroid photographs, a fourth lens is used after the analyzer.

The light source is a He-Ne gas laser, Spectra-Physics Model 120, equipped with a Model 332-337 spatial filter and beam expander. The beam expander eliminated the first two lenses of the original optical setup (Anderson, 1968, p. 104) and produces an optically pure, coherent, monochromatic light beam which is sufficiently intense to observe and record the interference fringes. The power output of the laser is about eight milliwatts. The laser beam has a diameter of 5 cm as it leaves the beam expander. It is focused on the midplane of the sample cell and masked to the region of interest by a 1 cm \times 3 cm slit. This prevents spurious reflections of laser light from the metal plates and reservoirs.

Biconvex positive lenses obtained from Special Optics, Cedar Grove, New Jersey, are used for L2 and L3. L1 and the modified Savart plates were the same as used previously (Anderson, 1968, pp. 104-5). A 3x microscope objective is used to focus the final image on the Polaroid camera back.

A 0.01mm x-y vernier telescope was purchased from The Ealing Corporation to replace the 0.1mm vernier microscope stage used previously to record the horizontal displacement of fringes (Anderson, 1968, p. 113). The frosted glass back of the Polaroid camera target does not produce a suitable image for monitoring fringe shifts with the x-y telescope. A target of translucent bond (typing) paper is

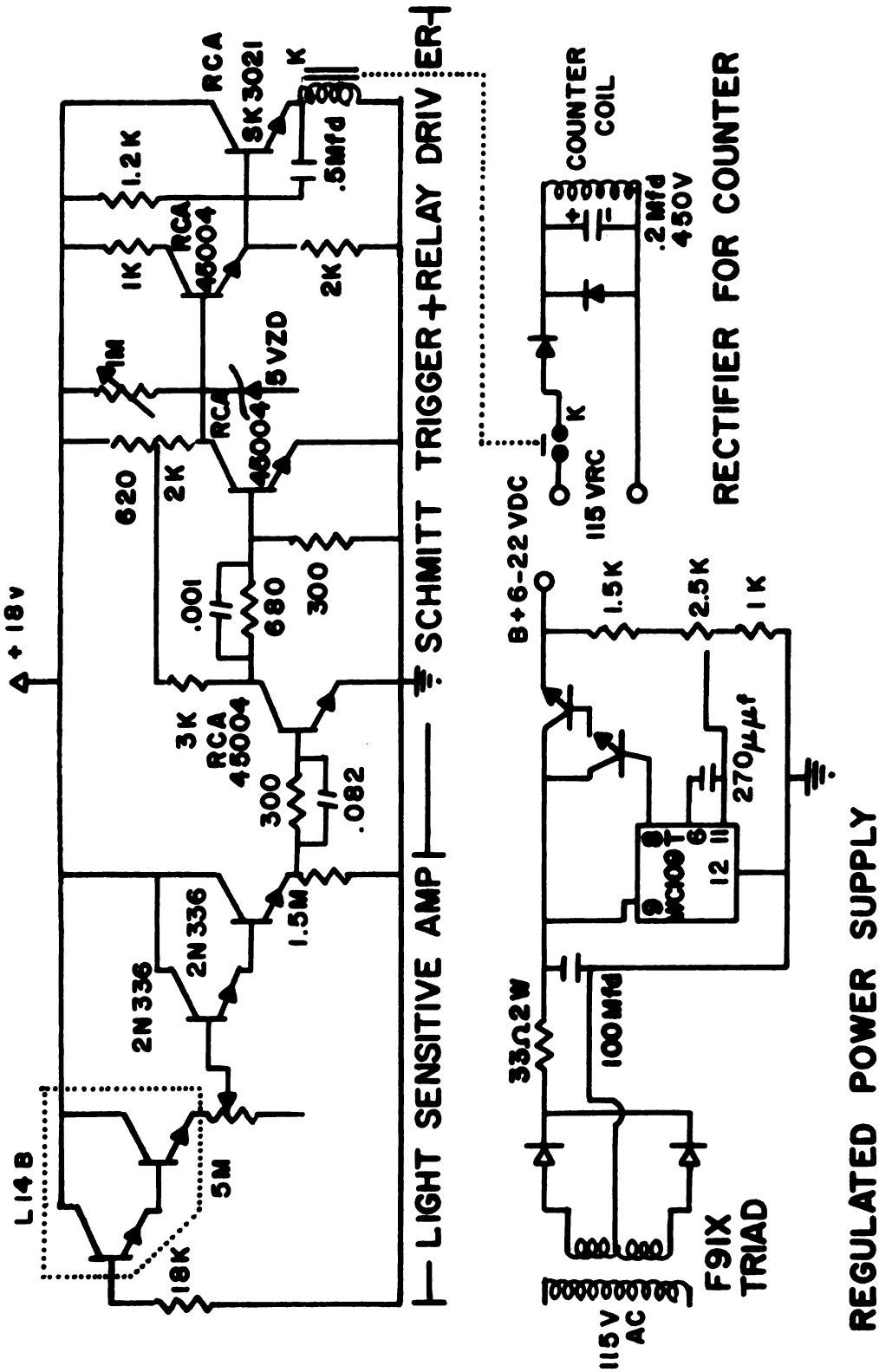
placed about one meter behind the camera. During an experiment the camera back is removed and the cell profile image focused on the paper. The x-y telescope is placed about 30cm behind the paper and used to record fringe motion.

The previous changes are improvements upon the original apparatus design. Two additions were made that have no analog in the original optical equipment: (1) a rotatable parallel plate has been placed in the optical train between the sample cell and L1; (2) a phototransistor is used to monitor fringe shifts during an experiment.

The parallel plate makes it possible to adjust the cell profile vertically in the final image plane without adjusting the relative position of the lenses in the interferometer as Anderson had to do. Also, the cell image can be relocated on the center of L1 if the "bending" effect of the refractive index gradient moves the light beam out of the optical axis. Finally, it is possible to align the laser and sample cell on a different optical axis from the optical axis of the interferometer. The parallel plate is used to raise or lower the cell image into the interferometer optical axis.

A Photo-Darlington L14B (Allied Electronics, Chicago, Ill.) phototransistor is used in conjunction with a mechanical fringe counter and signal amplifier, built by Mr. Ronald Haas of the Chemistry Department electronics shop, to monitor the horizontal travel of the interference fringes. Figure 3.1

Figure 3.1.--Schematic diagram of laser fringe counter.



LASER FRINGE COUNTER

is a schematic diagram of the fringe counter. The transistor is mounted in the vernier microscope stage (previously used to measure fringe travel) and horizontally centered on the fringe chart area by locating the position of minimum voltage output. The transistor is vertically centered on the line corresponding to the midplane in the sample cell by means of a wire which is mounted in the middle of the back of the phototransistor and which extends horizontally 1 cm in each direction.

Two forms of data are available from the amplifier: (1) the digital output from a mechanical counter which records the total number of integral fringes that pass the transistor (a square wave pulsed by a Schmitt trigger activates the counter) and (2) the amplified output voltage of the transistor which is displayed on a strip chart recorder. The voltage output goes from a minimum (0.0 fringe displaced) to a maximum (0.5 fringe displaced) and back to a minimum (1.0 fringe displaced). Of course, the fringe displacement is seldom exactly an integral number of fringes. The fractional fringe is measured directly by the x-y vernier telescope as described in section C.

3. Data from Fringe Photographs. The vernier microscope stage was used by Anderson (1968, p. 113) to obtain spatial data from the Polaroid photographs of the interference fringes. Determination of 2β , the shearing distance in cell coordinates, is also calculated from this

type of measurement. A more sensitive method of measuring distances on the photos was suggested by Dr. Marc DeBacker. The photo of interest is mounted on an x-y recorder equipped with crosshairs instead of a pen. A stable and sensitive ($\pm 0.00001\text{v}$) variable voltage supply is used to buck the recorder and move the crosshairs from position to position on the photo. At each point, the x and y input voltages are read to 0.1mv on a Heath UDI digital voltmeter and are then used as the coordinates of that point. This method provides fast, efficient analysis of fringe distances and shapes to three significant figures.

C. Chemicals

Water used in the refractive index and thermal conductivity experiments was obtained from the MSU Brillouin Lightscattering group. It was triply-distilled deionized conductivity water.

The carbon tetrachloride, cyclohexane and benzene used were purchased from the J. T. Baker Chemical Company. These were spectrophotometric grade reagents and were used without further purification.

D. Data Reduction

Raw data obtained from a refractive index temperature derivative experiment includes the following:

1. Cell height and cell length.
2. Shear distance.

3. Temperatures of the upper and lower plates in the isothermal configuration, T_M^O .
4. The temperature difference at the steady state.
5. Total number of fringes displaced during the establishment of the temperature gradient.
6. X-Y fringe shape in the steady state.

Thermal conductivity experiments require all of these data, except 6. In this case the following are also required:

7. Time dependence of the change of the plate temperatures from the isothermal configuration to the steady state, i.e., strip chart recording of thermocouple voltage.
8. Time dependence of the interference fringe shift, i.e., strip chart recording of the phototransistor voltage.

Note that both experiments can be done simultaneously; the transient data lead to determination of the thermal conductivity and the steady state data lead to determination of the refractive index temperature dependence.

This section will be a discussion of how each datum is obtained experimentally and how it is reduced to a form that can be used to determine the temperature dependence of refractive index or the thermal conductivity.

1. Cell height and cell length. The cell height was measured to $\pm 0.0005\text{cm}$ by repeated micrometer readings. The cell length was measured to $\pm 0.001\text{cm}$ with a vernier

calipers. The results for the two cells are:

Cell 1 Length = 6.828cm Height = 0.8103cm

Cell 2 Length = 6.805cm Height = 3.0124cm

2. Shear distance. The shearing distance, 2β , is determined by measurements made on the photograph of a slit of known aperture, h , as described in Chapter II, section D. The slit photos resemble Figure 2.3. Two example photos are Figures 4.1(a) and 5.6(a). The distances between the four parallel lines are measured in a vertical plane chosen at random on the photograph. The vertical coordinate of each boundary is obtained by measurement with the x-y recorder as described in section B, 3. These coordinates are called $Y(1)$, $Y(2)$, $Y(3)$, $Y(4)$. The differences $|Y(1) - Y(3)|$ and $|Y(2) - Y(4)|$ are the magnified slit heights and the distances $|Y(2) - Y(1)|$ and $|Y(4) - Y(3)|$ are the magnified shear distances, $2D$. The shear distance in cell coordinates is obtained from the following equations (see Chapter II, section D):

$$mr = |Y(1) - Y(3)|/h , \quad |Y(4) - Y(2)|/h , \quad (3.1)$$

$$2\beta = |Y(2) - Y(1)|/mr , \quad |Y(3) - Y(4)|/mr . \quad (3.2)$$

Note that each measurement of four coordinates yields two determinations of the shear.

Numerical Example: Isothermal Slit Photo

$$\text{Slit} = 0.4580\text{cm}$$

$$Y(1) = 17.60 \quad Y(2) = 41.10 \quad Y(3) = 140.1 \quad Y(4) = 163.5$$

$$mr = |140.1 - 17.6| / 0.4580\text{cm} = 267.5\text{cm}^{-1}$$

$$mr = |163.5 - 41.1| / 0.4580\text{cm} = 267.3\text{cm}^{-1}$$

$$\begin{aligned} \text{Absolute Shear, } 2\beta &= |41.1 - 17.6| / 267.4\text{cm}^{-1} = 0.0879\text{cm} \\ &= |163.5 - 140.1| / 267.4\text{cm}^{-1} = 0.0875\text{cm} \end{aligned}$$

A computer program, SHEAR, was written to calculate the average shear from data collected from experimental photographs according to Eqs. (3.1) and (3.2). As many determinations of 2β as desired can be carried out.

3. Isothermal mean temperature, T_M^O . (The superscript O) means measurements conducted in the isothermal configuration to distinguish from the temperature symbols referring to the steady state; T_M , T_U , and T_L .) The voltages of the thermocouples connected to the upper and lower plates are measured with a Leeds and Northrup K-3 potentiometer immediately before the application of the temperature difference. The voltages are converted to temperatures from a calibration chart obtained previously (Anderson, 1968, p. 103). Usually, $T_M^O = T_U^O = T_L^O$. At times, the temperature readings are different for the two plates. These differences are less than 0.006K. T_M^O was calculated to be $(1/2)(T_U^O + T_L^O)$ where T_U^O and T_L^O are the temperatures of the upper and lower plates in the isothermal configuration.

4. Temperature difference at the steady state, ΔT .

When the steady state is attained (the fringes have stopped

moving), T_U and T_L are again measured by recording the thermocouple voltages. Their difference, $\Delta T = T_U - T_L$, is used directly in the calculations, and therefore any errors such as thermocouple reference bath drift or potentiometer null offset is present in both the T_U and T_L readings and is eliminated in the difference. T_M , the mean temperature in the steady state, is equal to $(1/2)(T_U + T_L)$.

5. Total number of fringes displaced during the establishment of the temperature gradient. A strip chart recording of the phototransistor output yields the total number of integral fringes that pass an arbitrary reference point. The fraction of fringe displaced after the last integral fringe is measured with the x-y vernier telescope. The telescope crosshairs are centered on a dark area of a fringe before the start of an experiment. The horizontal coordinate of this point is called X_O . It is noted in which horizontal direction the fringes are traveling during the experiment. After the steady state is reached, the horizontal coordinate X_L of the last fringe to pass the crosshairs is measured. The position X_N of the fringe that would next pass the crosshairs is also measured. The fractional fringe displacement is calculated from this equation:

$$\text{Fringe Fraction, } X/\delta = |X_O - X_L|/|X_L - X_N| \quad (3.3)$$

Numerical Example: Experiment v-15

$$X_O = 13.794$$

$$X_L = 14.535$$

$$X_N = 13.431$$

$$\begin{aligned} \text{Fringe fraction} &= |13.794 - 14.535| / |14.535 - 13.431| \\ &= 0.671 \end{aligned}$$

Strip chart indicated 6 integral fringes plus 0.5
to 1.0 fraction fringe

$$\text{Total fringe displacement} = 6.671$$

6. X-Y fringe shape. The steady state fringe shape data are collected from Polaroid photographs using the x-y recorder. These fringe shapes are often parabolas similar to Figure 2.4. Two types of reduced data are calculated from the photographs: (i) the total number of fringes displaced during the establishment of the temperature difference as a function of vertical coordinate and (ii) deviations from the midplane fringe shift as a function of vertical coordinate. Data of type (i) are obtained by adding the horizontal fringe shift measured previously in part 5 to the data of type (ii). Both of these types of data are tabulated in ordered pairs of dimensionless fringe shifts, X/δ , for each vertical photo position converted to cell coordinates (see Chapter II, section C).

Photos of the cell profile and a slit of known aperture are taken in the isothermal configuration and in the temperature difference steady state. The magnification factors, (mr) and (mr)*, are calculated from the slit photos.

Often it is discovered that the cell height calculated from the isothermal cell profile photograph is not equal the actual cell height. This is due to masking of the cell-plate boundary by sealant that leaks out of the boundary upon tightening of the plates. The amount of sealant cut off, assumed to be the same at the top and bottom cell boundaries, is calculated from the following equation:

$$\Delta h_{\text{cutoff}} = h - H/mr \quad (3.4)$$

where h is the measured cell height, H is the magnified apparent cell height, and (mr) is the isothermal magnification factor calculated from the isothermal slit photograph.

Equation 2.30,

$$y = [(Y - Y_{\text{mid}})/(mr)^*] \pm [h - H^*/(mr)^*] , \quad (2.30)$$

for conversion of photograph vertical coordinates to cell coordinates was modified to account for sealant cut-off:

$$y = [(Y - Y_{\text{mid}})/(mr)^*] - \{[h - H^*/(mr)^*] - \Delta h_{\text{cutoff}}/2.0\} . \quad (3.5)$$

This allows for the downward bending of the light beam that is required to lower the beam past the upper sealant boundary.

A computer program, FRINGE, was written which takes raw data from the x-y recorder and calculates the fringe shape data. A facsimile of a partial output from this program for a set of test data is shown in Figure 3.2.

7. Time dependence of plate temperature change. The following empirical equations (Anderson, 1968, p. 97) are used to describe the warming of the upper plate and the

**Figure 3.2.--Facsimile of computer output from program
FRINGE.**

SAMPLE DATA FOR FRINGE SHAPE DATA CONVERSION

FRINGE NUMBER 1 OF 2 FRINGES

SHEAR(CM)	CELL HIGHT(CM)	CELL LNTH(CM)	KT(1/DEG C)	DEL T(DEG C)
.10	.5	7.0	.0020	3.000

AMOUNT OF CELL CUTOFF DUE TO SEALANT = .05033 CM

M1	H1	M2	H2
.100000E+04	.449968E+03	.100000E+04	.399971E+03

APPARENT CELL HT(ISOTHERMAL)	APPARENT CELL HT(DELTA T)	DEL(Z=0)
.449967 CM	.399971 CM	.075013 CM

DISTANCE BETWEEN FRINGES =	.149989E+03	STD DEV =	.101685E-11
(PHOTO UNITS)			

FRINGE SHIFT WITHOUT 1ST DERIVATIVE

Z(CM)	X(FRINGES)
-.07246	.44524
-.05222	.31351
-.03198	.18177
-.01174	.05004
.02849	-.08009
.07373	-.20983
.11849	-.07289
.14824	.06284
.17788	.26524
.19752	.46684
.21716	.66844

FRINGE SHIFT WITH 1ST DERIVATIVE SHIFT ADDED

Z(CM)	X(FRINGES)
-.07246	40.26825
-.05222	40.13652
-.03198	40.00478
-.01174	39.87305
.02849	39.74291
.07373	39.61318
.11849	39.75011
.14824	39.88585
.17788	40.08825
.19752	40.28985
.21716	40.49145

cooling of the lower plate during the change from the isothermal configuration to the temperature difference configuration:

$$T_{\text{upper}} = T_M^O + (T_U - T_M^O) (1 - e^{-t/\gamma_U}) , \quad (3.6)$$

$$T = T_M^O, \quad t = 0$$

$$T = T_U, \quad t = \infty$$

$$T_{\text{lower}} = T_M^O - (T_M^O - T_L) (1 - e^{-t/\gamma_L}) . \quad (3.7)$$

$$T = T_M^O, \quad t = 0$$

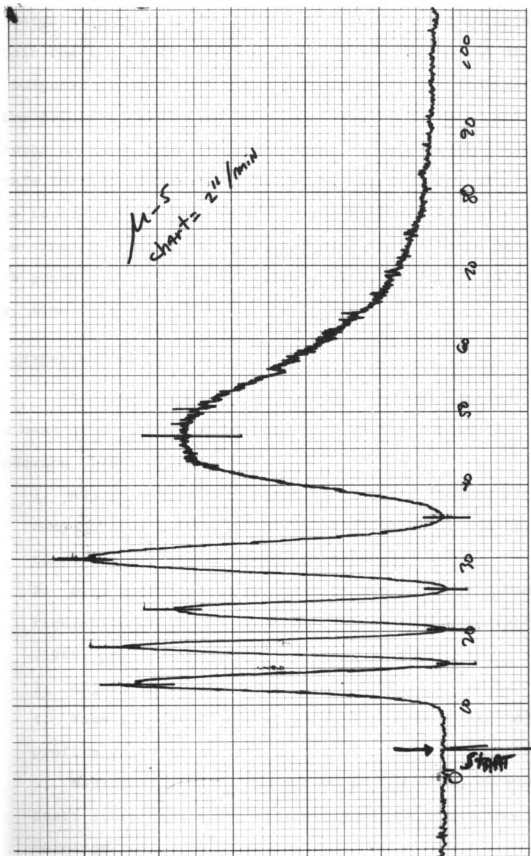
$$T = T_L, \quad t = \infty$$

In general, γ_U did not equal γ_L .

The raw data are obtained by reading the thermocouple voltage data in arbitrary units from the strip chart. A computer program, GAMMA, converts the strip chart coordinates to time and temperature and punches a data deck in a format appropriate for use in the generalized curvefitting program KINET (Nicely and Dye, 1971). KINET is used to obtain an ordinary least squares estimate of γ (all data point weights equal 1.0). Appendix C contains an outline of the procedure used to obtain parameter estimates.

8. Time dependence of the interference fringe shift. A typical strip chart recording (reduced in scale) of the phototransistor output voltage is shown in Figure 3.3. Note that the maxima are not equal. This prevents

Figure 3.3.--Strip chart record of phototransistor voltage output during fringe displacement of μ -5. The arrow indicates position of $t = 0$.



interpolation between half integer fringes. The horizontal scale reading is recorded for each of the maxima and minima. A computer program, TAU, is used to convert the arbitrary time points to real time by multiplying by the sec/unit factor obtained from the chart speed and subtracting the scale reading of zero time marked by the downward blip on the recording. Estimates of the experimental variance of the time and fringe positions are also made. These data are punched out in a KINET format. Typical fringe shift vs. time data are tabulated in Table 6.1.

E. Experimental Procedure

A description of how an experiment was carried out is best given in a step by step outline similar to that of Anderson (1968, pp. 128-137).

1. Adjust temperature baths to give the desired plate temperatures in the isothermal configuration and in the temperature difference configuration.
2. Fill and insulate the cell in the isothermal configuration using the technique described by Anderson (1968, pp. 132-3).
3. Adjust T_M^O if necessary.
4. Take slit photo for shear measurement. Take cell profile photo if desired.
5. Measure T_U^O and T_L^O and record on the strip charts. Start strip charts for thermocouples and phototransistor readings.

6. Adjust vernier telescope crosshairs to center of dark fringe. Adjust phototransistor to same position on an adjacent fringe.
7. Start application of temperature difference by switching water bath lever. Simultaneously, close shorting switch on phototransistor recorder momentarily to mark time zero.
8. When fringes have stopped moving, stop strip chart recorder. Measure T_U and T_L and record on strip charts. Measure fractional fringe with the vernier telescope. Take slit and cell profile photos if desired.
- 9-a. If data are to be recorded during decay of the temperature gradient, repeat steps 5, 6, 7 and 8, starting the experiment by switching back to the isothermal configuration.
- 9-b. If data during the decay of the temperature gradient are not desired, switch valve and wait for the fringes to stop moving. Repeat experiment from step 3.

Experiments were identified by the following code. Each filling of the cell was given a greek letter. Each repeated experiment on the same cell filling was assigned a consecutive number starting at one for each new filling. If the data were obtained during the establishment of a temperature gradient, the symbol E was added to the designation. If the data were obtained from the decay of the temperature gradient, the symbol D was added to the designation.

After many runs on a particular sample of liquid, the cell was disassembled, cleaned and stored. The raw data were reduced and were ready for analysis as described in Chapters IV, V and VI.

CHAPTER IV

TEMPERATURE DEPENDENCE OF REFRACTIVE INDEX

A. Introduction

This chapter contains working equations for the determination of the temperature dependence of the refractive index of liquids and experimental results for H_2O , CCl_4 , C_6H_{12} and C_6H_6 . The method uses the optical theory developed in Chapter II to calculate the temperature derivative behavior directly from the experimental fringe shift data observed when a temperature gradient of known magnitude is established in a liquid.

There has been little previous work on (dn/dT) for liquids. Bauer, Fajans and Lewin (1958) state that (dn/dT) is always negative for liquids. They note that the value of the derivative is unusually small, $-1.0 \times 10^{-4} \text{K}^{-1}$, for water and is relatively large, $-8 \times 10^{-4} \text{K}^{-1}$, for liquids with high absolute indices such as carbon disulfide. They also point out that the value, $-4.75 \times 10^{-4} \text{K}^{-1}$, commonly used to adjust data for organic liquids, is not adequate in many situations. Other references to (dn/dT) are found in light scattering work, for example, Coumou, et al. (1964). Previous experimental work is summarized in Table 4.1.

Table 4.1--Literature values for temperature dependence of refractive index at 25°C.

Liquid $n_{25^\circ}^{6328\text{\AA}}$ $-(dn/dT) \times 10^4$ $-(d^2n/dT^2) \times 10^6$ $(d^3n/dT^3) \times 10^{10}$				
H ₂ O	1.33162 ^d	1.04 ^a	3.0 ^a	100. ^a
		0.98 ^b		
		0.93 ^c	0.16 ^c	2200. ^c
		1.05 ^d	1.6 ^d	
		1.00 ^e	2.6 ^e	
CCl ₄	1.45586 ^d	5.75 ^f	0.0 ^f	0.0 ^f
		5.82 ^g	0.0 ^g	0.0 ^g
		6.08 ^d	0.0 ^d	330.0 ^d
		5.96 ^h		
		5.5 ⁱ		
		(6.48) ^j	(0.0004) ^j	(-194.0) ^j
		(5.95) ^k		
C ₆ H ₁₂	1.42205 ^f	5.47 ^f	0.0 ^f	0.0 ^f
		5.34 ^g	0.0 ^g	0.0 ^g
		5.44 ^h		
		(5.72) ^j	(0.509) ^j	(-0.66) ^j
		(5.44) ^k		
C ₆ H ₆	1.49511 ^d	6.35 ^f	0.0 ^f	0.0 ^f
		6.30 ^g	0.0 ^g	0.0 ^g
		(7.13) ^j	(0.017) ^j	(753.0) ^j
		(6.45) ^k		

All refractive index data are adjusted to 6328 \AA . () indicates values calculated from theory.

References.

^aTilton and Taylor, 1938.

^bWashburn (ICT), 1933.

^cBryngdahl, 1961.

References (continued).

^dWaxler, et al., 1964.

^eAndréasson, et al., 1971.

^fTimmermans, 1952; 1959 (see text).

^gCoumou, et al., 1964.

^hAnderson, 1968.

ⁱBauer, et al., 1958.

^jCalculated using Lorentz-Lorenz equation and density data of Wood, et al.; 1945, 1952.

^kCalculated from density data of Wood, et al., using modified L-L equation of Looyenga, 1965.

Table 4.1 lists previous literature values for the temperature dependence of the refractive index in terms of Taylor's series derivatives evaluated at $T_M = 25^\circ\text{C}$,

$$n(T) = n_{T=T_M} + \sum_{i=1}^{\infty} (1/i!) (d^i n/dT^i) (T - T_M)^i. \quad (4.1)$$

All of these values were obtained by curvefitting absolute refractive index data to various truncated forms of Eq. (4.1). Corrections to $6328 \overset{\circ}{\text{A}}$ were made when the data were obtained at other wavelengths. The many values from Timmermans (1950, 1959) were combined by Anderson (1968), who used a multiple regression least squares routine MULTREG.

This routine was also used in this work to obtain derivative values from the data of Waxler, et al. (1964). The values in brackets were calculated from the temperature dependence of the density by use of the Lorentz-Lorenz (L-L) equation,

$$(n^2 - 1)/(n^2 + 2) = (4\pi/3M)N_A\rho\alpha \quad (4.2)$$

where ρ is density, α is molecular electronic polarizability, M is the molecular weight and N_A is Avagadro's number, or from a modified form of the L-L equation (Looyenga, 1965) in which $(n^2 - 1)/(n^2 + 2)$ is replaced by $(n^{2/3} - 1)$.

B. Working Equations

The previous work tabulated in Table 4.1 suggests that for practical purposes Eq. (4.1) may be truncated after four terms,

$$\begin{aligned} n(T) = n_0 + n'(T - T_M) + (n''/2)(T - T_M)^2 \\ + (n'''/6)(T - T_M)^3 \end{aligned} \quad (4.3)$$

where

$$\begin{aligned} n_0 = n(T)_{T=T_M}, \quad n' = (dn/dT)_{T=T_M}, \\ n'' = (d^2n/dT^2)_{T=T_M} \text{ and } n''' = (d^3n/dT^3)_{T=T_M}. \end{aligned}$$

This is a specific refractive index property dependence equation as discussed in general in the optical theory, Eq. (2.35).

The temperature distribution in the liquid after the steady state is established has been determined from the transport equations of nonequilibrium thermodynamics by Horne and Anderson (1970)*:

$$T(z) = T_M + (\Delta T/h)z + (1/2)(\Delta T/h)^2 K_T [(h/2)^2 - z^2] \quad (4.4)$$

where

$$-h/2 \leq z \leq h/2, \quad \Delta T = T_H - T_C = T_U - T_L,$$

$$T_M = (T_H + T_C)/2, \quad K_T = (1/\kappa)(\partial \kappa / \partial T)_{T=T_M},$$

$$\kappa = \text{Thermal Conductivity}.$$

This is the specific property spatial distribution as discussed in the optical theory, Eq. (2.35).

Eq. (4.4) was obtained by a perturbation method (Horne and Anderson, 1970). In using Eq. (4.4), terms of order K_T^2 may not be retained without simultaneous retention of higher order terms such as $K_{TT} = (1/\kappa)(\partial^2 \kappa / \partial T^2)$. If we keep this restriction in mind, it is possible to obtain an expression for the refractive index as a function of the vertical coordinate; Eq. (4.4) is solved for $(T - T_M)$ and substituted into Eq. (4.3) to produce the following expression for $n(z)$:

* z is the vertical coordinate of the cell and y is the optical axis in this chapter. h is the cell height commonly labeled a .

$$\begin{aligned}
n(z) = & [n_0 + n'(\Delta T)^2 K_T/8] + [n'\Delta T/h] \\
& + [n''(\Delta T)^3 K_T/8h]z + [n''(\Delta T)^2/h^2 - n'(\Delta T)^2 K_T/2h^2] \\
& + [n'''(\Delta T)^4 K_T/16h^2]z^2 + [n'''(\Delta T)^3/6h^3] \\
& - [n''(\Delta T)^3 K_T/2h^3]z^3 + [n'''(\Delta T)^4 K_T/4h^4]z^4. \quad (4.5)
\end{aligned}$$

Terms in K_T are likely to be very small because $|K_T| \approx 10^{-3}$ (see Table 4.2).

Table 4.2--Literature values for $K_T \times 10^3$, temperature dependence parameter for thermal conductivity at 25°C.

H_2O	CCl_4	C_6H_{12}	C_6H_6
2.68 ^a	-2.10 ^b	-0.71 ^e	-1.75 ^e
	-1.84 ^c		-1.06 ^f
	-1.26 ^d		

References.

^aMcLaughlin, 1964.

^bTree and Leidenfrost, 1969.

^cTouloukian, et al., 1970.

^dChalloner, et al., 1958.

^eBriggs, 1957.

^fWeast (Handbook of Chemistry and Physics), 1959.

We now refer to the optical theory to predict the interference fringe behavior which results from the establishment of the refractive index distribution Eq. (4.5) in

the liquid. In order to obtain working equations of manageable size for this discussion, Eq. (2.22) in the form

$$X' = (X/\delta) = (a/\lambda)\Delta n(z) + B, \quad (4.6)$$

$$\Delta n(z) = n(z + \beta) - n(z - \beta), \quad a = \text{cell length},$$

will be used as the optical equation. However, the actual numerical analysis and the curvefitting performed on experimental data utilized Eq. (2.23) which contains the path length corrections, $\Delta S'(z)$ and $\Delta S''(z)$, due to the presence of a refractive index gradient. These terms contribute less than 1% to the total optical path length for our experimental arrangement.

If the total fringe shift from a reference line is measured during the establishment of the refractive index gradient, i.e., $X'(T=\infty) - X'(T=0)$, the constant B vanishes. Eq. (4.6) is then effectively,

$$X' = (a/\lambda)[n(z + \beta) - n(z - \beta)]. \quad (4.7)$$

Upon substitution of Eq. (4.5), Eq. (4.7) becomes:

$$\begin{aligned} X' = (a/\lambda) \{ & [2\beta n' \Delta T/h + \beta^3 n''''(\Delta T)^3/3h^3 + \beta n''(\Delta T)^3 K_T/4h \\ & - \beta^3 n''(\Delta T)^3 K_T/h^3] + [4\beta n''(\Delta T)^2/h^2 - 2\beta n'(\Delta T)^2 K_T/h^2 \\ & + \beta n''''(\Delta T)^4 K_T/4h^2 + 2\beta^3 n''''(\Delta T)^4 K_T/h^4] z \\ & + [\beta n''''(\Delta T)^3/h^3 - 3\beta n''(\Delta T)^3 K_T/h^3] z^2 \\ & + [2\beta n''''(\Delta T)^4 K_T/h^4] z^3 \} . \end{aligned} \quad (4.8)$$

The expression for the total horizontal fringe shift measured at $z=0$ is,

$$X' = (a/\lambda) 2\beta [n' \Delta T/h + \beta^2 n'''' (\Delta T)^3 / 6h^3 + n'' (\Delta T)^3 K_T / 8h - \beta^2 n'' (\Delta T)^3 K_T / 2h^3] \quad (4.9)$$

and

$$X' [\lambda/a(2\beta)] = (n' \Delta T/h) [1 + \beta^2 n'''' (\Delta T)^2 / 6n' h^2 + n'' (\Delta T)^2 K_T / 8n' - \beta^2 n'' (\Delta T)^2 K_T / 2n' h^2] . \quad (4.10)$$

Tables 4.1 and 4.2 list typical values for the parameters of Eq. (4.10). If $|n''| \leq 10^{-4}$ and $|n''''| \leq 2.4 \times 10^{-6}$, only the leading term of the R.H.S. of Eq. (4.10) is retained to 0.1% accuracy. Eq. (4.10) can then be solved for the first derivative of the refractive index with respect to temperature:

$$(dn/dT)_{T=T_M} = X' \lambda h / (\Delta T) a(2\beta) . \quad (4.11)$$

This is the final working equation for the determination of (dn/dT) . All of the quantities on the R.H.S. of Eq. (4.11) can be obtained by the experimental technique described in Chapter III.

Tilton and Taylor (1938) found that the refractive index temperature dependence for water exhibited second derivative behavior on the order of 3% of the first derivative (see Table 4.1). This would cause a parabolic refractive index distribution in the liquid that would be

manifested by straight fringes that are tilted from the vertical. The slope, m , of these tilted fringes at the center of the final image can be measured from the steady state photographs. Eq. (4.8) can be differentiated with respect to z to obtain a formula for (d^2n/dT^2) :

$$(\partial X'/\partial z)_{z=0} = m = (4a\beta/\lambda) [(\Delta T)^2/2h^2] (n'' - n'K_T) . \quad (4.12)$$

Eq. (4.12) can be rearranged to obtain

$$(d^2n/dT^2)_{T=T_M} = m\lambda h^2/(2\beta)a(\Delta T)^2 + n'K_T . \quad (4.13)$$

Eqs. (4.11) and (4.13) are calibration-free expressions for determining the temperature derivative behavior of the refractive index of liquids with a wavefront shearing interferometer.

C. A priori Error Estimates

We now estimate the expected uncertainty in (dn/dT) and (d^2n/dT^2) based on the precision with which the experimental quantities in Eqs. (4.11) and (4.13) can be determined.

Let a derived quantity U be a continuous differentiable function of measurable quantities X_1, X_2, X_3, \dots defined by,

$$U = U(X_1, X_2, X_3, \dots) . \quad (4.14)$$

The estimated variance (the square of the standard deviation) of U is obtained by the familiar propagation of error formula (Parratt, 1961; Wentworth, 1965):

$$\begin{aligned}\sigma_U^2 = & (\partial U / \partial X_1)^2 \sigma_{X_1}^2 + (\partial U / \partial X_2)^2 \sigma_{X_2}^2 \\ & + (\partial U / \partial X_3)^2 \sigma_{X_3}^2 + \dots\end{aligned}\quad (4.15)$$

The a priori estimated variance in (dn/dT) is given by the following expression derived from Eqs. (4.11) and (4.15):

$$\begin{aligned}[\sigma_{n'}^2 / (n')^2] = & (\sigma_{X'} / X')^2 + (\sigma_\lambda / \lambda)^2 + (\sigma_h / h)^2 \\ & + (\sigma_a / a)^2 + (\sigma_{2\beta} / 2\beta)^2.\end{aligned}\quad (4.16)$$

Typical values and experimental uncertainties for the quantities in Eq. (4.16) are listed in Table 4.3. These are the experimental standard deviations (rms error) for repeated observations of these quantities. Note that the relative uncertainty in 2β , the shearing distance in cell coordinates, is larger than any of the other relative uncertainties. When these numerical estimates are substituted into Eq. (4.16), we obtain an estimate for $\sigma_{n'}$,

$$\sigma_{n'} = 1.14 \times 10^{-2} |n'|. \quad (4.17)$$

The determination of (dn/dT) with an experimental uncertainty of about 1% is thus to be anticipated from this analysis. Note again that this uncertainty is due essentially entirely to the uncertainty in determining 2β .

Table 4.3--Typical values and experimental uncertainties of parameters in Eq. (4.11).

Quantity	Value (X_i)	Uncertainty (σ_{X_i})	$ (\sigma_{X_i}^2/X_i^2) $
X'	5.0 (fringes)	10^{-2} (fringe)	4×10^{-6}
λ	6.328×10^{-5} cm	10^{-9} cm	3×10^{-9}
h	0.81 cm	0.001 cm	1.5×10^{-6}
ΔT	5.0°K	0.003°K	1.6×10^{-7}
2β	0.09 cm	0.001 cm	1.2×10^{-4}
a	6.82 cm	0.005 cm	6×10^{-7}

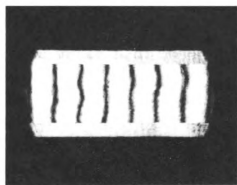
The derived value of (d^2n/dT^2) is directly proportional to m , the slope of the steady state fringes. The error in determining the slope would be expected to be larger than the uncertainty in the other quantities in Eq. (4.13). The following equation gives the uncertainty in the second derivative assuming that the error in the slope is the only important source of uncertainty:

$$\sigma_n^{2''}/(n'')^2 = (\sigma_m/m)^2. \quad (4.18)$$

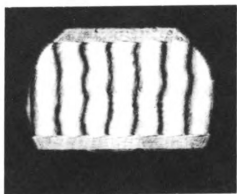
The slope was determined experimentally from a series of $(\Delta X'/\Delta z)$ measurements on the "best line" drawn by hand through a fringe. This measurement was repeated for several fringes in a family of steady state fringes (see Figure 4.1 (c)). Typical values were $m = 1.0$ fringe cm^{-1} and $\sigma_m = 0.07$. Using these data,

$$\sigma_{n''} = 7 \times 10^{-2} |n''| \quad (4.19)$$

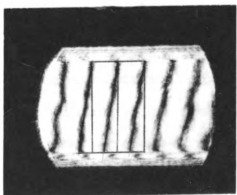
Figure 4.1--Interference fringe photographs: (a) isothermal slit photo, experiment v-13; (b) isothermal cell profile for water, experiment v-12; (c) steady state cell profile for water, $\Delta T = 5.597\text{K}$, experiment v-12.



a



b



c

Thus, we anticipate a 7% uncertainty in the determination of the second derivative (d^2n/dT^2).

D. Experimental Results for Water

Experiments were conducted upon water to determine $(dn/dT)_{25^\circ}$ at 6328 \AA . The qualitative behavior of the interference fringe pattern during the establishment of the temperature gradient in the water filled cell was as follows: The fringes were straight and vertical as shown in the photo Figure 4.1 (b) taken in the isothermal configuration. At the onset of the temperature difference, the fringes became extremely parabolic and the family of parabolas was shifted horizontally across the final image plane. Finally, the parabolas decayed away to the straight tilted fringes of Figure 4.1 (c) when the steady state temperature distribution was established.

This is the behavior we would predict from the literature values of K_T and (d^2n/dT^2) . The parabolic appearance of the fringes observed during the establishment of the temperature gradient is caused by the transient nonlinear temperature distribution in the liquid. When the temperature distribution reaches its essentially linear steady state, the parabolas become straight fringes which are slightly tilted due to the influence of the second order terms, Eq. (4.13).

Table 4.4 lists the experimental results for 30 determinations of $(dn/dT)_{25^\circ}$ for water. As described in

Table 4.4--Summary of experimental results for $(dn/dT)_{25^\circ}$
of water at $\lambda = 6328 \text{ \AA}$.

h = 0.8103cm			a = 6.828cm		2β = 0.0905cm	
ID	T _H	T _C	T _M	ΔT	X'	-(dn/dT)×10 ⁴
v-1E	27.903	22.183	25.043	5.720	6.873	0.997
v-2E	27.855	22.210	25.033	5.645	6.749	0.992
v-3E	27.857	22.240	25.049	5.617	6.747	0.997
v-4E	27.837	22.190	25.013	5.647	6.672	0.981
v-5E	27.793	22.260	25.027	5.533	6.579	0.987
v-6E	27.820	22.253	25.037	5.567	6.618	0.987
v-7E	27.813	22.283	25.048	5.530	6.596	0.990
v-8E	27.883	22.260	25.072	5.623	6.656	0.983
v-9E	27.863	22.350	25.107	5.513	6.579	0.991
v-10E	27.865	22.303	25.084	5.562	6.669	0.995
v-11E	27.843	22.350	25.097	5.493	6.537	0.988
v-12E	27.830	22.130	24.980	5.700	6.690	0.974
v-13E	27.805	22.307	25.056	5.498	6.602	0.997
v-14E	27.833	22.303	25.068	5.530	6.622	0.994
v-15E	27.843	22.280	25.062	5.563	6.671	0.995
(dn/dT) _E = -0.990 × 10 ⁻⁴				$\hat{\sigma} = 6.4 \times 10^{-7} = 0.69\%$		
ID	T _H	T _C	T _M	ΔT	X'	-(dn/dT)×10 ⁴
v-1D	27.890	22.183	25.036	5.707	6.838	0.994
v-2D	27.860	22.210	25.035	5.650	6.720	0.987
v-3D	27.867	22.250	25.059	5.617	6.632	0.980
v-4D	27.805	22.215	25.010	5.590	6.625	0.983
v-5D	27.788	22.266	25.027	5.521	6.531	0.982
v-6D	27.823	22.262	25.042	5.565	6.597	0.984
v-7D	27.796	22.273	25.034	5.523	6.518	0.979
v-8D	27.865	22.293	25.079	5.573	6.557	0.977
v-9D	27.855	22.330	25.093	5.525	6.573	0.987
v-10D	27.865	22.317	25.091	5.547	6.669	0.998
v-11D	27.840	22.350	25.095	5.490	6.549	0.990
v-12D	27.827	22.270	25.049	5.557	6.704	1.00
v-13D	27.796	22.323	25.059	5.473	6.601	1.00
v-14D	27.835	22.295	25.065	5.540	6.646	0.996
v-15D	27.843	22.283	25.063	5.560	6.662	0.994
(dn/dT) _D = -0.989 × 10 ⁻⁴				$\hat{\sigma} = 8.1 \times 10^{-7} = 0.82\%$		

Chapter III, each experiment had data collected during two different periods: (1) the fringe shift measured during the establishment of temperature gradient, labeled E and (2) the fringe shift measured during the decay of that same temperature gradient, labeled D. The experimental estimate of the standard deviation (scatter) is calculated from

$$\hat{\sigma}_{n'} = \{ [1/(j-1)] \sum_{i=1}^j (\hat{n}' - n_i')^2 \}^{1/2}, \quad (4.20)$$

$$\hat{n}' = (1/j) \sum_{i=1}^j n_i'.$$

There appears to be no statistical difference between the E and D experiments. A t-test on the averages from the two sets of experiments indicated that the null hypotheses, $\hat{n}'_E = \hat{n}'_D$, could not be rejected at the 99% level. Moreover, it was possible to verify the randomness of errors by use of the run test (Wilson, 1952) on the sign of the quantity $(0.989 - n_i' \times 10^4)$ for the sequence of experimental trials. This test indicated that the measurements were independent with random errors.

The final result for 30 determinations on water is

$$\left(\frac{dn}{dT} \right)_{25^\circ}^{6328\text{\AA}} = - 0.989 \times 10^{-4} \text{K}^{-1}, \quad (4.21)$$

$$\hat{\sigma}_{n'} = 7.35 \times 10^{-7}.$$

The experimental standard deviation is about 0.75%, which is comparable to but lower than the a priori estimate of 1% obtained in section C.

The steady state fringe pattern was photographed during four experiments, and the slope was obtained as discussed at the end of section C. The data and the values of the second derivatives calculated from Eq. (4.13) are shown in Table 4.5. The average of these results is

$$(d^2n/dT^2)_{25^\circ}^{6328\text{\AA}} = -2.34 \times 10^{-6} \text{K}^{-2}, \quad (4.22)$$

$$\hat{\sigma}_{n''} = 1.1 \times 10^{-7} = 4.6\% |n''|.$$

The experimental standard deviation of 4.6% is lower than the a priori 7% estimate.

Table 4.5--Summary of steady state fringe slope data for water.

ID	T_M	ΔT	$-m$	$-(d^2n/dT^2) \times 10^6$
v-12	24.980	5.597	0.906	2.21
v-13	25.056	5.543	0.972	2.39
v-14	25.068	5.563	0.936	2.30
v-15	25.062	5.616	1.03	2.46

The value obtained for the first derivative, $-0.989 \times 10^{-4} \text{K}^{-1}$, may be compared to the previous values listed in Table 4.1. Our value is about 5% lower than Tilton and Taylor (1938) and Waxler, et al. (1964) and about 6% higher than the number obtained by Bryngdahl (1961). The closest agreement is with the ICT value of $-0.98 \times 10^{-4} \text{K}^{-1}$ and with Andréasson, et al. (1971), $-1.00 \times 10^{-4} \text{K}^{-1}$. Tilton and Taylor's work on the absolute index of water has long

been considered definitive. However, their (dn/dT) values are obtained from an empirical equation used to interpolate the absolute index results. The uncertainties in their least squares parameters when applied to calculations of the derivative values are unknown and may be the source of the discrepancy. In any case our value is preferable because it is measured directly with an interferometric technique (i.e., a differencing technique) over a small temperature range. Bryngdahl's value was obtained in conjunction with a hot wire thermal conductivity experiment. His table of experimental results suggests that the scatter in his determination of (dn/dT) may be as great as 3%. Moreover, (dn/dT) is obtained as a derived quantity. The ICT value was obtained from a compilation of the data available in 1933. The work of Tilton and Taylor had not been completed at this time and is probably more accurate than the data used in the ICT determination. Andréasson, et al. (1971) used an interferometric technique which they claimed is comparable in precision to the method of Tilton and Taylor. The work of Andréasson, et al. is the most recent precision study on the refractive index of water.

The value determined for (d^2n/dT^2) is the same order of magnitude but slightly smaller than that obtained from Tilton and Taylor's data. This may again be due to the artifacts of their curvefitting process. Our value agrees well with Andréasson, et al. However, the effect

of an anomalous temperature distribution (see Chapter V) would cause the fringes to be tilted with a slope different from that predicted by Eq. (4.13). Our results may be in error if this effect is present for temperature distributions in water.

E. Results for CCl_4 ,
 C_6H_{12} , and C_6H_6

Experiments were conducted on three sensibly spherical nonelectrolytes; carbon tetrachloride, cyclohexane and benzene. Anderson (1968, p. 196) first observed anomalous parabolic steady state fringe patterns for the first two of these liquids:

The theory of the interferometer predicts that a uniform nonzero refractive index gradient should produce interference fringes identical to those for a zero gradient but shifted horizontally by some fixed distance. What we in fact observed for both CCl_4 and C_6H_{12} , when a temperature difference was imposed vertically, and a steady state temperature distribution developed, were curved interference fringes of a generally parabolic shape.

This anomalous parabolic behavior, observed also in the present work, will be discussed in detail in Chapter V.

Even though the fringes are parabolic in the steady state it is still possible to observe the gross horizontal shift of the family of fringes. Determinations of (dn/dT) could be made by measuring the midplane ($z = 0$) fringe shift and calculating the derivative from Eq. (4.11). Changes in $(\Delta T/h)$ were restricted to values of 1 K cm^{-1} or

less to prevent the light beam from being too far bent away from the optical axis.

The most extensive study was made on CCl_4 , with the experimental results shown in Table 4.6. CCl_4 was studied under three different sets of experimental conditions:

(i) observation of the fringe shift in the 8 mm cell on changing ΔT from 2.7K to 3.5K, $2\beta = 0.0844\text{cm}$; (ii) observation of the fringe shift in the 8 mm cell on changing ΔT from 0.0K to 0.95K, $2\beta = 0.0685\text{cm}$ and (iii) observation of the fringe shift in the 30 mm cell on changing ΔT from 0.0K to 5.6K, $2\beta = 0.0857\text{cm}$. The missing numbers in Table 4.6 correspond to determinations that were not completed or were rejected because of experimental difficulties. Usually these were related to maintaining and measuring the temperature difference, ΔT . Also, some of the numbers were rejected because the upper and lower plates were not isothermal at the start of an experiment. $(dn/dT)_{25^\circ}$ differed about 1% for the three sets of experiments. The grand average for 36 determinations and the calculated standard deviation are,

CCl_4

$$(dn/dT)_{25^\circ}^{6328\text{\AA}} = - 5.70 \times 10^{-4} \text{K}^{-1}, \quad (4.23)$$

$$\hat{\sigma}_{n'} = 8.2 \times 10^{-6} = 1.4\% |n'|.$$

Table 4.6--Summary of experimental results for $(dn/dT)_{25^\circ}$ of carbon tetrachloride at $\lambda = 6328 \text{ \AA}$.

CCl ₄ (i)						
		a = 6.828cm		h = 0.81026cm		2 β = 0.0844cm
ID	$\Delta T(1)$	$\Delta T(2)$	(ΔT)	T_M	x'	$-(dn/dT) \times 10^4$
v-2E	2.730	3.484	0.754	24.90	5.046	5.95
v-3E	2.730	3.491	0.761	24.93	4.823	5.64
v-4D	3.490	2.716	0.774	25.09	5.000	5.75
v-5E	2.716	3.501	0.786	24.90	5.000	5.66
v-6D	2.838	3.501	0.663	25.04	4.238	5.69
v-2D	3.431	2.765	0.666	24.98	4.282	5.72
v-3E	2.765	3.398	0.633	24.90	4.101	5.77
v-5E	2.738	3.485	0.747	24.84	4.959	5.90
v-6D	3.485	2.739	0.746	24.94	4.790	5.71
v-7E	2.739	3.416	0.677	24.93	4.255	5.58
v-10D	3.470	2.757	0.713	24.99	4.536	5.66

$$(dn/dT)_i = -5.73 \times 10^{-4} \quad \hat{\sigma} = 1.1 \times 10^{-5} = 1.9\%$$

CCl ₄ (ii)						
		a = 6.828cm		h = 0.81026cm		2 β = 0.06854cm
ID	T_H	T_C	T_M	ΔT	x'	$-(dn/dT) \times 10^4$
v-2E	25.513	24.568	25.040	0.945	4.814	5.58
v-4E	25.508	24.573	25.040	0.935	4.948	5.80
v-5E	25.495	24.542	25.019	0.953	4.879	5.61
v-6E	25.393	24.518	24.955	0.875	4.714	5.90
v-7E	25.498	24.505	25.001	0.993	5.137	5.67
v-8E	25.533	24.573	25.053	0.960	5.023	5.73
v-9E	25.493	24.598	25.045	0.895	4.708	5.76
v-10E	25.520	24.520	25.028	1.000	5.165	5.66
v-11E	25.490	24.541	25.010	0.949	4.905	5.67
v-12E	25.503	24.560	25.031	0.943	4.895	5.69
v-13E	25.478	24.583	25.030	0.895	4.639	5.67
v-14E	25.465	24.585	25.025	0.880	4.601	5.73
v-15E	25.495	24.582	25.038	0.913	4.721	5.67

$$(dn/dT)_{ii} = -5.70 \times 10^{-4} \quad \hat{\sigma} = 8.3 \times 10^{-6} = 1.5\%$$

Table 4.6--(continued).

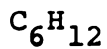
CCl ₄ (iii) a = 6.805cm h = 3.0124cm 2β = 0.08565cm						
ID	T _H	T _C	T _M	ΔT	x'	-(dn/dT) × 10 ⁴
ξ-3E	27.787	22.210	24.999	5.577	9.682	5.67
ξ-5E	27.750	22.240	24.995	5.510	9.509	5.64
ξ-6E	27.796	22.193	24.995	5.603	9.738	5.68
ξ-7E	27.863	22.258	25.061	5.605	9.727	5.68
ξ-8E	27.835	22.270	25.053	5.565	9.613	5.65
ξ-9E	27.950	22.285	25.118	5.660	9.786	5.65
ξ-10E	27.848	22.363	25.106	5.485	9.515	5.67
ξ-11E	27.857	22.343	25.100	5.514	9.642	5.72
ξ-12E	27.855	22.257	25.056	5.598	9.703	5.67
ξ-13E	27.813	22.270	25.042	5.543	9.539	5.63
ξ-14E	27.817	22.255	25.036	5.562	9.758	5.74
ξ-15E	27.884	22.268	25.076	5.616	9.681	5.64
(dn/dT) _{iii} = -5.67 × 10 ⁻⁴ $\hat{\sigma}$ = 3.3 × 10 ⁻⁶ = 0.58%						

Comparison of this result with the values listed in Table 4.1 shows that it agrees well with the literature values, $-5.82 \times 10^{-4} \text{K}^{-1}$ (Coumou, et al., 1964) and $-5.75 \times 10^{-4} \text{K}^{-1}$ (Timmermans; 1950, 1959). The value obtained by Anderson (1968), $-5.96 \times 10^{-4} \text{K}^{-1}$, is the result of a small number of experiments and depends on a calibration experiment. Waxler's value (1964) was obtained by curve-fitting data from three widely spaced temperatures, 25°C, 35°C and 55°C.

The results of 10 determinations of $(dn/dT)_{25^\circ}$ for cyclohexane are shown in Table 4.7. The average value and calculated standard deviation are,

Table 4.7--Summary of experimental results for $(dn/dT)_{25^\circ}$ of cyclohexane at $\lambda = 6328 \text{ \AA}$.

C_6H_{12} $a = 6.828\text{cm}$ $h = 0.81026\text{cm}$ $2\beta = 0.0869_8\text{cm}$						
ID	T_H	T_C	T_M	ΔT	x'	$-(dn/dT) \times 10^4$
κ -1E	25.415	24.623	25.02	0.792	5.000	5.45
κ -1D	--	--	24.96	0.792	5.009	5.46
κ -2E	25.405	24.628	25.01	0.777	5.000	5.56
κ -2D	--	--	24.98	0.777	4.919	5.47
κ -3E	25.430	24.613	25.02	0.817	5.000	5.28
κ -3D	--	--	25.01	0.817	5.000	5.28
κ -4E	25.430	24.610	25.02	0.820	5.025	5.29
κ -4D	--	--	24.99	0.820	4.975	5.24
κ -5E	25.417	24.622	25.02	0.795	4.965	5.39
κ -5D	--	--	25.01	0.795	4.965	5.39



$$(dn/dT)_{25^\circ}^{6328\text{\AA}} = -5.38 \times 10^{-4} K^{-1}, \quad (4.24)$$

$$\hat{\sigma}_{n'} = 1.0 \times 10^{-5} = 1.9\% |n'|.$$

This result agrees well with the previous values, $-5.34 \times 10^{-4} K^{-1}$ (Coumou, et al., 1964), $-5.47 \times 10^{-4} K^{-1}$ (Timmermans; 1950, 1959), and $-5.44 \times 10^{-4} K^{-1}$ (Anderson, 1968).

The results of eight determinations of $(dn/dT)_{25^\circ}$ for benzene are shown in Table 4.8. The average value and calculated standard deviation are,



$$(dn/dT)_{25^\circ}^{6328\text{\AA}} = -6.21 \times 10^{-4} K^{-1}, \quad (4.25)$$

$$\hat{\sigma}_{n'} = 4.9 \times 10^{-6} = 0.79\% |n'|.$$

Table 4.8--Summary of experimental results for $(dn/dT)_{25^\circ}$ of benzene at $\lambda = 6328 \text{ \AA}$.

C ₆ H ₆ a = 6.828cm h = 0.81026cm 2 β = 0.0869 ₈ cm						
ID	T _H	T _C	T _M	ΔT	x'	$-(dn/dT) \times 10^4$
$\lambda-1$	25.437	24.612	25.02	0.825	5.900	6.17
$\lambda-1$	--	--	25.04	0.825	5.849	6.12
$\lambda-2$	25.432	24.615	25.02	0.817	5.933	6.27
$\lambda-2$	--	--	25.05	0.817	5.928	6.26
$\lambda-3$	25.437	24.6112	25.03	0.825	5.964	6.24
$\lambda-3$	--	--	25.03	0.825	5.937	6.21
$\lambda-4$	25.426	24.607	25.02	0.819	5.882	6.20
$\lambda-4$	--	--	25.03	0.819	5.883	6.20

This value is only slightly lower in magnitude than the previous results, $-6.30 \times 10^{-4} \text{ K}^{-1}$ (Coumou, et al., 1965) and $-6.35 \times 10^{-4} \text{ K}^{-1}$ (Timmermans; 1950, 1959).

F. Discussion

These results for H₂O, CCl₄, C₆H₁₂ and C₆H₆ indicate that this technique is an accurate and precise method of determining (dn/dT) . It is superior to previous methods, where results were obtained by curvefitting of absolute index data over a large range of temperatures, typically 10°C to 50°C. Our measurements were made over a much smaller temperature range (24°C to 26°C) and, most important, (dn/dT) was determined directly.

The results indicate that values of (dn/dT) calculated from the temperature dependence of density using the Lorentz-Lorenz equation, Eq. (4.2), are too high by

the following percentage amounts: CCl_4 , 14%; C_6H_{12} , 6%; C_6H_6 , 15%. This suggests that further work is necessary, perhaps in the direction suggested by Looyenga (1965), whose equation yields results in better agreement with our values.

G. A Molecular
Calculation Using (dn/dT)

The temperature dependence of the refractive index may be interpreted molecularly for nonpolar sensibly spherical molecules (this restriction excludes water from this discussion) by electromagnetic equations of state (Amey, 1968) similar to the Lorentz-Lorenz equation, Eq. (4.2).

Böttcher (1952) has derived a two parameter version of this equation by starting from a more accurate approximation of the local field acting on a molecule in the liquid. His expression is

$$n^2 / [(n^2 - 1) (2n^2 + 1) \bar{V}] = (M/2\pi N_A) [\alpha^{-3} - r^{-3} (2n^2 - 2) / (2n^2 + 1)] \quad (4.26)$$

where r is the effective molecular radius. The model used by Böttcher assumes that the fluid is composed of sensibly spherical molecules whose polarizability and radius are independent of temperature and pressure.

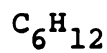
Langer and Montalvo (1968) and Waxler and Weir (1963) have used Eq. (4.26) to calculate r and α from

their experimental measurements of the pressure dependence of the refractive index. They obtain the pressure dependence of the specific volume from one of two sources in the literature; (i) direct measurements of the density as a function of pressure or (ii) experimentally determined constants for the Tait equation for liquids. They plot $n^2/[(n^2 - 1)(2n^2 + 1)\bar{V}]$ vs. $(2n^2 - 2)/(2n^2 + 1)$ and calculate α and r from, respectively, the slope and the intercept of the straight line ordinarily obtained.

We may use our experimental results for (dn/dT) and the literature values for the temperature dependence of specific volume in a similar analysis. The specific volume of CCl_4 and C_6H_{12} are given by Wood and Gray (1952) and the specific volume of C_6H_6 is given by Wood and Austin (1945) (T in these equations is in $^\circ\text{C}$):



$$\begin{aligned}\bar{V}(\text{in cm}^3\text{gm}^{-1}) = & 0.61233 + 7.294 \times 10^{-4}T \\ & + 7.22 \times 10^{-7}T^2 + 5.52 \times 10^{-9}T^3 . \quad (4.27)\end{aligned}$$



$$\begin{aligned}\bar{V}(\text{in cm}^3\text{gm}^{-1}) = & 1.2548 + 1.4362 \times 10^{-3}T \\ & + 2.529 \times 10^{-6}T^2 + 5.37 \times 10^{-9}T^3 . \quad (4.28)\end{aligned}$$

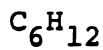


$$\begin{aligned}\bar{V}(\text{in cm}^3\text{gm}^{-1}) = & 1.1106 + 1.3105 \times 10^{-3}T \\ & + 1.477 \times 10^{-6}T^2 + 7.65 \times 10^{-9}T^3 . \quad (4.29)\end{aligned}$$

The refractive indices of CCl_4 , C_6H_{12} and C_6H_6 as a function of temperature are



$$n(T)^{6328\overset{\text{O}}{\text{\AA}}} = 1.45586 - 5.70 \times 10^{-4}(T - 25) \quad (4.30)$$



$$n(T)^{6328\overset{\text{O}}{\text{\AA}}} = 1.42205 - 5.38 \times 10^{-4}(T - 25) \quad (4.31)$$



$$n(T)^{6328\overset{\text{O}}{\text{\AA}}} = 1.49511 - 6.21 \times 10^{-4}(T - 25). \quad (4.32)$$

The values of $n_{25^\circ}^{6328\overset{\text{O}}{\text{\AA}}}$ are interpolated from the absolute index data of Waxler, et al. (1964) and Timmermans (1950, 1959).

The refractive index and the specific volume are obtained from Eqs. (4.27 - 4.32) for a range of temperatures and the quantities $(2n^2 - 2)/(2n^2 + 1)$ and $n^2/[(n^2 - 1)(2n^2 + 1)\bar{V}]$ are calculated. These numbers are fit to Eq. (4.26) by ordinary linear least squares to obtain the slope and intercept from which r and α are calculated. Table 4.9 shows values for a Böttcher plot from 20°C to 30°C calculated from Eqs. (4.27) and (4.30) for CCl_4 . Figure 4.2 is a graph of these numbers and is typical of the plots obtained for the liquids studied.

Table 4.9--Data for Böttcher plot of CCl_4 refractive index and specific volume temperature dependence.

$T^\circ (\text{C})$	$n(6328\text{\AA})$	\bar{V}	$(2n^2-2)/(2n^2+1)$	$n^2/(n^2-1)$	$(2n^2+1)\bar{V}$
20.00	1.45871	.62725	.4291		.57229
21.00	1.45814	.62801	.4288		.57235
22.00	1.45757	.62878	.4284		.57242
23.00	1.45700	.62955	.4281		.57248
24.00	1.45643	.63032	.4277		.57254
25.00	1.45586	.63110	.4273		.57259
26.00	1.45529	.63187	.4270		.57265
27.00	1.45472	.63265	.4266		.57271
28.00	1.45415	.63344	.4262		.57277
29.00	1.45358	.63422	.4259		.57283
30.00	1.45301	.63501	.4255		.57289

It was found empirically that the value of $n_{25^\circ}^{6328\text{\AA}}$ used in the calculation does not greatly affect the values of r or α obtained. However, r and α are very sensitive to the value of (dn/dT) . Therefore, small errors introduced by interpolation to 6328\AA would not affect the final estimates of r and α .

Table 4.10 summarizes the polarizabilities and effective molecular radii calculated from our data. Also listed are the previous values obtained from the analysis of pressure dependence data and the values calculated by Waxler and Weir (1963) directly from molar volume data.

Our values for the effective molecular radius are about 16% higher than those obtained by Waxler and Weir while the polarizabilities agree within 6%. However, our values for r agree well with the radii calculated by

Figure 4.2--Böttcher plot for CCl_4 ; $n^2/[(n^2-1)(2n^2+1)\bar{V}]$
vs. $(2n^2-2)/(2n^2+1)$.

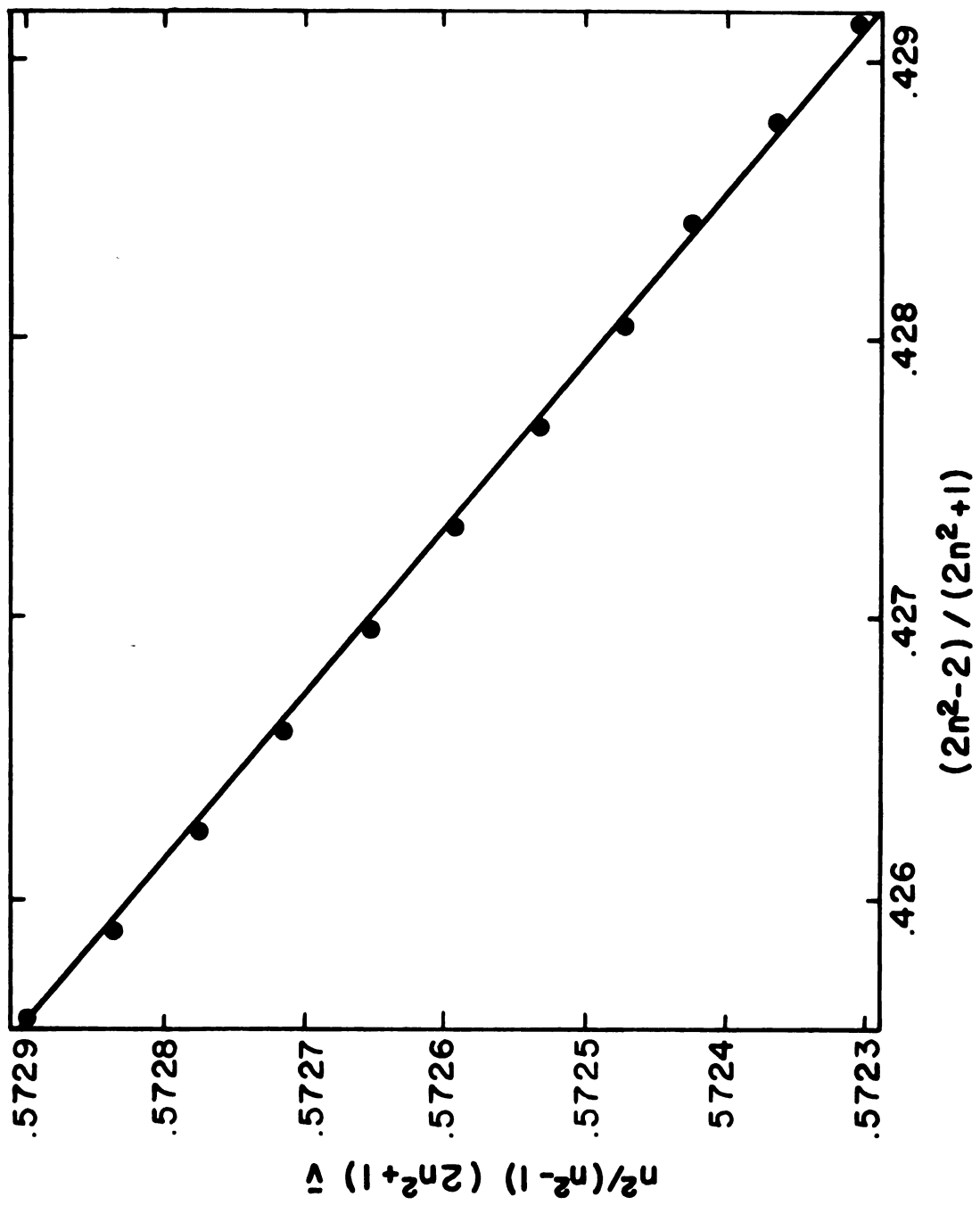


Table 4.10--Effective molecular radii and polarizability
for CCl_4 , C_6H_6 and C_6H_{12} .

Source	Liquid	$r(\text{\AA})$	$\alpha(\text{\AA})^3$
a	CCl_4	3.46	10.55
	C_6H_6	3.25	10.30
	C_6H_{12}	3.24	10.65
b	CCl_4	2.93	9.88
	C_6H_6	2.93	9.86
c	CCl_4	3.33	
	C_6H_6	3.40	

^aThis work.

^bCalculated from pressure dependence of n , Waxler and Weir, 1963.

^cCalculated from molar volume, op. cit.

Waxler and Weir directly from the molar volume data. It appears that the pressure dependence and temperature dependence experiments are not equivalent.

The precise physical meaning of the "effective" radius is not clear. It may correspond to a correlation distance between molecules or to the "cavity" occupied by a simple molecule in the liquid. Since the refractive index is manifested molecularly by the displacement of the molecule's electrons, the effective radius should be related to the scattering cross-section of the individual

molecules. Clearly, a more complete theoretical treatment is necessary here; perhaps these results can suggest directions for future work.

H. Suggestions for Further Work

Although accurate and reproducible results were obtained with the apparatus described in the preceding pages, the basic experimental techniques can be improved in four ways.

(1) Improved Temperature Control. Anderson (1968) suggests methods of maintaining and changing the temperature of the metal plates that may be more efficient than circulating water baths. The possibility of electrical heating and constant temperature cooling coils being balanced by a proportional controller should also be considered.

(2) Determination of Shear. As pointed out in section C, the error in determining the absolute shearing distance 2β is the largest contributor to the experimental uncertainty in (dn/dT) . A slit of precise and uniform aperture would improve the determination of 2β as described in Chapter III. Wallin and Wallin (1970) have described a method for determining the shear by passing the laser beam backwards through Q1, L1 and L2 and measuring the beam separation directly. They claim that use of this technique lowered the uncertainty in the absolute shear by an order of magnitude.

(3) Cell Sealant. The liquid of interest is sealed in the sample cell with a viscous stopcock grease (Dow "FS" Fluorosilicone) applied between the metal plates and the top of the glass cell walls. Use of a teflon gasket on top of the glass walls would eliminate the problem of sealant extrusion from the metal-glass boundary when pressure is applied to the metal plates. This would improve the optical quality of the fringe image (compare Figure 4.1(a) and Figure 4.1(b)) and would also eliminate danger of contamination of the sample liquid with the sealant.

(4) Digital Data Acquisition. A significant modification of the apparatus would be the installation of a small digital computer (for example, PDP 8E) to record the data during a run. This would eliminate the tedious and time consuming process of obtaining the time dependent temperature change and fringe shift data from a strip chart recorder output. This changeover would be relatively easy because the data are available as an electrical outputs and these could be easily interfaced to the analog input of a computer. It is likely that accuracy would also be improved.

Many further experiments can be performed in the determination of (dn/dT) for liquids. The most obvious is the determination of (dn/dT) at several different mean temperatures. This would make possible the calculation of the 2nd and 3rd derivatives from the change (if any)

in the first derivative with temperature. Tabulation of data from a series of chemically related compounds would indicate trends that may suggest further improvements in the electromagnetic equation of state. (dn/dT) values are useful to workers performing light-scattering and depolarization experiments.

Finally, this technique could possibly be used to determine (dn/dT) for mixtures. However, the fringe shift would have to be measured before the onset of thermal diffusion because the formation of the mass fraction gradient also causes the fringes to move horizontally (Horne and Anderson, 1971). A small temperature gradient in a large cell would minimize the effects of thermal diffusion.

CHAPTER V

ANOMALOUS PARABOLIC FRINGE SHAPES

A. Introduction

The steady state fringe shapes observed for carbon tetrachloride, cyclohexane and benzene in the 8mm cell were anomalously parabolic (see Chapter IV, section E). Examination of the literature (Table 4.1) indicates that for CCl_4 , C_6H_{12} and C_6H_6 , unlike water which has a significant (d^2n/dT^2) , the first derivative is the only nonzero term in the power series expansion of refractive index, Eq. (4.3). Second and third derivatives of the order of magnitude of 10^{-8} to 10^{-10} would not cause detectable fringe shifts. A priori, we would therefore expect a refractive index derivative experiment on, for example, CCl_4 to proceed as follows: straight vertical fringes in the isothermal configuration would become parabolic due to the initial nonlinear temperature distribution at the onset of the temperature difference. These parabolas would be shifted horizontally across the final image plane and would decay away to vertical or very slightly tilted straight fringes. What in fact was observed experimentally was behavior identical to that described by Anderson (1968):

the steady state fringes remain parabolic in shape with the ends of the parabolas extending in the direction of travel of the horizontal fringe shift. Typical steady state photographs for the three liquids are shown in Figure 5.1, (a), (b), (c). These parabolas do not move horizontally with time after reaching the steady state (5-8 min.), nor do they change shape even after 36 hours of a maintained temperature gradient.

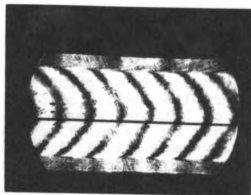
B. Analysis of the Parabolic Steady State Fringe Shapes

There are several possible explanations for the anomalous parabolic fringe shapes for CCl_4 , C_6H_{12} and C_6H_6 . These include (1) nonlinear temperature dependence of the refractive index, (2) nonlinear (sigmoidal) steady state temperature distribution, and (3) 2nd order optical effects.

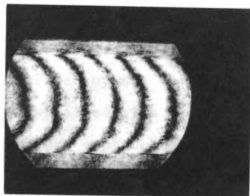
(1) Nonlinear temperature dependence of the refractive index. This is the interpretation we put forth at an early stage of this research (Olson, et al., 1970). The notion was first described by Bartelt (1968) and Anderson (1968, pp. 196-200):

Analysis of the refractive index data from the literature for the two pure compounds showed that only a linear dependence on temperature was statistically significant. Use of those data and the working equations for the interferometer required that the temperature distribution inside the liquid be sigmoidal in shape in order to explain the shape of the interference fringes.

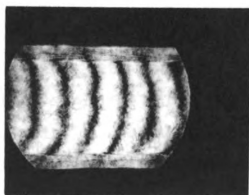
Figure 5.1--Interference fringe photographs: (a) steady state cell profile of CCl_4 in 8mm cell, $\Delta T = 2.73\text{K}$, solid line (—) indicates midplane of cell, (b) steady state cell profile of C_6H_{12} in 8mm cell, $\Delta T = 2.79\text{K}$, (c) steady state cell profile of C_6H_6 in 8mm cell, $\Delta T = 2.79\text{K}$.



a



b



c

Such a temperature distribution would, in turn, require either anomalous variations in the thermal conductivity of the liquid or some inexplicable apparatus effect. Believing that the thermal conductivity is a well-behaved function of the temperature, and that our apparatus caused no strange effects (since the same temperature difference, applied to water, gave the expected straight fringes), we turned our attention to the validity of the reported values of the temperature dependence of the refractive index for CCl_4 and C_6H_{12} .

Since only second order thermal conductivity temperature dependence affects the value of $(dT/dz)_0$, and since the effect is less than 0.1° , we have, at the center of the cell, $(dT/dz)_0 = \Delta T/a \dots$, therefore second and higher temperature derivatives are obtainable from fringe shape analysis.

If the temperature distribution is essentially linear, i.e., described by Eq. (4.4), then parabolic fringes would be explained by a cubic form of the refractive index temperature dependence formula, Eq. (4.3). KINET was used to curvefit the steady state parabolic fringe shape data (see Appendix C) using Eqs. (2.23), (4.3) and (4.4). Literature values of K_T (Table 4.1) and our experimental values of (dn/dT) (Eqs. (4.23), (4.24) and (4.25)) were used so that (d^2n/dT) and (d^2n/dT^3) were the only adjustable parameters. The average results and uncertainties calculated with KINET are shown in Table 5.1.

Note that $(\Delta T/h)$ for this series of experiments was $\approx 3.5\text{Kcm}^{-1}$. This caused the light beam from the cell to be bent out of the interferometer optical axis and required that the rotatable parallel plate and L1 be adjusted

Table 5.1--Results of curvefitting for alleged nonlinear temperature dependence of refractive index.

Liquid	$(d^2n/dT^2) \times 10^5$	$\hat{\sigma} \times 10^5$	$-(d^3n/dT^3) \times 10^5$	$\hat{\sigma} \times 10^5$
CCl_4	1.77	0.13	7.10	0.30
C_6H_{12}	1.94	0.30	5.84	0.30
C_6H_6	1.51	0.24	2.78	0.25

to return the light beam to the optical axis. This type of adjustment was not necessary during the (dn/dT) experiments where $(\Delta T/h) \approx 1.0 K cm^{-1}$.

Superficially, it appears that the nonlinear $n(T)$ explanation is entirely satisfactory since the data were easily fit to this model. However, there are two objections to this interpretation:

(i) The refractive index equation obtained would not reproduce the literature refractive index behavior (the values obtained for (d^2n/dT^2) and (d^3n/dT^3) are about 10^3 larger than indicated by previous experimental or theoretical studies (Table 4.1)). Upon substitution of the numerical values from Table 4.7 into Eq. (4.2), we obtain for C_6H_{12} ,

$$n(T) = n_{25^\circ} - 5.38 \times 10^{-4}(T - 25) + 9.70 \times 10^{-6}(T - 25)^2 - 9.73 \times 10^{-6}(T - 25)^3. \quad (5.1)$$

Figure (5.2) is a plot both of Eq. (5.1) and the absolute refractive index from the literature. Note the gross differences at 25°C and 30°C. This type of behavior would be easily detectable with a conventional critical angle refractometer since variations would occur in the 3rd decimal place. However, Coumou, et al. (1964) measured the absolute index at 20°, 25°, 30° and 40° and noted only linear behavior.

In order to eliminate this problem, a gaussian form of the refractive index temperature equation was postulated,

$$n(T) = n_{25^{\circ}} + (dn/dT)_{25^{\circ}}(T - 25) + e^{-\epsilon(T - 25)^2} [\phi(T - 25)^2 + \theta(T - 25)^3] \quad (5.2)$$

This equation was fit to the steady state fringe data and the results are shown in Table 5.2. Note that the exponential parameter ϵ is very poorly determined as indicated by the very large estimated standard deviation. The 2nd and 3rd derivatives are of the same order of magnitude as before. Eq. (5.2) produces the correct absolute index behavior at all temperatures. However, this type of equation suggests that $|(d^2n/dT^2)|$ and $|(d^3n/dT^3)|$ are maximal at 25° and decay away to zero everywhere else. This sort of singular behavior is not physically reasonable nor theoretically satisfying.

Figure 5.2--Temperature dependence of refractive index of C_6H_{12} . The solid line (—) is Eq. (5.1) and the broken line (- - -) is the linear behavior predicted by the literature (Table 4.1).

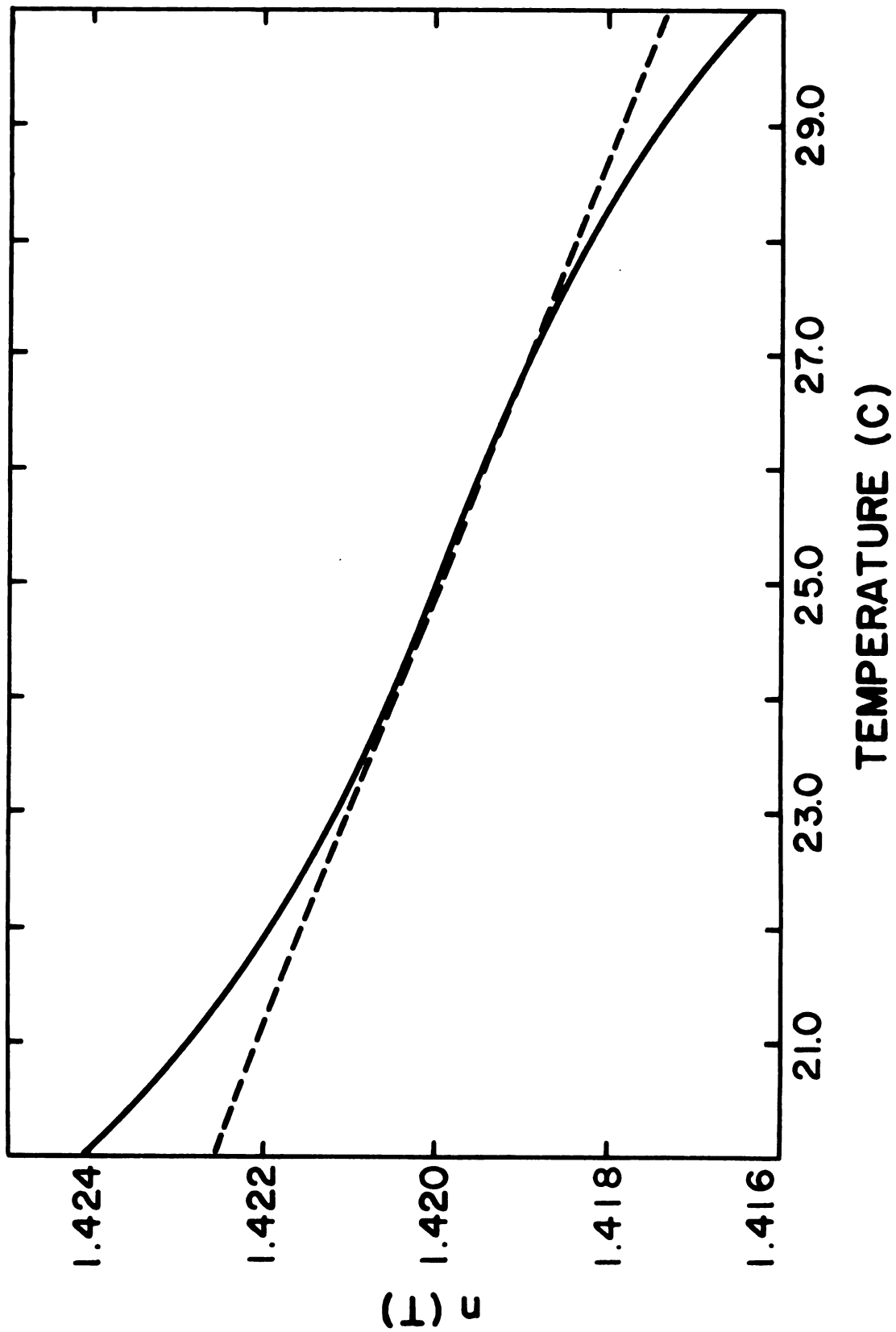


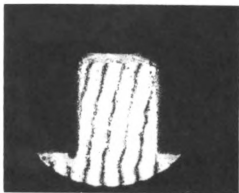
Table 5.2--Results of curvefitting for gaussian nonlinear refractive index temperature dependence equation.

Liquid	$\hat{\epsilon} \times 10^3$	$\hat{\sigma} \times 10^3$	$\hat{\phi} \times 10^6$	$\hat{\sigma} \times 10^6$	$\hat{\theta} \times 10^5$	$\hat{\delta} \times 10^5$
CCl_4	-7.9	38.0	8.73	0.31	-1.13	0.050
C_6H_{12}	24.4	57.0	10.4	0.50	-0.998	0.057
C_6H_6	-223.0	130.0	6.68	0.50	-0.461	0.028
$10^5 \times (d^2 n / dT^2) = 2\phi$			$10^5 \times (d^3 n / dT^3) = 6\theta$			
CCl_4	1.74		-6.78			
C_6H_{12}	2.08		-5.99			
C_6H_6	1.34		-2.77			

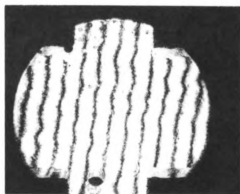
(ii) Experiments on CCl_4 in the 30mm cell gave results for the higher derivatives which were quite different from those obtained in the 8mm cell. Steady state fringe data for water and CCl_4 were obtained using the 30mm cell with $(\Delta T/h) \approx 3.3\text{K cm}^{-1}$ ($\Delta T \approx 10\text{K}$, $h \approx 3\text{cm}$). This is comparable to $(\Delta T/h) \approx 3.5\text{K cm}^{-1}$ for the 8mm cell experiments ($\Delta T \approx 2.80\text{K}$, $h \approx 0.8\text{cm}$). The mean temperature was also 25°C in the large cell.

The entire cell profile could not be placed on one photograph. Consequently, three photos of the cell profile were taken for water (Figure 5.3) and CCl_4 (Figure 5.4). A composite drawing of the complete cell profile made from these photographs is shown in Figure (5.5). These drawings have been marked to indicate the region of an 8mm cell.

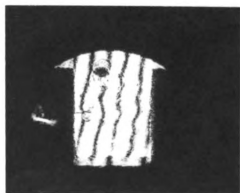
Figure 5.3--Interference fringe photographs. This is the steady state cell profile of H_2O in 30mm cell, $\Delta T = 10.83\text{K}$: (a) top (1/3) of cell, (b) middle (1/3) of cell, (c) bottom (1/3) of cell.



a



b



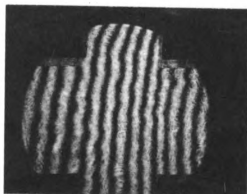
c

Figure 5.4--Interference fringe photographs. This is the steady state cell profile of CCl_4 in 30mm cell, $\Delta T = 10.22\text{K}$: (a) top (1/3) of cell, (b) middle (1/3) of cell, (c) bottom (1/3) of cell.

110



a

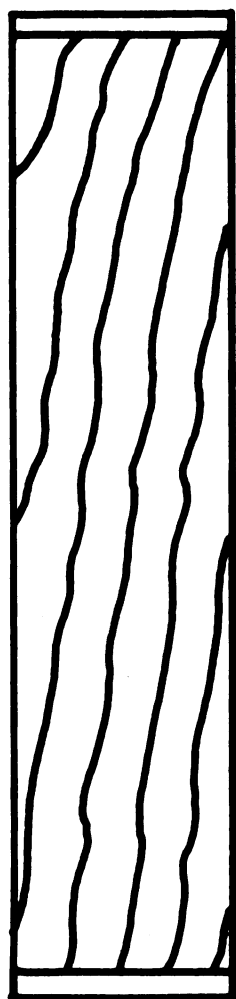


b

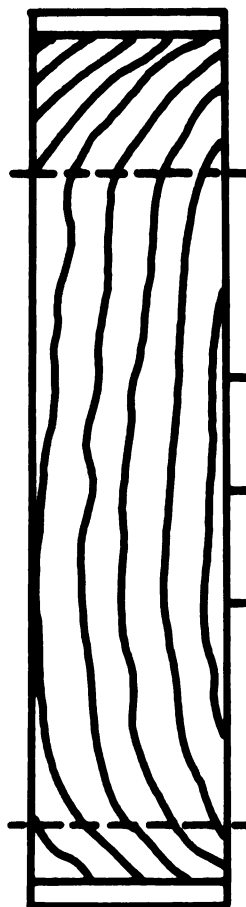


c

Figure 5.5--Steady state cell profile of CCl_4 and H_2O in 30mm cell. This composite drawing was made from Figures 5.3 and 5.4. The broken line (- - -) indicates the "break" in the CCl_4 fringes.

 H_2O

$Z = 0.4$
 $Z = 0.0$
 $Z = -0.4$

 CCL_4

$Z = 0.4$
 $Z = 0.0$
 $Z = -0.4$

The general appearance of the steady state fringes for water is the same as in the 8mm cell: straight fringes that are slightly tilted from the vertical. However, the CCl_4 fringe shape is vastly different in the two different cells. In the center region of Figure (5.5) which corresponds to the central 8mm, the fringes are nearly straight. If (d^2n/dT^2) and (d^3n/dT^3) were actually the values in Table 5.1, the fringes in the center of Figure (5.5) should be similar to Figure (5.1(a)) since the mean temperature, $(\Delta T/h)$ and the shear are almost identical.

The data from Figure (5.5) were fit to the cubic refractive index temperature equation using KINET. The following results were obtained:

$$\begin{array}{lcl}
 \text{CCl}_4 & 30\text{mm cell} & \\
 \hline
 (d^2n/dT^2)_{25^\circ} & \leq -4.4 \times 10^{-7} \approx 0 & (5.3) \\
 \hat{\sigma} & = 10 \times 10^{-7} & \\
 (d^3n/dT^3)_{25^\circ} & = -0.75 \times 10^{-5} & \\
 \hat{\sigma} & = 0.077 \times 10^{-5} &
 \end{array}$$

The value of the 3rd derivative (responsible for parabolicity) has decreased by an order of magnitude. An intensive physical property of the liquid should be independent of the height of the cell in which the liquid is contained.

Another experimental test was carried out. Since the (dn/dT) of water is about $(1/6)$ the value of (dn/dT) for CCl_4 , the refractive index gradient is smaller in water than in CCl_4 for identical $(\Delta T/h)$ conditions;

$$(\partial n / \partial z)_{z=0} \approx (\Delta T/h)_{z=0} (dn/dT)_{T=25^\circ} \quad (5.4)$$

For

$$(\Delta T/h) \approx 3.0 K \text{ cm}^{-1} ,$$

$$\begin{array}{c} H_2O \\ \hline \end{array} \quad (\partial n / \partial z)_{z=0} \approx 3.0 \times 10^{-4} \text{ cm}^{-1} , \quad (5.5)$$

$$\begin{array}{c} CCl_4 \\ \hline \end{array} \quad (\partial n / \partial z)_{z=0} \approx 17 \times 10^{-4} \text{ cm}^{-1} . \quad (5.6)$$

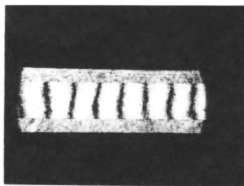
We decided to subject water to a large temperature difference to see if parabolic behavior could be produced if the refractive index gradient was similar in magnitude to that in the nonelectrolyte experiments. Figure (5.6(b)) shows photographs of steady state for water with $(\Delta T/h) = 20 K \text{ cm}^{-1}$.

The fringes continue to tilt from the vertical in response to the large $(\Delta T/h)$ as predicted by Eq. (4.13). Parabolic steady state fringes could not be produced for water.

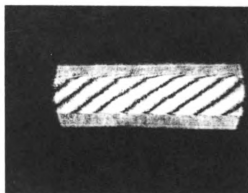
(2) Nonlinear temperature distribution. If the refractive index is well represented by the formula,

$$n(T) = n_{25^\circ} + (dn/dT)(T - 25) , \quad (5.7)$$

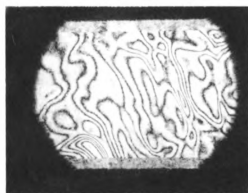
Figure 5.6--Interference fringe photographs: (a) Isothermal slit photo for H_2O in 5mm cell, (b) steady state cell profile of H_2O in 5mm cell, $\Delta T = 10.09\text{K}$, (c) fringe pattern produced by free convection in CCl_4 heated from below.



a



b



c

then a sigmoidal spatial temperature distribution in the steady state would produce parabolic fringes. We know that the temperature distribution should be sigmoidal during the establishment of the temperature difference (Ingle, 1971, Figure 1, p. 97), but this nonlinearity should decay away so that the steady state $T(z)$ is Eq. (4.3). Even for water we observed parabolas at the beginning of the experiment that decayed away to straight fringes in the steady state.

We write Eq. (5.8) as an empirical model for an essentially linear steady state temperature distribution with parameters S_1 and S_2 to introduce nonlinearity,

$$T(z) = (\Delta T/h)z + S_1[z^2 - (h/2)^2] + S_2 \{z[z^2 - (h/2)^2]\} + T_M. \quad (5.8)$$

S_2 causes the distribution to become sigmoidal while S_1 causes the distribution to be skewed (unsymmetric) about $z = 0$.

Eqs. (5.8) and (5.7) were used with the complete optical equation, Eq. (2.23), to fit the steady state parabolic fringe data with KINET. Table 5.3 shows results for representative CCl_4 , C_6H_{12} and C_6H_6 data.

The experimental values of S_1 and S_2 were used to calculate the steady state temperature distributions from Eq. (5.8) and Eq. (4.4). The results are tabulated in Table 5.4.

Table 5.3--Results of curvefitting for nonlinear temperature distribution equation.

Liquid	$S_1 \times 10^2$	$\sigma \times 10^2$	$S_2 \times 10$	$\sigma \times 10$
CCl_4	-14.4	0.64	7.54	0.21
C_6H_{12}	-7.30	0.38	7.92	0.15
C_6H_6	-7.06	0.42	3.17	0.16

Note that the maximum difference in the two temperature distributions is 0.028K. It is apparent that this is not a drastic deviation. The s-shaped temperature distribution shown would not be inconsistent with the theoretical analysis of the steady state temperature distribution because the deviation is less than the claimed accuracy of the temperature equation (Horne and Anderson, 1970).

The steady state fringe shape data for CCl_4 in the 30mm cell were not fit to the empirical temperature equation because of the sharp breaks in the fringe shape indicated in Figure 5.5. The break is more apparent when looking at the actual photographs, Figure 5.4. There appear to be three distinct regions: (a) sharply tilted fringes near the top of the cell, (b) a center region of almost straight fringes, and (c) sharply tilted fringes near the bottom of the cell. Curvefitting difficulties were encountered because the optical equation delta functions, $\Delta n(z)$, $\Delta S'(z)$ and $\Delta S''(z)$, are not continuous across the

Table 5.4--Experimental and theoretical steady state temperature distributions for CCl_4 in 8mm cell, $\Delta T = 2.80^\circ\text{C}$, $K_T = -2.0 \times 10^{-3}$.

$z(\text{cm})$	$T^\circ\text{C}$ (Theory)	$T^\circ\text{C}$ (Experiment)
.405	26.4000	26.4000
.385	26.3298	26.3263
.365	26.2596	26.2533
.344	26.1895	26.1809
.324	26.1193	26.1091
.304	26.0491	26.0380
.284	25.9790	25.9673
.263	25.9089	25.8972
.243	25.8387	25.8274
.223	25.7686	25.7582
.203	25.6985	25.6892
.182	25.6284	25.6207
.162	25.5584	25.5524
.142	25.4883	25.4843
.122	25.4182	25.4165
.101	25.3482	25.3489
.081	25.2781	25.2814
.061	25.2081	25.2140
.041	25.1381	25.1466
.020	25.0680	25.0793
-.000	24.9980	25.0120
-.020	24.9280	24.9446
-.041	24.8581	24.8771
-.061	24.7881	24.8094
-.081	24.7181	24.7416
-.101	24.6482	24.6736
-.122	24.5782	24.6053
-.142	24.5083	24.5367
-.162	24.4384	24.4678
-.182	24.3684	24.3985
-.203	24.2985	24.3287
-.223	24.2286	24.2586
-.243	24.1587	24.1879
-.263	24.0889	24.1167
-.284	24.0190	24.0449
-.304	23.9491	23.9725
-.324	23.8793	23.8995
-.344	23.8095	23.8257
-.365	23.7396	23.7513
-.385	23.6698	23.6760
-.405	23.6000	23.6000

three regions. The physical significance of these three regions will be discussed in section C.

(3) 2nd Order Optical Effect. There is a possibility that the parabolicity could in some way be the result of the optical components of the interferometer acting on the wavefront after it leaves the cell. The wavefront, having passed through a refractive index gradient, is distorted. This possibility is remote in that explicit account of the gradient is made in the theory derived in Chapter II.

Empirical tests were performed which included tilting the Savart plates at different angles, adjusting the polarization analyzer, and slightly changing the angle of incidence of the light beam on L1. None of these affected the parabolicity in any unusual way that would suggest that critical adjustment of a particular component is necessary.

Note that benzene has the largest value of (dn/dT) for the liquids studied. Therefore the benzene filled cell contained the largest refractive index gradient for the experiments on CCl_4 , C_6H_{12} and C_6H_6 when $(\Delta T/h) \approx 3.5K\text{ cm}^{-1}$. However, Figure 4.1 shows that the degree of parabolicity of the benzene fringes is the smallest of the three. This suggests that the size of the gradient and the resulting nonlinear optical effects are not responsible for the parabolicity.

C. Discussion

Rejecting the possibility of an optical effect, there are two alternatives for explanations of the parabolic steady state fringe shape. We pointed out earlier in the optical theory that to analyze the fringe shape with respect to a property varying in the vertical coordinate in the liquid, either the refractive index property dependence, in this case $n(T)$, or the property spatial distribution, $T(z)$, must be specified beforehand. If we claim to know $T(z)$ exactly as Eq. (4.4), then the data indicate nonlinear refractive index behavior that is drastically different from anything ever observed or predicted before. However, if we accept $n(T)$ as a linear function, then the data indicate that $T(z)$ is slightly different (a maximum of $\approx 0.2\%$) from the theoretically predicted temperature distribution. We therefore conclude that the temperature distribution in the steady state is slightly sigmoidal and that this perturbation is the cause of the parabolic fringes observed for CCl_4 , C_6H_{12} , and C_6H_6 .

It is important to note that the effect is small in magnitude compared to the gross linear character of the temperature distribution as described by Eq. (4.4). Because of this, thermal diffusion experiments that use Eq. (4.4) to describe the steady state temperature distribution (Anderson, 1968; Horne and Anderson, 1971) are not in any

way affected by the discovery of a sigmoidal temperature perturbation. The mass distribution response to this small a temperature variation would not be detectable. In like manner, the development of the thermal conductivity experiment discussed in Chapter VI is not affected by this discovery.

The experimental evidence at this time suggests that the physical cause of the sigmoidal perturbation is a wall effect related to the liquid-metal boundaries at the top and bottom of the sample cell. Radiation heat flux, horizontal heat flux through the glass walls, the heterogeneous mechanism of "wetting" of the metal surfaces, adsorption of the liquid on the metal and dissolution of the sealant at the liquid-metal interface are possible causes of a wall effect. The theory of metal-liquid interactions at a boundary has not been developed so that a quantitative theoretical analysis is not possible. In addition, the vertical heat flux through the liquid does not vanish at the boundaries. Anomalous behavior of the heat flux would, of course, be manifested in a perturbation of the temperature distribution.

The suggestion of a wall effect is supported by the peculiar appearance of the CCl_4 steady state fringes in the 30mm cell. We have already noted the sharp break in the fringes near the top and bottom boundaries of the cell profile. The region of extreme curvature extends

about 4.6mm from the top boundary and about 3.9mm from the bottom boundary (taking into account the cutoff due to the light beam bending). If these two regions were joined together to form an 8.5mm fringe pattern, the resulting parabolas would be similar to those actually observed in 8mm cell. This suggests that the boundary influence on the temperature distribution extends about 4-5mm into the liquid from each of the metal boundaries.

The suggestion that the metal-liquid boundary could influence the temperature distribution in this type of apparatus was also made by Longworth (1957). He noted peculiar behavior of the temperature gradient established in water contained in a sandwich cell whose upper and lower boundaries were, at different times, silver, stainless steel or Koroseal (a gasket material). By use of Rayleigh interferometry, he determined that the gradient of refractive index was markedly larger near the upper and lower boundaries of the cell. This behavior could not be explained by the known behavior of refractive index or thermal conductivity. Longworth referred the origin of the wall effect notion to Bates (1933) who made the following statement concerning the temperature distribution in water and red oil contained in a similar sandwich type apparatus with a vertical heat flux: "A surface effect is present at the interface of a stationary liquid and a solid during the transmission of heat normal to the face, and should properly be considered."

In our investigation, water, so often the exception in physical properties of liquids, exhibits "normal" steady state fringe behavior. Some physical properties of water, CCl_4 , C_6H_{12} , and C_6H_6 are compared in Table 5.5. Significantly, the thermal conductivity of water exhibits unusual behavior in that it increases with temperature and has noticeable nonlinear temperature dependence (McLaughlin, 1964). This indicates that the sigmoidal perturbation is not due to anomalous behavior in the thermal conductivity. Moreover, the fact that water is probably structured due to hydrogen bonding would tend to reduce the influence of a wall effect.

Further experiments should be performed for a series of sample cells whose heights are intermediate between 8mm and 30mm. Different materials should be tried as the upper and lower thermostating boundaries. These experiments would indicate if the distance from the upper and lower walls to the "break" in the fringes (see Figures 5.4 and 5.5) is a constant. Observation of the steady state fringe pattern for other liquids, especially hydrogen bonded liquids, would indicate trends, which would be useful in beginning a theoretical treatment of the phenomenon. Finally, experiments should be conducted at different mean temperatures.

Table 5.5--Summary of some physical properties of H_2O , CCl_4 , C_6H_{12} and C_6H_6 at 25°C .

Liquid	κ	K_T	ρ	\bar{C}_p	η	γ	T_B
H_2O	60.8^c	2.68^c	0.997^a	4.18^a	0.894^a	72.0^a	100.0^a
CCl_4	10.3^b	-1.84^b	1.584^e	0.85^b	0.904^h	26.1^a	76.7^a
C_6H_{12}	12.4^d	-0.71^d	0.774^e	1.84^g	0.900^h	26.5^a	80.1^a
C_6H_6	16.0^a	-1.75^b	0.874^f	1.72^a	0.608^a	28.2^a	80.7^a

κ = Thermal conductivity $\times 10^2$, $\text{J m}^{-1} \text{sec}^{-1} \text{K}^{-1}$.

$K_T = (1/\kappa) (\partial\kappa/\partial T)_{25^\circ} \times 10^3$.

ρ = Density, g cm^{-3} .

\bar{C}_p = Specific heat capacity at constant pressure, $\text{J g}^{-1} \text{K}^{-1}$.

η = Viscosity $\times 10^2$, $\text{g cm}^{-1} \text{sec}^{-1}$.

γ = Surface tension, dynes cm^{-1} .

T_B = Boiling point at atm., $^\circ\text{C}$.

References.

^aWeast (Handbook of Chemistry and Physics, 44th edition), 1963.

^bTouloukian, 1970.

^cMcLaughlin, 1964.

^dBriggs, 1957.

^eWood and Gray, 1952.

^fWood and Austin, 1945.

^gTimmermans, 1950.

^hHammond and Stokes, 1955.

CHAPTER VI

PURE THERMAL CONDUCTION

A. Introduction

The observation and theory of heat flow in matter is the oldest and most fundamental problem in the study of transport phenomena. It was the first transport process to be precisely described by a linear law when Fourier (1822) stated his famous relation for heat flow in one dimension,

$$q = -\kappa(\partial T/\partial X) . \quad (6.1)$$

If a system is perturbed by a temperature gradient, Eq. (6.1) indicates that a heat flux, q , will occur (i.e., heat will flow) toward the colder part of the object. This heat flux will tend to restore the system to equilibrium. The dimensions of the heat flux are (energy) (time)⁻¹ (distance)⁻², and the proportionality factor κ , the thermal conductivity, has dimensions of (energy) (time)⁻¹ (distance)⁻¹ (temperature)⁻¹.

In a recent review, McLaughlin (1964) considers the importance of the study of thermal conductivity of liquids:

The subject of the thermal conductivity of liquids and dense gases is important for two main reasons: firstly, because its study can help in giving a better understanding of the basic molecular processes involved in transport phenomena in general, and secondly, because of its significance in technological applications.

B. Experimental Methods

The experimental methods of determining thermal conductivity are divided into two types: (1) steady state methods and (2) transient methods. A recent general discussion can be found in Tyrrell (1961).

(1) Steady state methods. A liquid is contained in a vessel with geometrically well defined boundaries, for example, between two concentric cylinders. If a constant heating source is maintained in one of the boundaries, a steady state heat flux will be present in the liquid. In this case Eq. (6.1) can be approximated by

$$Q/A = \kappa(\Delta T/d) , \quad (6.2)$$

where Q is the energy produced in the heating surface per unit time, A is the area of the heating surface, d is the separation of the boundaries of the liquid and ΔT is the steady temperature difference between the liquid boundaries. This treatment assumes that κ is independent of temperature over this ΔT . The thermal conductivity experiment is begun by applying a constant heat flux through an initially isothermal liquid (this is usually accomplished by means

of electrical heating with constant current passing through a resistor of known value). The steady state temperature difference ΔT is measured when no further temperature variation is detected in the liquid. This number and the geometric constants can be used to calculate κ from Eq. (6.2).

Energy may be transported through the liquid by two mechanisms in addition to pure conduction described by Eqs. (6.1) and (6.2). These are: (i) convection, which is the bulk transfer of mass from the hot area of the liquid to the cold area, and (ii) radiation of energy from one boundary of the liquid to the other. Care must be taken to eliminate these mechanisms when designing a thermal conductivity apparatus. Heating from the top of a horizontal layer downward is commonly done to minimize convection, while maintaining a small temperature difference tends to minimize the effect of radiation.

The main sources of error in steady state methods are (i) measurement of Q (calorimetry), (ii) elimination of "heat leaks" so that the entire heat flux generated at the boundary of the liquid is transported through the liquid, (iii) minimization of the effects of convection and radiation energy transfer and (iv) the careful machining and measurement of the cell geometry necessary to obtain the surface area, A . A recent careful application of this method including a systematic discussion of the experimental errors has been made by Tree and Leidenfrost (1969).

(2) Transient methods. The only previous time dependent experimental method of determining thermal conductivity is the "hot wire" experiment. In this method the development of the temperature of an electrically heated wire immersed in the liquid of interest is observed. In principle the temperature rise of the wire will depend on the rate of the conduction of heat away from the wire in the surrounding liquid and therefore on the thermal conductivity of the liquid. Extensive theoretical treatments have produced several equations describing the temperature of the wire as a function of time (McLaughlin, 1964). A commonly used equation is,

$$T_2 - T_1 = (Q/\ell 4\pi\kappa) \ln(t_2/t_1) , \quad (6.3)$$

where T_2 is the temperature of the wire at time t_2 , T_1 is the temperature of the wire at time t_1 and ℓ is the length of the wire. The thermal conductivity is calculated from the slope of a plot of the temperature of the wire against log time. However, after a time convection begins in the liquid surrounding the wire. Consequently all measurements must be made before the onset of convection, which is indicated by deviations from Eq. (6.3). Additional experimental errors include those discussed above for steady state methods. A recent exhaustive theoretical treatment of this method and a carefully designed computerized experiment on toluene are described by McLaughlin and Pittman (1971).

C. A New Transient Method

Tyrrell (1961, p. 299) noted that in principle the experimental apparatus used for steady state measurements could be used in transient methods:

The above methods are all steady state methods, but cells of similar geometrical form (parallel plates) could in principle be used to determine the heat conductivity from the rate of establishment of the thermal gradient in the liquid layer. It is possible to envisage several methods by which this might be done, for example by adapting optical methods used for diffusion measurements. . . ., but the practical difficulties cannot be negligible because no accurate measurements have been carried out using techniques of this kind.

The fringe shift produced by a wavefront shearing interferometer during the establishment of a temperature gradient in a liquid as described in Chapters III and IV should be a time dependent measurement of the rate of establishment of the thermal gradient. In order to design a quantitative transient experiment to determine the thermal conductivity, three basic problems must be solved:

(1) Description of the boundary conditions. A systematic and reproducible method of applying and maintaining a temperature difference across the boundaries of the liquid is necessary. The thermostated metal plates are the boundaries of the liquid contained in the sample cell. The time dependence of the temperature of the upper and lower plates is described by the following equations,

$$T_U(t) = T_M^O, \quad T_L(t) = T_M^O, \quad t \leq t_s ;$$

$$T_U(t) = T_M^O + (T_U^\infty - T_M^O) (1 - e^{-t/\gamma_U}), \quad (6.4)$$

$$T_L(t) = T_M^O - (T_M^O - T_L^\infty) (1 - e^{-t/\gamma_L}), \quad (6.5)$$

$$t \geq t_s = 0 ,$$

where t_s is the time when the plates are switched from the isothermal configuration to the temperature difference configuration, T_M^O is the temperature of the plates in the isothermal configuration, T_U^∞ and T_L^∞ are the steady state values ($t = \infty$) of the plate temperatures and γ_U and γ_L are adjustable relaxation parameters determined by curvefitting of experimental data (Chapter II).

(2) A method of monitoring temperature changes. A sensitive method of monitoring changes of temperature in the vertical coordinate of the liquid is necessary. The fringe shift produced by a wavefront shearing interferometer can be used in conjunction with the already determined temperature dependence of refractive index to measure the temperature gradient in the sample cell at the midplane ($z = 0$).

(3) Theoretical description of the temperature in the liquid. An equation for the spatial and temporal development of the temperature of the liquid is necessary to analyze the temperature changes. Ingle (1971) has obtained a $T(z,t)$ function that can be combined with our

optical theory to analyze the horizontal fringe shifts in terms of the thermal conductivity.

The method outlined above is called pure thermal conduction because it is the simplest experimental arrangement. It requires no calorimetry, no complex geometrical measurements and, moreover, it is performed in an apparatus demonstrated to be free of convection (Anderson, 1968). Convection in the cell would be manifested by abnormal fringe behavior similar to that shown in Figure 5.2 (c).

D. Theory of the Time Dependent Fringe Shift

Ingle (1971, pp. 77-101) developed an equation to describe the temperature of a liquid as a function of time and position when the liquid is contained in a rectangular parallelepiped cell such as described in Chapters III and IV and is subject to boundary conditions Eqs. (6.4) and (6.5). Her analysis is based on the perturbation scheme described by Horne and Anderson (1970) for the temperature distribution in a binary liquid undergoing thermal diffusion. This approach takes into account the variability with temperature of the transport coefficients.

Ingle assumed that (i) the temperature gradient is applied only in the vertical direction with no horizontal effects and (ii) the lateral cell walls are adiabatic so that there is no horizontal heat flux through the lateral

walls. Hence, heat and matter flow only in the vertical direction, and there is no steady state convection when the liquid is heated from above (for liquids which expand upon heating). She began with the appropriate transport equations, simplified where possible, and then applied the perturbation scheme to the set of partial differential equations describing the transfer of mass and energy in the cell. The temperature equation obtained is of the form,

$$T(z,t) = T_M + T_0(z,t) + T_1(z,t) + T_2(z,t) \dots \quad (6.6)$$

where T_0 is the result for constant coefficients, T_1 is the result when first derivatives of coefficients are retained, T_2 is the result when second derivatives and products of first derivatives are retained, and so forth to any order. Each of the T_n , $n = 0,1,2,\dots$, was obtained by Fourier transforms.

Numerical analysis indicated (Ingle, 1971, pp. 98-101) that T_0 alone is a very good representation of the temperature distribution because each succeeding term in the solution Eq. (6.6) is 10^{-3} to 10^{-4} smaller in magnitude than its predecessor. In addition, T_1 was found to be symmetric about $z = 0$, so that its derivative is zero at $z = 0$ for all t and would add nothing to a temperature difference measured about $z = 0$.

Her Eq. (4.20) will be used as $T(z,t)$ for the analysis of the time dependent fringe shift:

$$\begin{aligned}
T(z,t) = & T_M + [(z/h) + (1/2)](T_U - T_M)[1 - \exp(-t/\gamma_U)] \\
& + [(z/h) + (1/2)](T_M - T_L)[1 - \exp(-t/\gamma_L)] \\
& + \sum_{n=1}^{\infty} (-1)^n (\pi n)^{-1} \{ [4n^2(\gamma_U/\tau) - 1]^{-1} (T_U - T_M) \\
& \times [\exp(-t/\gamma_U) - \exp(-4n^2 t/\tau)] \\
& + [4n^2(\gamma_L/\tau) - 1]^{-1} (T_M - T_L) [\exp(-t/\gamma_L) - \exp(-4n^2 t/\tau)] \} \\
& \times \sin(2n\pi z/h) \\
& + \sum_{\ell=0}^{\infty} (2/\pi) (-1)^\ell (2\ell+1)^{-1} \{ [(2\ell+1)^2(\gamma_U/\tau) - 1]^{-1} (T_U - T_M) \\
& \times \{ \exp[-(2\ell+1)^2 t/\tau] - \exp(-t/\gamma_U) \\
& - [(2\ell+1)^2(\gamma_L/\tau) - 1]^{-1} (T_M - T_L) \\
& \times \{ \exp[-(2\ell+1)^2 t/\tau] - \exp(-t/\gamma_L) \} \} \cos[(2\ell+1)\pi z/h] \}. \quad (6.7)
\end{aligned}$$

The thermal relaxation time τ is

$$\tau = h^2 (\rho \bar{C}_p)_0 / \pi^2 \kappa_0, \quad (6.8)$$

where \bar{C}_p is the specific heat capacity, ρ is the density and κ is the thermal conductivity. The subscript 0 indicates the value of these quantities at T_M . Note that the "thermal diffusivity," $\alpha = \rho \bar{C}_p / \kappa$, is the quantity determined by the experiment. If values for ρ and \bar{C}_p are previously known, κ can be determined.

It was shown in Chapter IV that for experimental purposes, the refractive index is adequately represented by the equation,

$$n(T) = n_{T=T_M} + n'_{T=T_M} (T - T_M) . \quad (6.9)$$

If Eq. (6.7) is solved for $[T(z,t) - T_M]$ and substituted into Eq. (6.9), the result is a time dependent refractive index spatial distribution in the liquid,

$$n(z,t) = n_{z=0} + n'_{T=T_M} [T(z,t) - T_M] . \quad (6.10)$$

We now refer to the optical theory to predict the interference fringe behavior resulting from the establishment of the time dependent refractive index distribution, Eq. (6.10), in the liquid. The optical equation, Eq. (4.7), is

$$X' = (X/\delta) = (a/\lambda) [n(z+\beta) - n(z-\beta)] . \quad (6.11)$$

If we consider the case of horizontal fringe shifts, X'_0 measured as a function of time for the midplane ($z = 0$) of the cell, Eq. (6.11) may be written,

$$X'_0(t) = (a/\lambda) \{n'_{T=T_M} [T(\beta, t) - T(-\beta, t)]\} , \quad (6.12)$$

where Eq. (6.10) has been solved for $z = 0$ and substituted into the difference expression of Eq. (6.11).

Eq. (6.12) may be used to analyze the time dependent fringe shift data obtained experimentally as described in Chapter III. The explicit optical equation, obtained by substituting Eq. (6.7) into Eq. (6.12), is a very long and complicated expression. A Fortran subroutine, TEMP, was written to evaluate Eq. (6.7) for any given values of β , t ,

γ_U , γ_L , T_U , T_L , T_M and τ . The infinite series were automatically truncated in each calculation using the criteria discussed by Ingle (1971, p. 94). This subroutine was subsequently used with a special subroutine EQN for the general curvefitting program KINET to determine thermal conductivity from curvefitting of fringe shift vs. time data. These subroutines are listed in Appendix B.

E. Experimental Results for Water and CCl₄

Fringe shift vs. time data measured at ($z = 0$) were available from refractive index temperature dependence experiments ν and μ (see Tables 4.4 and 4.6) and these data were analyzed as an experimental test of Eq. (6.12). A typical set of data are listed in Table 6.1. The variance of the time and fringe shift values for each data point were estimated from the reading error on the strip chart recording. The fringe maxima and minima were not as clearly defined in the final stages of the experiment as in the early stages, so the variances are larger for longer times. This is because the fringes were "slowing down" and consequently the recorder pen stayed at a maximum value for a longer period of time (see Figure 3.3).

One major experimental difficulty was encountered. During some of the runs the photo transistor was not exactly in the center of a fringe minimum at the start of

Table 6.1--Fringe shift data for experiment v-4.

Data Point	Time(sec)	σ_t^2	X'(fringe number)	$\sigma_{X'}^2$
1.	0.0	0.360	0.00	0.010
2.	19.1	0.014	0.50	0.010
3.	23.4	0.014	1.00	0.012
4.	27.8	0.014	1.50	0.010
5.	31.6	0.014	2.00	0.010
6.	36.7	0.014	2.50	0.010
7.	41.3	0.014	3.00	0.010
8.	47.2	0.014	3.50	0.010
9.	53.2	0.014	4.00	0.010
10.	62.3	0.032	4.50	0.010
11.	72.4	0.130	5.00	0.014
12.	89.2	0.360	5.50	0.023
13.	114.1	0.706	6.00	0.026
14.	194.8	5.760	6.50	0.032
15.	402.4	0.032	6.67 ^a	0.040

^aThis number was obtained from the steady state measurement of the fractional fringe shift, see Table 4.4.

an experiment. This was due to movement of the fringe pattern, variations in the phototransistor voltage amplifier characteristics and changes in the laser intensity. Consequently, these runs exhibited gross errors in the calculated thermal conductivity. They are labeled with an (*) in the tables of experimental results and are not included in the calculation of the final average or the experimental standard deviation.

Experimental results for 15 trials on water from the data of experiment v are listed in Table 6.2. Note that the γ_U and γ_L values are relatively constant. Three sets of results are listed corresponding to the number of data points included in the curvefitting. This number of data points corresponds to a starting time, t_{start} , for the first data point. The values of κ are different for the three sets.

The early time data should not be included in the curvefitting of the fringe shift data for two a priori reasons: (1) the perturbation scheme's higher order contributions would be largest at the start of an experiment, and (2) the initial temperature change of the plates is probably not completely exponential as described by Eqs. (6.4) and (6.5). Because of this we would not expect Eq. (6.12) to fit the very short time data points.

There was experimental evidence for choosing the data set with $N = 11$, $t_{\text{start}} = 3\text{sec}$: Figure (6.1) is a plot of the average standard deviation of the thermal conductivity calculated by KINET for each set of data. This number indicates the "goodness of fit" of the data with Eq. (6.12). It is a minimum for the data with $N = 11$; i.e., for data beginning with points at $t = 3\text{sec}$. Apparently there are two opposing influences on the goodness of fit: (1) the inclusion of early time data points is not theoretically allowed and (2) fitting only the long

Table 6.2--Summary of experimental results for thermal conductivity of water, $J\ m^{-1}\ sec^{-1}\ K^{-1}$.

		$\rho_{25^\circ}^a = 0.997044\ g\ cm^{-3}$		$\bar{C}_{P25^\circ}^a = 4.1796\ J\ g^{-1}\ K^{-1}$			
ID	$\gamma_L(sec)$	$\gamma_U(sec)$	$\kappa_{25^\circ}^b \times 10^2$	$\hat{\sigma}_\kappa \times 10^2$	$\kappa_{25^\circ}^c \times 10^2$	$\hat{\sigma}_\kappa \times 10^2$	$\hat{\sigma}_\kappa \times 10^2$
v-1	30.3	42.2	58.5 ₉	0.95	59.1 ₀	0.98	59.2 ₆
v-2*	--	--	62.5 ₈	1.01	63.0 ₄	0.88	63.0 ₅
v-3*	30.8	41.8	57.9 ₄	0.98	58.4 ₇	1.03	58.5 ₂
v-4	30.5	44.5	60.2 ₄	0.84	60.9 ₃	0.71	61.2 ₇
v-5	30.3	41.4	60.9 ₈	0.90	61.8 ₃	0.73	62.0 ₇
v-6	30.6	41.4	59.7 ₂	0.80	60.1 ₉	0.80	60.2 ₃
v-7	31.3	39.9	59.9 ₅	0.90	60.5 ₉	0.99	60.6 ₀
v-8	31.0	41.5	61.5 ₃	0.84	62.2 ₅	0.74	62.6 ₂
v-9	31.0	42.1	62.1 ₃	0.89	62.9 ₅	0.76	63.3 ₉
v10*	28.7	41.7	56.0 ₀	0.97	56.4 ₃	1.05	56.3 ₄
v-11*	31.4	44.0	63.6 ₈	0.99	64.6 ₁	0.86	65.1 ₆
v-12	31.2	42.1	60.9 ₈	1.17	62.3 ₉	0.72	62.8 ₅
v-13*	31.2	41.7	67.8 ₁	1.14	68.8 ₆	1.00	69.3 ₃
v-14	31.3	36.3	59.8 ₁	0.95	60.2 ₇	1.00	60.4 ₅
v-15*	--	--	64.9 ₂	1.20	66.0 ₈	1.07	66.7 ₅

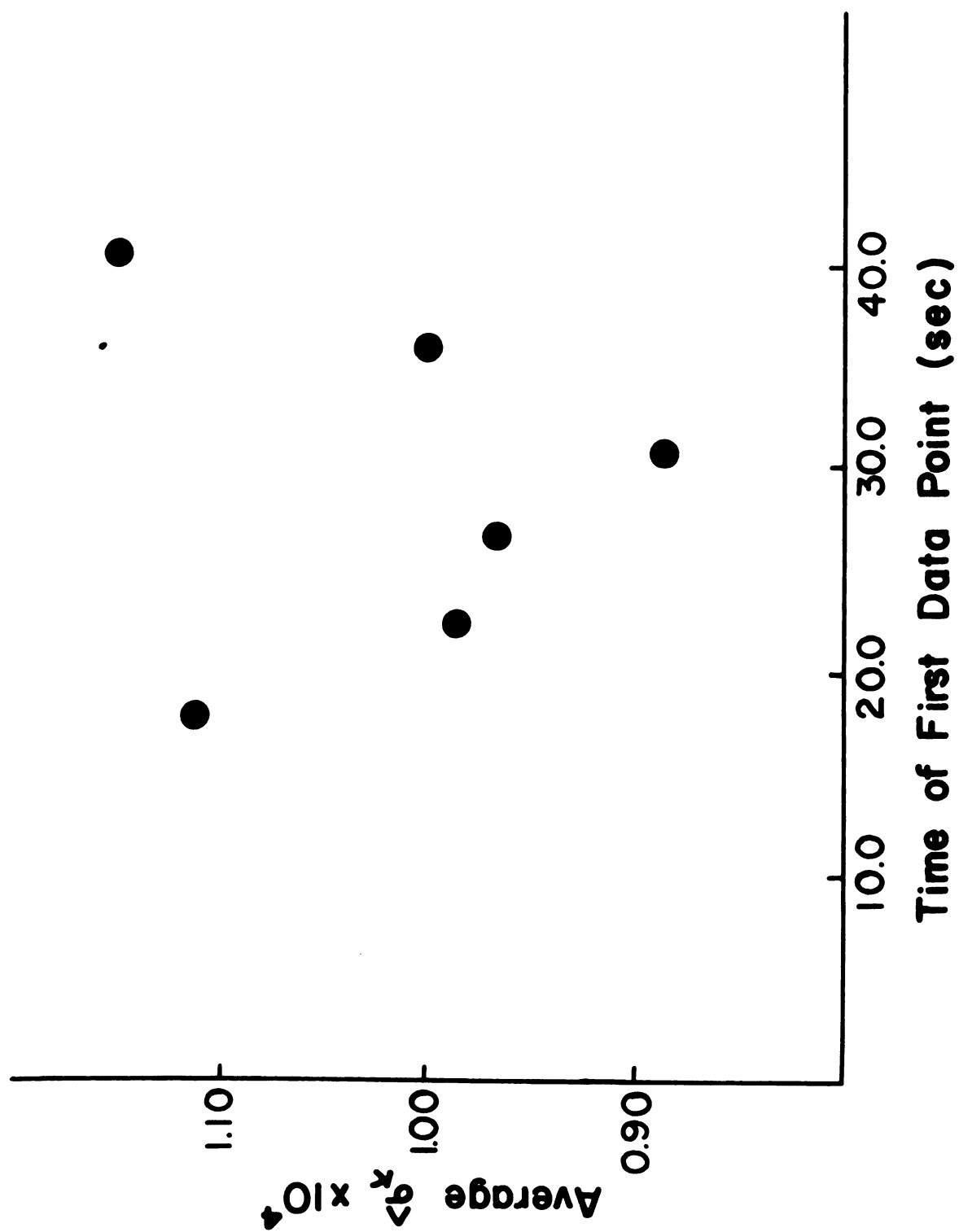
^aWeast (Handbook of Chemistry and Physics, 44th edition), 1963.

^bNumber of data points = N = 12, $t_{start} = 28sec$.

CN = 11, $t_{start} = 31sec$.

dN = 10, $t_{start} = 37sec$.

Figure 6.1--"Goodness of fit" plot for thermal conductivity
fitting of data from experiment v.



time "flat" end of the curve also produces a poor fit. Further evaluation of this process is necessary before definitive experiments can be performed. Figure 6.2 is a plot of the data from experiment v-4 and the calculated curve from KINET.

The average for nine acceptable determinations of the thermal conductivity of water at 25°C is,

$$\begin{aligned} \kappa_{25^\circ}^{\text{H}_2\text{O}} &= 61.17 \times 10^{-2} \text{ J m}^{-1} \text{ sec}^{-1} \text{ K}^{-1}, \\ \hat{\sigma}_\kappa &= 1.26 \times 10^{-2} = 2.06\% \kappa. \end{aligned} \quad (6.13)$$

This number compares well with the value, $60.74 \times 10^{-2} \text{ J m}^{-1} \text{ sec}^{-1} \text{ K}^{-1}$, recommended by McLaughlin (1964) from a least square fit of the results of several workers. Our value is quite close to that determined by Challoner, et al. (1958), $61.2 \times 10^{-2} \text{ J m}^{-1} \text{ sec}^{-1} \text{ K}^{-1}$. However, the experimental precision of our method reflected in the 2% scatter is large compared to the 0.5% to 1% precision claimed for the steady state and hot wire experiments.

Experimental results for 13 trials on CCl_4 from the data of experiment μ are listed in Table 6.3. Only data collected after $t = 31 \text{ sec}$ were used in the curve-fitting. Note that values of γ_U and γ_L contain more scatter compared to the water experiment. This is probably due to the difficulty involved in maintaining the smaller ΔT required in the case of CCl_4 to prevent excessive ray bending.

Figure 6.2--Plot of fringe shift at $z = 0$ as a function of time. The circles are the experimental points from v-4 and the solid line (—) is the least squares curve calculated from KINET.

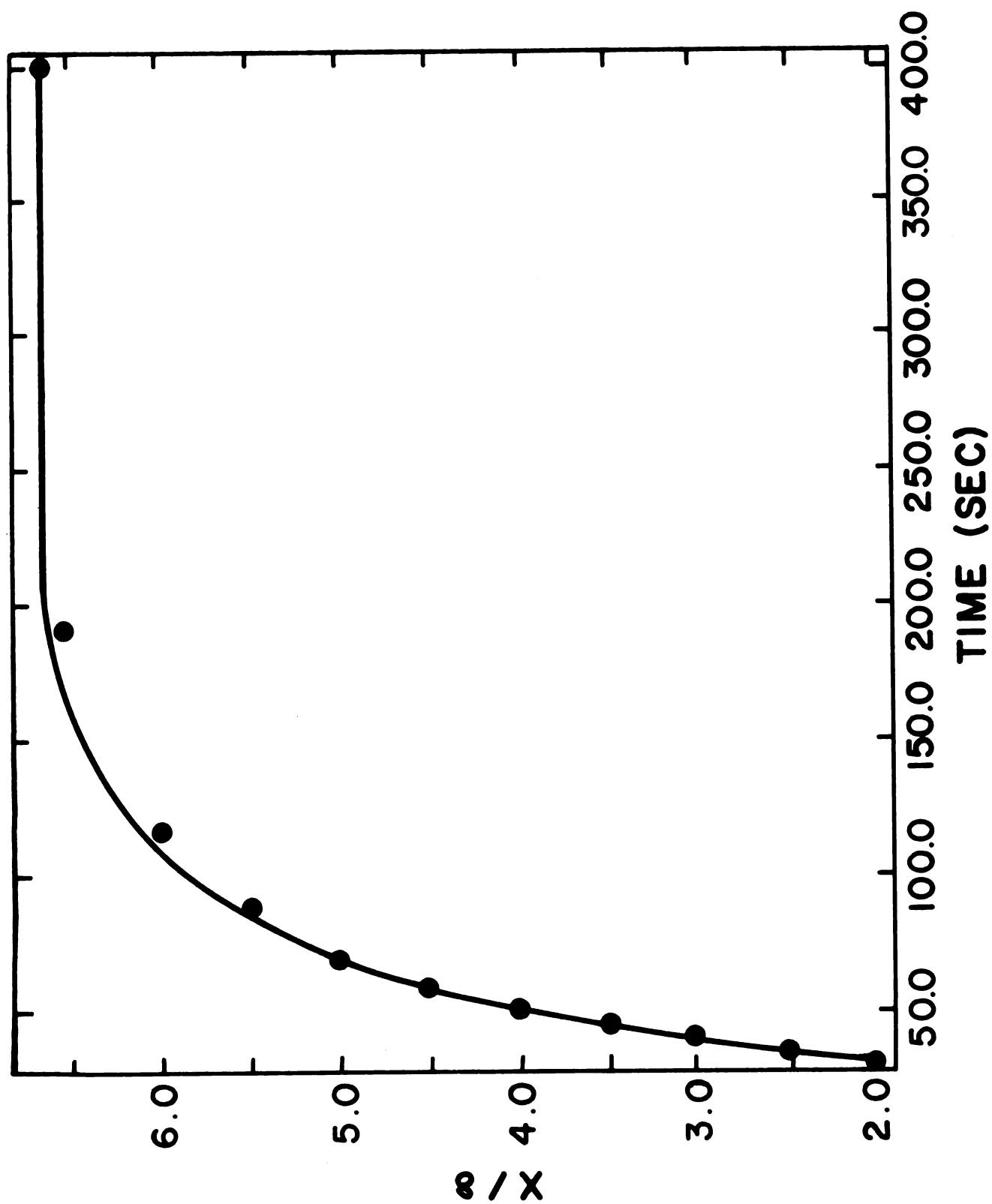


Table 63.--Summary of experimental results for thermal conductivity of CCl_4 , $\text{J m}^{-1} \text{sec}^{-1} \text{K}^{-1}$.

$\rho_{25^\circ}^a = 1.584 \text{ g-cm}^{-3}$ $\bar{C}_{p25^\circ}^b = 0.854 \text{ J g}^{-1} \text{K}^{-1}$				
ID	$\gamma_U(\text{sec})$	$\gamma_L(\text{sec})$	$K_{25^\circ} \times 10$	$\hat{\sigma}_K \times 10$
$\mu-2$	42.3	30.6	1.15 ₆	0.023
$\mu-4$	33.4	30.5	1.11 ₀	0.014
$\mu-5$	39.4	30.4	1.16 ₈	0.024
$\mu-6^*$	34.3	34.7	1.36 ₀	0.022
$\mu-7$	39.7	29.2	1.21 ₃	0.018
$\mu-8$	36.0	31.0	1.16 ₅	0.013
$\mu-9$	38.3	31.4	1.17 ₆	0.015
$\mu-10$	37.4	28.6	1.16 ₈	0.014
$\mu-11$	36.2	27.9	1.13 ₉	0.008
$\mu-12$	39.1	29.1	1.17 ₅	0.014
$\mu-13$	31.2	30.1	1.06 ₇	0.007
$\mu-14$	34.4	28.4	1.04 ₁	0.016
$\mu-15$	36.1	31.4	1.13 ₅	0.012

^aWood and Gray, 1952.

^bTouloukian, 1970.

The average for 12 acceptable determinations of the thermal conductivity of CCl_4 at 25°C is,

CCl_4

$$\kappa_{25^\circ} = 1.14_3 \times 10^{-1} \text{ J m}^{-1} \text{ sec}^{-1} \text{ K}^{-1}, \quad (6.14)$$

$$\hat{\sigma}_\kappa = 0.049 \times 10^{-1} = 4.3\% \kappa.$$

This result can be compared to the recommended value, $1.04 \times 10^{-1} \text{J m}^{-1} \text{sec}^{-1} \text{K}^{-1}$, obtained by Touloukian (1970) from a weighted least squares fit of the "best" data. Our value is about 10% higher than this accepted value. The thermal conductivity of CCl_4 has been a source of controversy for many years. Compilations by Tyrrell (1961) and Tree and Leidenfrost (1969) show that values as high as $1.5 - 1.6 \times 10^{-1} \text{J m}^{-1} \text{sec}^{-1} \text{K}^{-1}$ have been determined over the years. Woolf and Sibbitt (1954) obtained a value of $1.14 \times 10^{-1} \text{J m}^{-1} \text{sec}^{-1} \text{K}^{-1}$ in a series of experiments on different liquids during which they obtained correct values for the thermal conductivity of water. In view of these divergent results, CCl_4 was a poor choice as a standard to test a new method. Toluene would have been a much better choice (McLaughlin; 1964, 1971).

Again the precision of our determinations is worse than the normal scatter associated with the classical methods.

F. Discussion

The experiments discussed in section E indicate that the method of pure thermal conduction is a viable technique and warrants further investigation and development. Because of the small number of experiments and in view of the experimental scatter, the specific results for water and carbon tetrachloride must be considered as

preliminary and the determination of definitive values postponed until the technology of the experiment is optimized.

The National Bureau of Standards recently (NSRDS News, March 1972) listed criteria for use in the critical evaluation of thermal conductivity experiments:

1. A direct experimental assessment of radiative losses.
2. Experimental proof of the absence of convection.
3. A discussion of parasitic conduction and of the efforts made to estimate its magnitude and correct for it.
4. A discussion of the temperature-gradient measurement including specification of the size of the temperature difference and a discussion of the relation of the measured temperature difference and the gradient in the fluid.
5. A discussion of the method of measuring heat flow and its accuracy.
6. Experimental confirmation that the measured thermal conductivity is independent of the magnitude of the temperature gradient (Fourier's law).
7. The determination of the geometrical constants of the system.
8. The geometry of the temperature field.
9. Accommodation coefficients.
10. If the experimental method is a relative method, the calibration and proof of validity of the method.
11. The purity and composition of the sample.
12. Specification of the state variables, including the temperature, at the position in the cell at which the thermal conductivity is measured.

Although this list was intended for the steady state experiments discussed in section B, we note: (a) numbers 2, 3, 4, 6, 7, 8, 11 and 12 are automatically or easily satisfied by our method, (b) numbers 5, 9 and 10 do not apply and (c) criterion number 1 requires further investigation for our method.

Experimental improvements would include all of the modifications discussed at the end of Chapter IV, especially digitalized data collection. In addition, there are some suggestions in the literature (Tyrrell, 1961; McLaughlin and Pittman, 1971) that a smaller cell height would be advantageous. A cell height in the 4-5mm range would tend to eliminate any possibility of a horizontal heat flux. Bartelt (1968) has considered this problem in some detail for a pure thermal diffusion experiment.

Finally, a critical review of the development of Eq. (6.7) should be made in order explicitly to consider the problem of radiation energy transfer and metal-liquid boundary effects.

BIBLIOGRAPHY

.

.

BIBLIOGRAPHY

- Amey, R. L., "The Electromagnetic Equation of State Data," Pure Dense Fluids, H. L. Frisch, Ed. (Academic Press, New York, 1968).
- Anderson, T. A., Ph.D. Thesis, Michigan State University, 1968.
- Andréasson, S. P., S. E. Gustafsson, and N. O. Halling, J. Opt. Soc. Am., 61, 595 (1971).
- Bartelt, J. L., Ph.D. Thesis, Michigan State University, 1968.
- Bates, O. K., Ind. Eng. Chem., 25, 431 (1933).
- Bauer, N., K. Fajans, and S. Z. Lewin, Technique of Organic Chemistry, Vol. I., A. Weissberger, Ed. (Wiley (Interscience), New York, 1958).
- Beck, J. V., Parameter Estimation in Engineering and Science, Preliminary Edition (Mich. State Univ., E. Lansing, Mich., 1972).
- Becsey, J. G., Gene E. Maddox, Nathaniel R. Jackson, and J. A. Bierlein, J. Phys. Chem., 74, 1401 (1970).
- Bevington, P. R., Data Reduction and Error Analysis for the Physical Sciences (McGraw Hill Book Co., New York, 1969).
- Böttcher, C. K., Theory of Electric Polarization (Elsevier Publ. Co., Amsterdam, 1952).
- Briggs, D. K. H., Ind. Eng. Chem., 49, 418 (1957).
- Bryngdahl, O., Acta Chem. Scand., 11, 1017 (1957).
- _____ and S. Ljunggren, J. Phys. Chem., 64, 1264 (1960).
- _____, Arkiv. Fysik, 21, 289 (1961).
- _____, J. Opt. Soc. Am., 53, 571 (1963).
- _____, J. Opt. Soc. Am., 59, 142 (1969).

- Challoner, A. R., H. A. Grundy, and R. W. Powell, Proc. Roy. Soc. (London), A245, 259 (1958).
- Coumou, D. J., E. L. Mackor, and J. Hijmans, Trans. Faraday Soc., 60, 1539 (1964).
- Deming, W. E., Statistical Adjustment of Data (John Wiley and Sons, Inc., New York, 1943).
- Efroymsen, M. A., Mathematical Methods for Digital Computers, Vol. 1, A. Ralston and H. S. Wilf, Eds. (John Wiley and Sons, New York, 1960).
- Fourier, J. B. L., Théorie Analytique de la Chaleur (Paris, 1822).
- Gustafsson, S. E., J. G. Becsey, and J. A. Bierlein, J. Phys. Chem., 69, 1016 (1965).
- Hamilton, W. D., Statistics in Physical Science: Estimation, Hypothesis Testing, and Least Squares (Ronald Press Co., New York, 1964).
- Hammond, B. R. and R. H. Stokes, Trans. Faraday Soc., 51, 1641 (1955).
- Horne, F. H. and T. G. Anderson, J. Chem. Phys., 53, 2332 (1970).
- _____, J. Chem. Phys., 55, 2831 (1971).
- Ingelstam, E., J. Opt. Soc. Am., 47, 536 (1957).
- Ingle, S. E., Ph.D. Thesis, Michigan State University, 1971.
- Langer, D. W. and R. A. Montalvo, J. Chem. Phys., 49, 2836 (1968).
- Longworth, L. G., Ann. N. Y. Acad. Sci., 46, 211 (1945).
- _____, Ind. Eng. Chem. (Anal.), 18, 219 (1946).
- _____, J. Am. Chem. Soc., 69, 2510 (1947).
- _____, J. Am. Chem. Soc., 74, 4155 (1952).
- _____, J. Phys. Chem., 61, 1557 (1957).
- Looyenga, H., Molecular Phys., 9, 501 (1965).

- McLaughlin, E., Chem. Rev., 34, 389 (1964).
- _____ and J. F. T. Pittman, Phil. Trans. R. Soc. (London), 270A, 557 (1971).
- Mitchell, M. and H. J. V. Tyrrell, J. Chem. Soc., Faraday Trans. II, 68, 385 (1972).
- Nicely, V. A. and J. L. Dye, J. Chem. Ed., 48, 443 (1971).
- Olson, J. D., T. G. Anderson, J. L. Bartelt, and F. H. Horne, American Chemical Society National Meeting (September, 1970).
- Parratt, L. G., Probability and Experimental Errors in Science (John Wiley and Sons, New York, 1961).
- Svennson, H., Opt. Acta, 1, 25 (1954).
- _____ and R. Forsberg, Opt. Acta, 1, 90 (1954).
- _____, Opt. Acta, 3, 164 (1956).
- Tilton, L. W. and J. K. Taylor, J. Research NBS, 20, 419 (1938).
- Timmermans, J., Physico-Chemical Constants of Pure Organic Compounds (Elsevier, New York, 1950).
- _____, Physico-Chemical Constants of Binary Systems, Vol. I (Interscience, New York, 1959).
- Touloukian, V. S., Ed. Thermophysical Properties of Matter (Plenum Press, New York, 1970).
- Tree, D. R., and W. Leidenfrost, "Thermal Conductivity Measurements of Liquid Toluene," Thermal Conductivity, Proceedings of the Eighth Conf., Ho and Taylor, Eds. (Plenum Press, New York, 1969).
- Tyrrell, H. J. V., Diffusion and Heat Flow in Liquids (Butterworths, London, 1961).
- Wallin, L. E., J. Chem. Phys., 52, 552 (1970).
- _____ and K. Wallin, Opt. Acta, 17, 381 (1970).
- Washburn, E. W., Ed., International Critical Tables of Numerical Data (McGraw-Hill, New York, 1933).

Waxler, R. M., and C. E. Wier, J. Research NBS, 67A, 163 (1963).

_____, C. E. Weir, and H. W. Schamp, Jr., J. Research NBS, 68A, 489 (1964).

Weast, R. C., Ed. Handbook of Chemistry and Physics (Chemical Rubber Pub. Co., Cleveland, 1959).

_____, Ed. Handbook of Chemistry and Physics (Chemical Rubber Pub. Co., Cleveland, 1963).

Wentworth, W. E., J. Chem. Ed., 42, 96 (1965).

Wilson, E. B., An Introduction to Scientific Research (McGraw Hill, Inc., New York, 1952).

Wolberg, J. R., Prediction Analysis (D. Van Nostrand Co., Inc., Princeton, N. J., 1967).

Wolter, H., Handbuch der Physik, Vol. XXIV, S. Flugge, Ed. (Springer Vorlag, Berlin, 1956).

Wood, S. E. and A. E. Austin, J. Am. Chem. Soc., 67, 480 (1945).

_____, and J. A. Gray, III, J. Am. Chem. Soc., 74, 3729 (1952).

Woolf, J. R. and W. L. Sibbitt, Ind. Eng. Chem., 46, 1947 (1954).

APPENDICES

APPENDIX A

ORIGINAL OPTICAL THEORY OF BRYNGDAHL

In the original derivation of the optical theory for the wavefront shearing interferometer, Bryngdahl (1963) used the mean value theorem to replace the difference function ΔV of Eq. (2.15). We give here a brief summary of his treatment for comparison to the results of Chapter II. The equation number from his original article is given after the Appendix equation number.

Bryngdahl uses the mean value theorem:

If $a \leq x \leq b$,

$$(f(b) - f(a))/(b-a) = \Delta f(x)/\Delta x = f'(a + \theta \Delta x)$$

for some θ , $0 \leq \theta \leq 1$,

to write Eq. (2.14) as,

$$\begin{aligned} mrx = & \ell \{ V'_x [mrx + \theta_1 (b_1/2), mry + \theta_2 (mb_1/2)] \} \\ & + m\ell \{ V'_y [mrx + \theta_1 (b_1/2), mry + \theta_2 (mb_1/2)] \} \\ & - (\ell/b_1) [(\phi/k) - \chi'] + mrx \, 0(i^2), \end{aligned} \quad (A.1) (27)$$

where $-1 < \theta_1 < 1$ and $-1 < \theta_2 < 1$

Next, Bryngdahl limits consideration to refractive index variations in the y coordinate and expands V'_y by use of the mean value theorem to give,

$$\begin{aligned} \text{mr}x &= m\ell V'(y) + \theta_2 (m^2 \ell b_1/2) V''[mry + \theta_2 \theta_3 (mb_2/2)] \\ &\quad - (\ell/b_1) [(\phi/k) - \chi'] + \text{mr}x_0(i^2) , \end{aligned} \quad (\text{A.2}) (29)$$

where $-1 < \theta_3 < 1$.

Since,

$$V(mry) = w(ry) = W(y) ,$$

$$V'(mry) = (1/mr) W'(y) ,$$

$$V''(mry) = (1/m^2 r^2) W''(y) ,$$

Eq. (A.2) may be written,

$$\begin{aligned} \text{mr}x &= (\ell/r) W'(y) + (\theta_2 \ell b_1/2r^2) W''[y + \theta_2 \theta_3 (b_1/2r)] \\ &\quad - (\ell/b_1) [(\phi/k) - \chi'] + x_0(i^2) . \end{aligned} \quad (\text{A.3}) (31)$$

At this point, Bryngdahl substitutes the path length expression, Eq. (2.16), into Eq. (A.3) to obtain his final working equation:

$$W(y) = an(y) ,$$

$$X = \text{mr}x = A(\Delta n/\Delta y) + B \quad (\text{A.4}) (32)$$

where $A = (a\ell/b_1)$, $\Delta y = (b_1/r)$ and

$$B = - (\ell/b_1) [(\phi/k) - \chi'] .$$

Equation (A.4) may be rewritten,

$$X = (a\ell/b_1^2) r \Delta n + B . \quad (\text{A.5})$$

Equation (A.5) is dimensionally incorrect because the quantity $(a\ell/b_1^2)$ should have the units of distance.

The first quantity in Eq. (A.3), (ℓ/r) , does not contain b_1 so that the subsequent definition of A in Eq. (A.4) should be,

$$A = (a\ell/r) . \tag{A.6}$$

APPENDIX B

SUBROUTINES EQN AND TEMP

These subroutines were used to evaluate Eq. (6.7) during least squares fitting of experimental data from thermal conductivity experiments. KINET was used to perform the parameter estimation. A program listing and instructions for use of KINET can be obtained from the authors (Nicely and Dye, 1971).

SUBROUTINE EQN is the part of KINET that can be modified to the particular user's application. EQN evaluates the difference between the experimental fringe shift and the value calculated by use of SUBROUTINE TEMP for a specific choice of the thermal conductivity. An iterative procedure minimizes the sum of the squares of these differences.

The following pages are a listing of these subroutines exactly as they were used in Chapter VI.

```

SUBROUTINE EON
  COMMON KOUNT,ITAPE,JTAPE,IWT,LAP,XINCR,NOPT,NOVAR,NOUNK,X,U,ITMAX,
  1WTX,TEST,I,AV,RESID,IAR,EPS,ITYP,XX,RXTYP,DXII,FOP,FO,FU,P,ZL,TO,E
  2IGVAL,XST,T,DT,L,M,JJJ,Y,DY,VECT,NCST,CONST
  DIMENSION X(4,100), U(20), WTX(4,100), XX(4), FOP(100), FO(100), F
  1U(100), P(20,21), VECT(20,21), ZL(100), TO(20), EIGVAL(20), XST(10
  20), Y(10), DY(10), CONST(16)
  GO TO (2,3,4,5,1), ITYP
1 CONTINUE
  ITAPE=60
  JTAPE=61
  WRITE (JTAPE,6)
6 FORMAT(* THERMAL CONDUCTIVITY FITTING*)
  NOUNK = 1
  NOVAR=2
  RETURN
2 CONTINUE
  RHO = 0.997044$ CPBAR = 4.1796
  PI = 3.14159
  DF = 1.0
  GAMMAU = CONST(7) $GAMMAL = CONST(8)
  DELTU = CONST(9)-CONST(11) $DETL = CONST(11)-CONST(10)
  CLLT = CONST(1)
  CLHT = CONST(2)
  SHEAR = CONST(3)
  DNNT = CONST(4)
  S = SHEAR/2.0
  S = S/CLHT
  TAU = ((CLHT**2)*RHO*CPBAR)/((PI**2)*U(1))
  TIME = XX(1)
  CALL TEMP (TAU,TIME, S,GAMMAU,GAMMAL,DELTU,DETL,TZ)
  TPLUS = TZ
  CALL TEMP (TAU,TIME,-S,GAMMAU,GAMMAL,DELTU,DETL,TZ)
  TMINUS = TZ
  FRIN = (DF*CLLT/(6.328E-05))*DNNT*(TPLUS-TMINUS)
  FRIN = ABS(FRIN)
  RESID = FRIN-XX(2)
  RETURN
3 CONTINUE
  RETURN
4 CONTINUE
  RETURN
5 CONTINUE
  RETURN
END

```

```

SUBROUTINE TEMP (TAU,TIME,ZOA,GAMMAU,GAMMAL,DELTU,DETL,TZ)
  DIMENSION TERM(150),TEST(150)
  IF(TIME.EQ.0.0) GO TO 500
  DENOM = ABS(4.0*GAMMAU/TAU - 1.0)
  IF (DENOM.LT.1.0E-06) PRINT 20
  DENUM = ABS(4.0*GAMMAL/TAU - 1.0)

```

```

IF ( DENUM.LT.1.0E-06) PRINT 20
DENOM = ABS(GAMMAU/TAU - 1.0)
IF (DENOM.LT.1.0E-06) PRINT 40
DENUM = ABS(GAMMAL/TAU - 1.0)
IF (DENUM.LT.1.0E-06) PRINT 50
TT = TIME/TAU
PI = 3.14159
TZ = 0.0
ITMAX = 0
DO 200 I=1,150
TEST(I) = 0.0
200 TERM(I) = 0.0
TA = (DELTU*(1.0 - EXP(-TIME/GAMMAU)) + DELTL*(1.0 - EXP(-TIME/
1 GAMMAL)))*ZOA
TB = 0.5*DELTU*(1.0-EXP(-TIME/GAMMAU))-0.5*DELTU*(1.0-EXP(-TIME
1/GAMMAL))
TZ = TA + TB
NT = 0
2 NT = NT + 1
A = FLOAT(NT)
AA = 2.0*A
AA2 = AA**2
DUMSIN = 1.0/(A*PI)*(DELTU/(AA2*GAMMAU/TAU-1.0)*(EXP(-TIME/GAMMAU
1) - EXP(-AA2*TT)) + DELTL/(AA2*GAMMAL/TAU - 1.0)*(EXP(-TIME/GAMM
2AL) - EXP(-AA2*TT)))*SIN(AA*PI*ZOA)
L = NT/2
RND = L
RNDUM = A/2.0
IF (RND.LT.RNDUM) DUMSIN = -DUMSIN
NMIN = NT -1
B = FLOAT(NMIN)
BB = 2.0*B + 1.0
BB2 = BB**2
DUMCOS = 2.0/(PI*BB)*(DELTU/(BB2*GAMMAU/TAU - 1.0)*(EXP(-BB2*TT)
1-EXP(-TIME/GAMMAU))-DELTU/(BB2*GAMMAL/TAU - 1.0)*(EXP(-BB2*TT)
2-EXP(-TIME/GAMMAL)))*COS(BB*PI*ZOA)
L = NT/2
RND = L
RNDUM = B/2.0
IF (RND.LT.RNDUM) DUMCOS = -DUMCOS
TERM(NT) = DUMSIN + DUMCOS
IF(NT.GT.3) GO TO 1005
TZ = TZ + TERM(NT)
1005 IF(NT.EQ.7) GO TO 3
GO TO 2
3 CALL TEST1(TERM,TEST,TA,ITMAX,NT)
22 NT = NT + 1
NTD = NT + 1
IF(ITMAX.EQ.1) GO TO 1
A = FLOAT(NT)
AA = 2.0*A
AA2 = AA**2
DUMSIN = 1.0/(A*PI)*(DELTU/(AA2*GAMMAU/TAU-1.0)*(EXP(-TIME/GAMMAU
1) - EXP(-AA2*TT)) + DELTL/(AA2*GAMMAL/TAU - 1.0)*(EXP(-TIME/GAMM

```

```

2AL) = EXP(-AA2*TT))*SIN(AA*PI*ZOA)
L = NT/2
RND = L
RNDUM = A/2.0
IF (RND.LT.RNDUM) DUMSIN = -DUMSIN
NMIN = NT - 1
B = FLOAT(NMIN)
BB = 2.0*B + 1.0
BB2 = BB**2
DUMCOS = 2.0/(PI*BB)*(DELTU/(BB2*GAMMAU/TAU - 1.0)*(EXP(-BB2*TT)
1-EXP(-TIME/GAMMAU))-DETL/(BB2*GAMMAL/TAU - 1.0)*(EXP(-BB2*TT)
2-EXP(-TIME/GAMMAL)))*COS(BB*PI*ZOA)
L = NT/2
RND = L
RNDUM = B/2.0
IF (RND.LT.RNDUM) DUMCOS = -DUMCOS
TERM(NT) = DUMSIN + DUMCOS
A = FLOAT(NTD)
AA = 2.0*A
AA2 = AA**2
DUMSIN = 1.0/(A*PI)*(DELTU/(AA2*GAMMAU/TAU-1.0)*(EXP(-TIME/GAMMAU
1) - EXP(-AA2*TT)) + DELTL/(AA2*GAMMAL/TAU - 1.0)*(EXP(-TIME/GAMM
2AL) = EXP(-AA2*TT))*SIN(AA*PI*ZOA)
L = NT/2
RND = L
RNDUM = A/2.0
IF (RND.LT.RNDUM) DUMSIN = -DUMSIN
NMIN = NTD - 1
B = FLOAT(NMIN)
BB = 2.0*B + 1.0
BB2 = BB**2
DUMCOS = 2.0/(PI*BB)*(DELTU/(BB2*GAMMAU/TAU - 1.0)*(EXP(-BB2*TT)
1-EXP(-TIME/GAMMAU))-DETL/(BB2*GAMMAL/TAU - 1.0)*(EXP(-BB2*TT)
2-EXP(-TIME/GAMMAL)))*COS(BB*PI*ZOA)
L = NT/2
RND = L
RNDUM = B/2.0
IF (RND.LT.RNDUM) DUMCOS = -DUMCOS
TERM(NTD) = DUMSIN + DUMCOS
TZ = TZ + TERM(NT)
DT0 = TZ + TERM(NTD)
CALL TEST2(TERM,TEST,TZ,DT0,ITMAX,NT,NTD)
IF(NT.GT.100) GO TO 6
GO TO 22
500 TZ = 0.0
GO TO 1
6 PRINT 10
10 FORMAT(* THE SERIES HAS FAILED TO CONVERGE AFTER 100 TERMS*)
20 FORMAT(* 4.0GAMMAU = TAU*)
30 FORMAT(* 4.0GAMMAL = TAU*)
40 FORMAT(* GAMMAU = TAU*)
50 FORMAT(* GAMMAL = TAU*)
GO TO 1
1 CONTINUE

```

```

7 RETURN
END

```

```

SUBROUTINE TEST1(TERM,TEST,TA,ITMAX,NT)
DIMENSION TEST(150),TERM(150),SUM(5)
NT = 3
DO 1 I =1,3
S = 0.0
DO 2 J=1,I
2 S = TERM(J) + S
1 SUM(I)=S
TEST(1) =(TERM(1)/(TA+ SUM(1)))*100.0
TEST(2)=((TERM(1)+TERM(2))/(SUM(2)+TA))*100.0
TEST(3)=((TERM(3)+TERM(2))/(SUM(3)+TA))*100.0
DO 7 I=1,3
7 TEST(I) = ABS(TEST(I))
IF(TEST(1).LT.0.01) GO TO 4
IF(TEST(2).LT.0.1) GO TO 5
IF(TEST(3).LT.0.1) GO TO 6
GO TO 100
4 CONTINUE
GO TO 101
5 CONTINUE
GO TO 101
6 CONTINUE
101 ITMAX = 1
100 CONTINUE
RETURN
END

```

```

SUBROUTINE TEST2(TERM,TEST,TZ,DT0,ITMAX,NT,NTD)
DIMENSION TERM(150),TEST(150)
TST = 0.0
TST = ((TERM(NT) + TERM(NT-1))/TZ)*100.0
TEST(NT) = ABS(TST)
TEST(NTD) = ABS(((TERM(NT)+TERM(NTD))/DT0)*100.0)
TST = ABS(TST)
IF(TST.LT.0.1) GO TO 1
GO TO 2
1 CONTINUE
ITMAX = 1
2 RETURN
END

```

APPENDIX C

PARAMETER ESTIMATION

A. Introduction

The theory of parameter estimation from experimental data has been considered by many workers (Bartelt, 1968; Wentworth, 1965; Hamilton, 1964; Beck, 1972; Wolberg, 1967). The maximum likelihood estimation method described by Wentworth has been successfully translated into a versatile computer program KINET (Nicely and Dye, 1971).

During the course of our research it was often necessary to apply these various curvefitting methods to various experimental techniques (for example, the thermal conductivity experiment of Chapter VI). This Appendix gives an outline of the procedure used to obtain parameter estimates. The outline was written for use with KINET but the goals and pitfalls of the procedure apply equally to other least squares methods. The purpose of this outline is (i) to suggest a systematic way of approaching the practical application of parameter estimation methods and (ii) to describe some of the problems commonly encountered.

B. Procedure for obtaining parameter estimates

I. Construct a Test Problem

A. Select an equation to fit the data. This can be a theoretical equation of definite form or can be a phenomenological approximation like a Taylor's series expansion. MULTREG (Anderson, Appendix H, 1968) is useful for choosing among a set of linearly related parameters if only an empirical equation is required.

B. Take the selected equation and generate (by hand or computer) a set of test data using an experimentally reasonable range of variables and values of the parameters. Put the equation into subroutine EQN of KINET and read in the test data. Use estimates of the parameters determined as you would from an experiment. KINET should give back exact replicas of the parameters with very small standard deviations. If this does not happen, there are several possibilities: (1) Subroutine EQN may not be doing what you think it is. Computers do exactly what they are told. (2) The equation may be "too non-linear" for the Taylor series in method one of KINET to be valid; that is, the initial guesses of the parameters may be outside the radius of convergence for the truncated series. Try minimization by method two in KINET. (3) Do not attempt to obtain too much information from the data. An equation having a

large number of parameters for a small number of data points will possibly produce meaningless (or nonunique) results.

C. Add randomly generated errors to the test data to see if KINET can still calculate the true input parameters. Increase the variance until the program no longer gives the correct results. This will give an indication of how well determined the experimental data must be and will help in design of the experiment.

II. Transform the Experimental Data

A. Reduce the data to a form containing the experimental observations and their variance. Decide on values of the variance in each experimental variable or, if that is not possible, estimate the relative variance of the variables and use arbitrary variances reflecting this ratio. Consider alternate estimates of the variance, especially under varying experimental conditions. Avoid combining a number of experimental variables into a derived quantity and using it as the experimental observation because this tends to produce correlations among the data points which may bias the parameter estimates. However, repeated experiments of the same type may be combined into a smaller set of data using the "spread" of the data points as a guide for estimating the variance. Finally, obtain estimates for the initial guesses of the parameters by a linear approximation of the equation or by other means such as graphing or the values of previous workers.

B. Punch data in the prescribed format and read into KINET using the form of subroutine EQN tested in part I.

III. Analyze KINET Output

A. Examine the parameter estimates. Are they mathematically and chemically reasonable? Is there any other external information that can be used to check the reasonableness of the estimates? A common example of this type of check occurs in chemical kinetics. Rate constants must be independent of the initial concentrations of the reacting species. If data from different initial concentration conditions give widely varying values of the rate constant, suspicion should be cast on the rate law even though the equation appears to "fit" the data in each individual case. Compare the parameter estimates to literature values or theoretically derived values.

B. Calculate the relative error of each parameter,

$$\text{relative error} = |(\hat{\sigma}_{U_i})/U_i|, \quad (\text{C.1})$$

where $\hat{\sigma}_{U_i}$ is the estimated standard deviation of parameter U_i . Relative errors greater (especially much greater) than one indicate an equation of the wrong form or a parameter which cannot be determined from the experimental data.

C. Examine the variance-covariance matrix and multiple correlation coefficients. The multiple correlation coefficient is a measure of the total linear dependence of

the parameter on all the other parameters. There will usually be some dependence among the parameters. However, as a qualitative guide, multiple correlation close to one may indicate a parameter or parameters that cannot be determined uniquely from the data. In this case a different equation (or data) should be considered. Bevington (1969) and Hamilton (1964) discuss tests for the statistical significance of the correlation coefficients.

D. Perform "Goodness of Fit" Tests. It is often necessary to know how well a particular equation "fits" the data. This can provide experimental evidence that one theory is "more likely" than an alternate. Several tests of this type are available. In addition, the quality of the parameters as discussed in sections A and B would also indicate a "goodness of fit" for the data.

Three methods are generally used to test "goodness of fit": (1) The randomness of the residuals. (2) The fraction of data points lying outside of a statistical confidence limit interval constructed from the parameters and their estimated errors. (3) The χ^2 test.

(1) The sign of the residuals should be distributed randomly among the data points. If not, this indicates a poor choice for the fitting equation. See Wilson (1952).

(2) A confidence interval can be constructed about the derived line using the estimated variances and covariances for the parameters, the propagation of error

formula, and an appropriate "t" value. An equation for the construction of an interval can be found in Wolberg (1967, p. 64). If a large percentage of the data points lie outside the constructed interval, the validity of the equation may be suspect. Individual data points may also be examined in order to investigate the source of their error. Obvious sources of error such as miscopied data or gross error in measurement should be considered before casting doubt on the equation.

(3) Under certain conditions, the χ^2 test can be applied to the quantity, $S/(N - m)$.

S = the minimum sum of the weighted residuals

$(N - m)$ = the number of degrees of freedom;

N = experimental observations

m = parameters

This test applies rigorously only when the true variances of the observations are known. The method of application is discussed in Wolberg (1967, p. 67). A χ^2 table lists the probability that $S > \chi^2$ for various values of $(N - m)$. Two different equations could be tested with the χ^2 distribution and the ratio, (S_1/S_2) , may constitute an F test for statistically significant difference between the two theories.

At the completion of these tests, the investigator may have evidence that the "goodness of fit" is not satisfactory. As Wentworth (1965) states, "he may (1) re-examine

his experimental procedure and techniques for bias errors not properly taken into account, and/or (2) reinvestigate the problem from a theoretical standpoint to find a more representative function."